Materials Science & Engineering R 166 (2025) 101057

Contents lists available at ScienceDirect

Materials Science & Engineering R

journal homepage: www.elsevier.com/locate/mser

Single-atom engineered sensors for volatile organic compounds

Sowjanya Vallem [a,b], Malayil Gopalan Sibi [c], K. Keerthi [d], Anam Giridhar Babu [e], Vishaka Goyal [c], EA Lohith [d], N.V.V. Jyothi [d], K. Praveena [f], Kasibhatta Sivakumar [f], T.G. Satheesh Babu [a,b], P.V. Suneesh [a,b], Hari Bandi [g], Daniel-Ioan Stroe [h], Sada Venkateswarlu [c,*], Aristides Bakandritsos [c,i,**], Rajenahally V. Jagadeesh [c,j,**], Radek Zboril [c,i,**]

[a] Department of Chemistry, Amrita School of Physical Sciences Coimbatore, Amrita Vishwa Vidyapeetham, Coimbatore 641112, India
[b] Amrita Biosensor Research Laboratory, Amrita School of Engineering Coimbatore, Amrita Vishwa Vidyapeetham, India
[c] Nanotechnology Centre, Centre for Energy and Environmental Technologies, VSB-Technical University of Ostrava, 17. listopadu 2172/15, Poruba, Ostrava 708 00, Czech Republic
[d] Department of Chemistry, Sri Venkateswara University, Tirupati, Andhra Pradesh 517502, India
[e] Department of Basic Sciences, SR University, Warangal, Telangana 506371, India
[f] Department of Chemistry, Sri Venkateswara Arts College (TTD's), Tirupati, Andhra Pradesh 517502, India
[g] Department of Electronics and Information Convergence Engineering, Institute for Wearable Convergence Electronics, Kyung Hee University, 1732 Deogyeong-daero, Giheung-gu, Yongin-si, Gyeonggi-do 17104, Republic of Korea
[h] Department of Energy, Aalborg University, Aalborg 9220 Denmark
[i] Regional Centre of Advanced Technologies and Materials, Czech Advanced Technology and Research Institute, Palacky University, Olomouc, Slechtitelu 27, Olomouc 77900, Czech Republic
[j] Leibniz-Institut fur Katalyse e.V., Albert-Einstein-Str. 29a, Rostock D-18059, Germany

ARTICLE INFO

Keywords:
Single atom engineered sensors
Volatile organic compounds
Metal support interactions
Density functional theory
Machine learning

ABSTRACT

The efficient and precise detection of trace-level volatile organic compounds (VOCs) is critically important for environmental monitoring, industrial safety, and public health. In this context, single-atom (SA) materials have emerged as a new frontier in sensor technology, offering unparalleled atom and energy efficiency, along with maximal exposure to active sites. Compared to conventional nanoparticle and bulk sensors, SA-based platforms exhibit superior sensitivity, selectivity, and tunability. This review presents a comprehensive overview of the advances in single-atom engineering (SAE) for VOC detection. We systematically discuss the design principles, fabrication methods, and sensing mechanisms of various SA-based sensors, including chemiresistive gas sensors (CGS), metal oxide semiconductors (MOS), microelectromechanical systems (MEMS), field effect transistors (FETs), and electrochemical sensors. Special attention is given to the roles of heteroatom doping, vacancy engineering, and support interactions in modulating the sensing performance. This review also highlights how advanced spectroscopic tools provide insight into SA-analyte interactions and how computational approaches, particularly density functional theory (DFT) and emerging machine learning (ML) techniques, aid in the rational design of next-generation sensors. Finally, we outline the current challenges and propose future research directions aimed at achieving scalable synthesis, long-term stability, and real-world deployment of SA-based VOC sensors. This review aims to guide future innovations in SA sensor technologies, setting the stage for transformative advances in VOC detection.

* Corresponding author.
** Correspondence to: Nanotechnology Centre, Centre for Energy and Environmental Technologies, VSB-Technical University of Ostrava, 17. listopadu 2172/15, Ostrava 708 00, Czech Republic
E-mail addresses: venkateswarlu.sada@vsb.cz (S. Venkateswarlu), a.bakandritsos@upol.cz (A. Bakandritsos), jagadeesh.rajenahally@catalysis.de (R.V. Jagadeesh), radek.zboril@upol.cz (R. Zboril).

https://doi.org/10.1016/j.mser.2025.101057
Received 10 April 2025; Received in revised form 4 June 2025; Accepted 25 June 2025
Available online 2 July 2025

1. Introduction

The rapid urbanization has led to a significant rise in the use of personal care products, cleaning chemicals, paints, solvents, air fresheners and others. The extensive utilization of these daily life products has resulted in the release of carbon-based volatile organic compounds (VOCs) into the atmosphere (both indoor and outdoor), which create substantial health and environmental risks [1–4]. According to the World Health Organization (WHO), VOCs such as formaldehyde, methyl (alkyl)amines, alcohols, benzene derivatives, light hydrocarbons and halogen compounds have adverse effects on human health, including an increased risk of leukemia, lung damage, dyspnea, throat infection, and other issues [5–7] (Scheme 1). The WHO and the European Union (EU) define VOCs as organic compound with a boiling point below 250 °C at 1 atm [8–10]. Given the concerns related to human health, environmental monitoring, and healthcare diagnostics, the development of eco-friendly, low-cost, and easily accessible sensors for the detection and estimation of VOCs is highly essential [11]. However, conventional detection methods such as gas chromatography and protein-based biosensors are often expensive, difficult to operate, and unsuitable for real-time monitoring of the diverse analytes [12–15].

In this context, gas sensors, including chemiresistive sensors, metal oxide semiconductor gas sensors, electrochemical sensors, and microelectromechanical system sensors, are among the most advanced devices for air quality monitoring [13–15]. Generally, most of the sensors are fabricated using n-type metal oxide nanoparticles (NPs) such as ZnO, In_2O_3, WO_3, Fe_2O_3, and SnO_2 as well as p-type metal oxide nanoparticles like CuO, Cr_2O_3, and Co_3O_4 [16–20]. However, pristine metal oxide nanoparticles based sensors suffer from low response toward the analytes, poor stability, and limited selectivity [21]. To address these limitations, researchers have developed heterostructures with heterojunctions, such as SnO_2/Fe_2O_3@rGO, SnO_2/NiO, SnO_2/Au@In_2O_3, and SnO_2/ZnO. Similarly, sensors incorporating metal nanoparticles embedded in metal oxides ($ZnFe_2O_4$), or doped with noble metal nanoparticles (Pt, Pd, Au, Ru) have shown enhanced sensing capabilities and higher selectivity compared to non-noble metal catalysts. This improvement is primarily attributed to the high catalytic activity and electronic sensitization effects governed by the Schottky barrier mechanism [22–27]. However, several obstacles hinder the widespeared use of noble metal nanoparticle in gas sensor technologies. One key limitation is that only the outer surface atoms of the nanoparticles participate in the sensing reactions, which restricts atom utilization and reduces the overall response rate [28]. Additionally, issues such as limited availability and higher price as well as difficulties in controlling the active sites of noble metal nanoparticles, and particle-agglomeration remain significant challenges. The detection and removal of hazardous pollutants using advanced nanomaterials has gained significant attention due to increasing environmental and health concerns. In addition to widely studied noble metal-based nanoparticles, the group led by Md. Rubel et al. explored earth-abundant mesoporous silica-based nanoparticles (NPs) functionalized with chelating organic ligands as effective sensor platforms for the selective detection and removal of toxic contaminants [29–42]. However, silica NPs often encapsulate or coordinate metal ions within organic ligands, which reduces the fraction of accessible metal active sites. Moreover, the insulating nature of silica and the static characteristics of organic ligands limit electronic modulation. Organic ligands may also introduce background signals or steric hindrance and typically rely on weak, non-specific interactions (e.g., chelation), thereby compromising the selectivity and sensitivity of the sensing process [43]. In our group, S. Venkateswarlu and colleagues have developed a variety of metallic nanoparticle-based catalysts, including Au/C carbon dots, Co_3O_4, ZrO_2, graphene-based composites, metal-organic frameworks (MOFs), covalent organic frameworks (COFs), and carbon dot-based materials. These nanostructures have been employed in electrochemical and photoluminescence sensors for the detection of a broad spectrum of organic molecules such as dopamine, glucose, regorafenib, uric acid, and folic acid, as well as toxic heavy metal ions including Hg^{2+} and Pb^{2+} [44–49]. In our previous work, we also reported the detection of volatile organic compounds (VOCs), including ethylenediamine, diisopropylamine, and dioxane, using environmentally benign carbon onion-based catalysts [50]. Furthermore, we successfully utilized carbon dots as photoluminescent (PL) thermal sensors [51]. More recently, our research has shifted toward the development of next-generation single-atom-based sensors. In particular, we have demonstrated that copper single atoms exhibit excellent electrocatalytic activity for the sensitive and selective detection of dopamine [52]. These findings underscore the promising potential of single-atom catalysts (SACs) in the advancement of high-performance chemical sensing technologies.

Developing effective heterojunctions through heterogeneous systems can significantly enhance the catalytic activity and selectivity towards the VOCs, enabling ultra-low-level detection, selectivity, long-term stability, and green fuel production [53–56]. Owing to their maximum atom efficiency, low energy consumption, unique metal support interface, tunable coordination environments, and well-defined active sites, single atoms (SAs) facilitate effective adsorption and trigger the catalytic conversion of gas molecules, leading to high sensitivity in sensor technologies [57–59]. From the last decade, SAs have opened new avenues in chemical engineering, energy, catalysis, biotechnology, environmental science, and sensor technologies [60–68]. With respect to the applications in sensor-technology, X. Chen et al. investigated the electronic behavior of Sc and Ti SAs decorated on a graphdiyne catalyst for

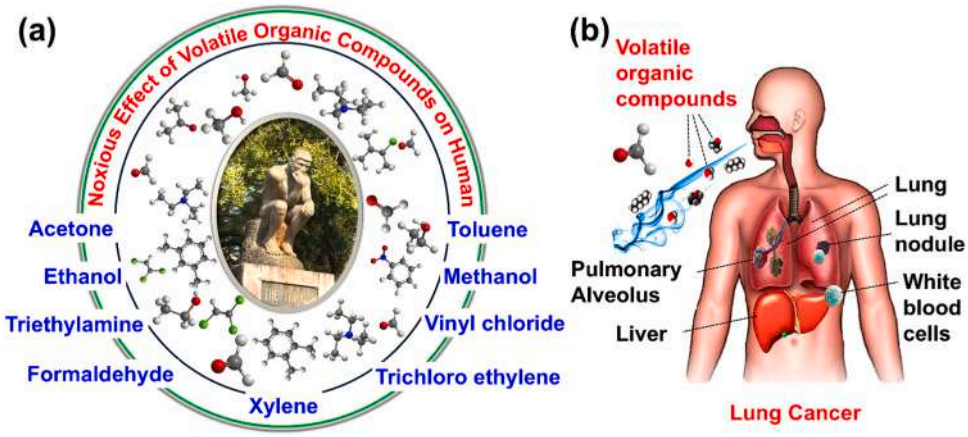

Scheme 1. (a) Schematic representation of various volatile organic compounds (VOCs). (b) Noxious effects on human health such as lung cancer. Reprinted with permission from Ref. [7].

formaldehyde (HCHO) detection in 2017 and summarized the timeline of SAs based on various sensors, including SAES for VOC detection (Fig. 1a, b) [69]. Since then, SAE has been integrated with 1-dimensional (1D), 2-dimensional (2D), and 3-dimensional (3D) metal oxides, selenides, sulfides, metal-organic frameworks (MOFs), and MXenes to generate heterojunctions with abundant active sites such as PtSA@SnO_2, Pt-Vo-W, RhSA@SnO_2, AuSAs@SnO_2, AuSA@In_2O_3, CoSA-CeO_2@SnO_2, CuSAs@$WO_{2.7}$, RuSA@SnS_2, PtSAs@ZnO, PtSA@MXene, and PdSAs@cMOF for the ultra-low detection of VOCs by CGS, MOS, FET, MEMS, and electrochemical techniques [70–74] (Scheme 3c,d).

Based on the increased applications of single atoms, many comprehensive reviews have been reported on SAs-based energy conversion, storage, and environmental applications [75–77]. In addition, few reviews are also focused on single-atom sensor technology related to purification of contaminated gases, biomedical, environmental monitoring, and food safety assays [57,58,68,78,79]. However, to the best of our knowledge, until now no comprehensive reviews have been published on the specific topic of single atom engineered sensors (SAES) for VOC detection (Scheme 2) [78,79]. Hence, we turned our interest to writing an in-depth review on the development and applications of single atom engineered sensors (SAES) for the detection of volatile organic compounds.

This review discusses the impact of coordination environments, heteroatom and defect engineering, as well as other physical parameters in SAES. We also highlight the integration of SAES with various low-dimensional substrates, ranging from 0D to 3D systems. To elucidate the synergetic interactions between SAs and target VOCs, advanced spectroscopic techniques play a key role. In this context, we summarize the characterization of SAES using in situ/operando diffuse reflectance infrared Fourier transform spectroscopy (DRIFTS), Raman spectroscopy, X-ray absorption near edge structures (XANES), and Extended X-ray absorption fine structure (EXAFS). Furthermore, we discuss the application of density functional theory (DFT) for mechanistic insights (Scheme 1d) and the use of advanced ML strategies to accelerate the development of SAES technology for VOC detection. Finally, we summarize current limitations and outline future opportunities for these multidimensional substrates supported by SAES to monitor hazardous VOCs and other environmental pollutants.

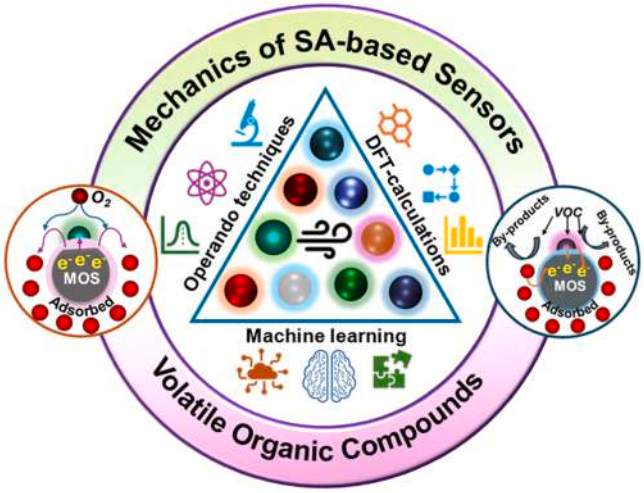

Scheme 2. Graphical representation of the overall concept of the SAs engineered VOCs sensor, operando techniques, DFT studies, and machine learning models.

1.1. Scope of this review and SAES

Despite rapid advancements in single-atom catalysts (SACs) for energy conversion and environmental catalysis, their emerging application in chemical sensing, particularly for the detection of volatile organic compounds (VOCs), remains significantly underexplored and fragmented across isolated studies. VOCs are highly toxic, volatile, and environmentally persistent, posing serious health and ecological risks. Thus, the development of sensitive, selective, and stable detection platforms is of critical importance. Conventional VOC sensors, based on metal oxides, silica nanoparticles, or carbon-based composites, often

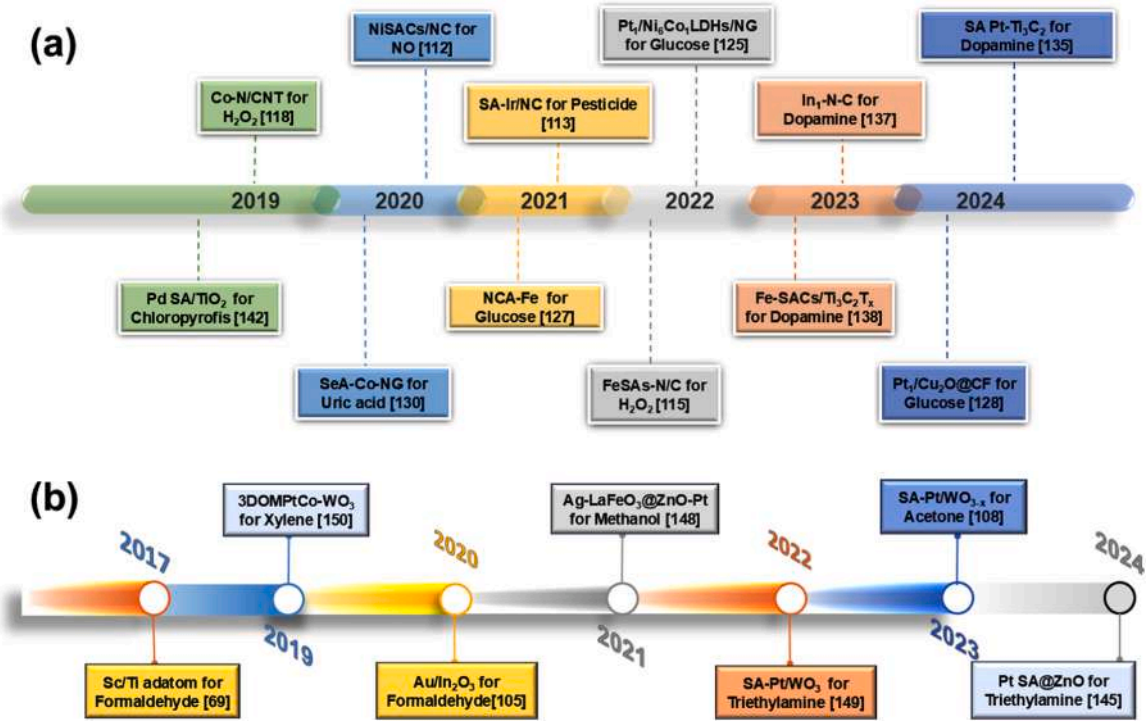

Fig. 1. (a) The timeline of single atom based various sensors. (b) Timeline of single-atom engineered VOCs sensors.

suffer from inherent drawbacks such as high operating temperatures, limited selectivity, and poor long-term stability under real-world conditions (Table 1) [80–87]. In contrast, SACs offer unique advantages, including maximum atomic efficiency, highly tunable coordination environments, and superior selectivity arising from their atomically dispersed active centers and strong metal support interactions. These characteristics position SACs as ideal candidates for next-generation chemical sensors. Although several reviews have comprehensively addressed the catalytic and biomedical applications of SACs, there is currently no focused and critical review that systematically explores their role in VOC detection. Considering the escalating demand for high-performance VOC sensors in indoor air quality monitoring, environmental surveillance, industrial safety, and wearable electronics, this review aims to fill this critical gap. The overall theme of the review is illustrated in (Scheme 3), which presents selected examples highlighting the synthesis of single-atom catalysts (SACs) supported on various morphologies, such as 2D MXene and nitrogen-doped carbon. It also depicts the working models of chemiresistive and electrochemical sensors designed for VOC detection. By consolidating recent progress, identifying existing challenges, and highlighting future opportunities, this work provides a timely and essential resource for advancing SAC-based VOC sensing technologies.

2. Single atom-based sensors

Single atoms in sensor technology have led to significant advancements due to their distinctive characteristics and advantages, including high atomic efficiency and tunable electronic properties. These features enable the development of highly sensitive, selective, and rapid detection sensors. SACs and single atom nanozymes are particularly fascinating for their ability to replicate natural enzymes with enhanced catalytic activity and selectivity [88,89].

Interestingly, SAs play a crucial role in biosensors, electrochemical sensors, and photoelectrochemical sensors, enabling precise detection of biomolecules and environmental analytes, even at ultra-low concentrations. Specifically, single-atom nanozymes have emerged as attractive biosensors due to their efficient atom utilization, enhanced selectivity, and stability, making them suitable for a wide range of biosensing applications. These nanozymes can mimic natural enzymes, which makes them valuable for detecting biological molecules, ions, organisms, and viruses [90]. Similarly, SAES demonstrates improved biomarker detection performance, broadening their applicability across various fields [57,91]. SAs are increasingly recognized as critical components of photoelectrochemical (PEC) sensors, enhancing sensitivity and selectivity. Researchers have developed novel biosensing technologies that utilize SACs to monitor biological substances in complex environments. These sensors, which integrate the unique properties of SAs with advanced PEC systems, deliver unprecedented performance across a wide range of applications [88,92].

2.1. Heteroatom engineering of SAs

Heteroatom engineering of SAs involves the strategic insertion of heteroatoms (atoms other than the principal element in the system) into the structure of SACs [93]. This approach tunes the electrical, structural, and chemical properties of SACs, making them better suited for a variety of applications, including catalysis, energy devices, and sensors such as CGS, MOS, FFT, MEMS, and PEC.

Heteroatoms such as boron (B), nitrogen (N), phosphorous (P), oxygen (O), sulfur (S), and fluorine (F) in the support material or near the single atom influence the local coordination and electronic environment. They modify the charge distribution and d-band center of the metal atom, facilitate more active sites, and improve its catalytic and sensor activity [94]. The following recent developments highlight the importance of heteroatoms in SAE (Fig. 1).

A nitrogen-rich, high-surface conductive metal-organic framework (cMOF) has been employed as an effective single-atom support via a unique electrochemical deposition method (Fig. 2a). The generated Pd SAs are stabilized in a PdN_4 coordination by interplanar sites in the cMOF while preserving the porosity of the catalyst. This PdN_4 moiety, with its preserved porosity, enables high selectivity and sensitivity to the target gas analyte [95]. Another interesting approach involves the design of dual heteroatoms that have SACs, a guest B heteroatom is doped alongside the nitrogen moiety via a one-pot pyrolysis process (Fig. 2b). This method effectively tunes charge transfer and modulates the electronic structure of Fe atoms by generating various FeBNC coordination models, which lower the energy barrier and enhance the peroxide-like activity of single atom nanozymes [96].

Similarly, a chemical etching coordination approach has been developed to enable the direct coordination of Fe-SAs with N and S heteroatoms (Fig. 2c). The coordination of the low electronegative S atom can tune the 3D orbital of Fe-SAs electronic structure and activate catalytic sites for more effective reaction [97]. Meanwhile, the two-dimensional graphitic carbon nitride (gCN) creates a stable coordination network with N moiety, which prevents the agglomeration of Pt SAs (4.3 wt%) even at elevated temperatures and provides more active sites, as shown in the STEM image (Fig. 2d) [72]. Beyond mono-and di-heteroatom strategies, H. Zhou et al. expanded single-atom engineering to include tri-heteroatom coordination. They developed an Mn-based single-atom porous carbon frame catalyst coordinated with N, S, and P (Fig. 2e). The incorporation of multiple heteroatoms introduces additional lone pairs of electrons, which stabilize Mn SAs. Advantageously, the high selectivity is attributed to the presence of multi-hierarchical pores in the as prepared Mn SACs [98].

In SAE, the use of environmentally benign heteroatoms, such as boron (B), in combination with biopolymers as nitrogen (N) atom

Table 1
Comparison of SACs, metal oxide nanoparticles, and organic ligand-chelated silica nanoparticles in sensor applications.

S. No	Parameter	Metal Oxide Nanoparticles (MONPs)	Organic Ligand-Chelated Silica NPs	Single-Atom Catalysts (SACs)	SAC Advantage	Ref
1	Metal atom utilization	Low-to-moderate (bulk or surface-bound)	Partial (due to buried/ chelating ligands)	100 % (all atoms are active sites)	Maximum atom efficiency	[80]
2	Conductivity	Generally low (e.g., TiO_2, ZnO), may need conductive additives	Insulating silica core	High (with conductive supports: MXene, graphene)	Faster electron transfer	[81]
3	Chemical stability	High thermal and chemical stability	Moderate (ligands degrade in pH/UV)	Excellent (strong metal–support anchoring)	Tuned coordination gives both stability and selectivity	[82]
4	Selectivity	Moderate, depends on surface defect chemistry	Ligand-specific, often not robust	Tunable via atom type and coordination (e.g., Co–N)	Designer active sites enhance target recognition	[83, 84]
5	Detection limit	Moderate-to-low (affected by agglomeration and surface activity)	Moderate (ligand–analyte dependent)	Ultra-low (ppb to ppt)	Trace-level sensitivity due to unique adsorption	[85]
6	Harsh environment compatibility	Stable, but may suffer surface passivation	Weak (ligands degrade easily)	Stable in acidic, basic, ionic, oxidative media	Strong anchoring and inert supports resist deactivation	[86]
7	Multifunctionality	Redox-active, photocatalysis possible	Limited to ligand type (e. g., fluorescence)	Sensing, catalysis, and remediation	Versatile integration with other functions	[87]

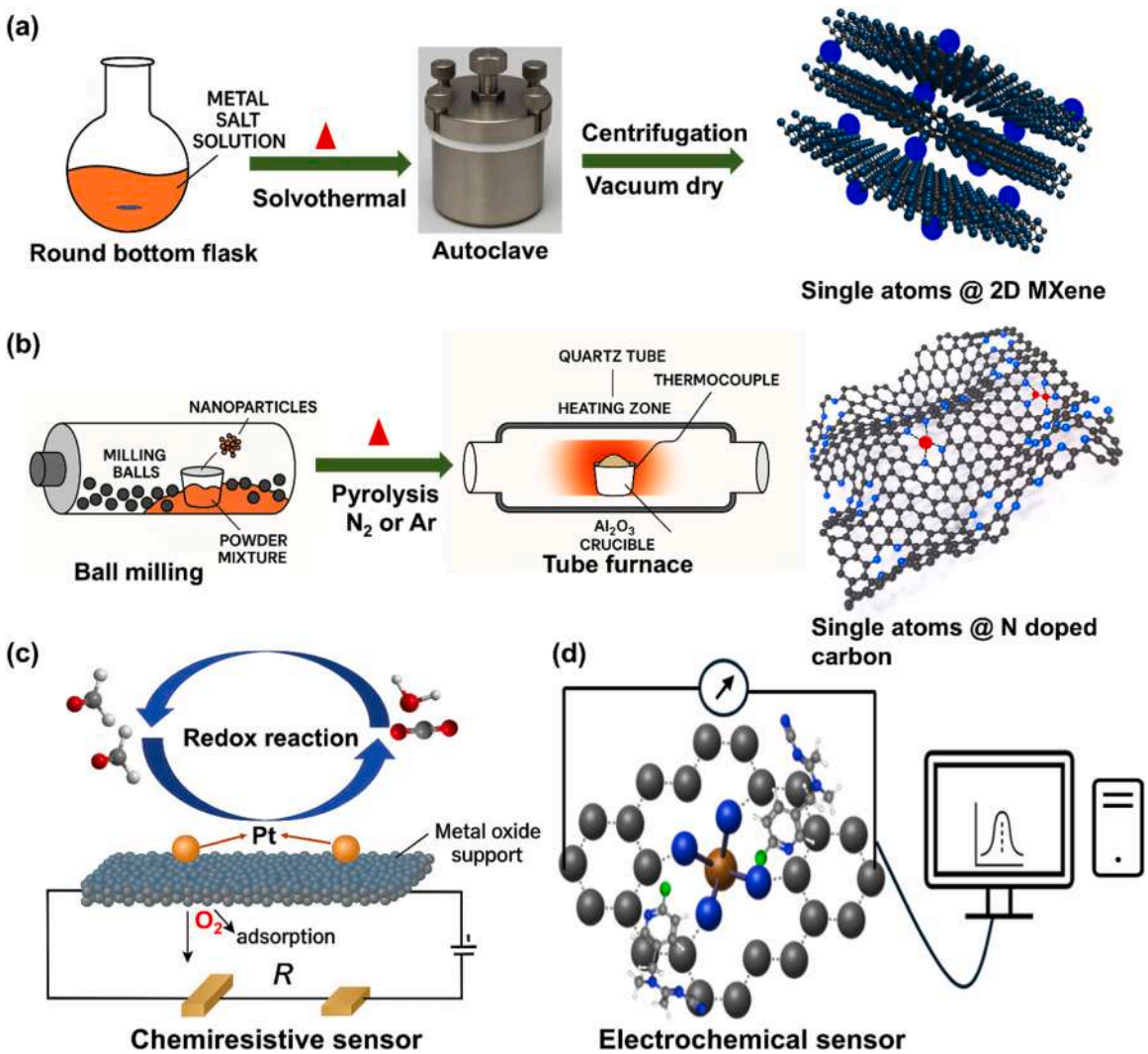

Scheme 3. (a, b) Schematic illustrations of the synthesis of SACs via different methods and morphologies, including solvothermal and pyrolysis techniques. (c, d) Schematic representations of chemiresistive and electrochemical sensor models for VOC detection.

precursors, is an intriguing approach for developing eco-friendly single-atom catalysts. To design a high surface area hierarchical porous single-atom network, C. Xu et al. utilized boric acid and chitosan as B and N heteroatom sources. They synthesized B and N coordinated, high-loading Co SAs (4.2 wt%) within a hierarchical porous carbon framework via a one-pot pyrolysis strategy (Fig. 2f). Interestingly, at high temperatures, the formation of boron oxide prevents Co agglomeration, allowing for the uniform dispersion of isolated SAs with Co-N-B-C coordination. This also generates effective active sites for efficient electrochemical reactions [99].

The above SAE coordination strategies illustrate the significance of heteroatoms in preventing aggregation and leaching. Heteroatoms provide anchoring sites for SAs (such as N and S dopants in carbon supports), thereby stabilizing them and increasing the resilience of SACs under operating conditions [100]. Specific heteroatoms can synergize with SAs, enhancing reactant adsorption and reducing activation energy. Additionally, they may introduce defects that serve as additional active sites. By strategically manipulating the type and position of heteroatoms, SACs can be tailored to preferentially interact with specific reactants, thereby improving selectivity in sensor technology [101].

2.2. Defect engineering in single atom-based sensors

Defect engineering of SAs involves the deliberate introduction or manipulation of atomic-level flaws in materials to stabilize or modify the properties of individual atoms. This emerging field is essential for advancing applications in catalysis, energy storage, and sensor technology [102]. Defect engineering includes creating and altering vacancies, as well as managing defects and grain boundaries in host materials such as carbon substrates, MXene, and metal oxides. For SAs, defect sites act as anchor points, stabilizing individual atoms or clusters on the substrate. Due to their high surface energy, SAs tend to agglomerate into larger clusters. Defects help to prevent agglomeration by creating high-energy sites that enhance interactions with the SAs and thus between the target molecules and the active sensing sites of the sensor material [103]. Various synthesis techniques, including plasma treatment, chemical etching, thermal annealing, and ultraviolet (UV)

irradiation [104], can create different types of defects, such as vacancy, substitutional, topological, strain-induced, and surface defects, all of which effectively increase the sensing properties (Fig. 3). On the other hand, metal oxide semiconductors for gas sensing have their practical application often limited by poor sensitivity, low selectivity, and high operating temperature requirements. Single atom engineering (SAE) presents a promising approach to overcome these challenges by enhancing the stability, selectivity, and sensitivity of metal oxide semiconductor gas sensors. By introducing SAs at defects or vacant sites in extremely low concentrations, activation energy and operating temperatures can be significantly reduced. This approach also provides

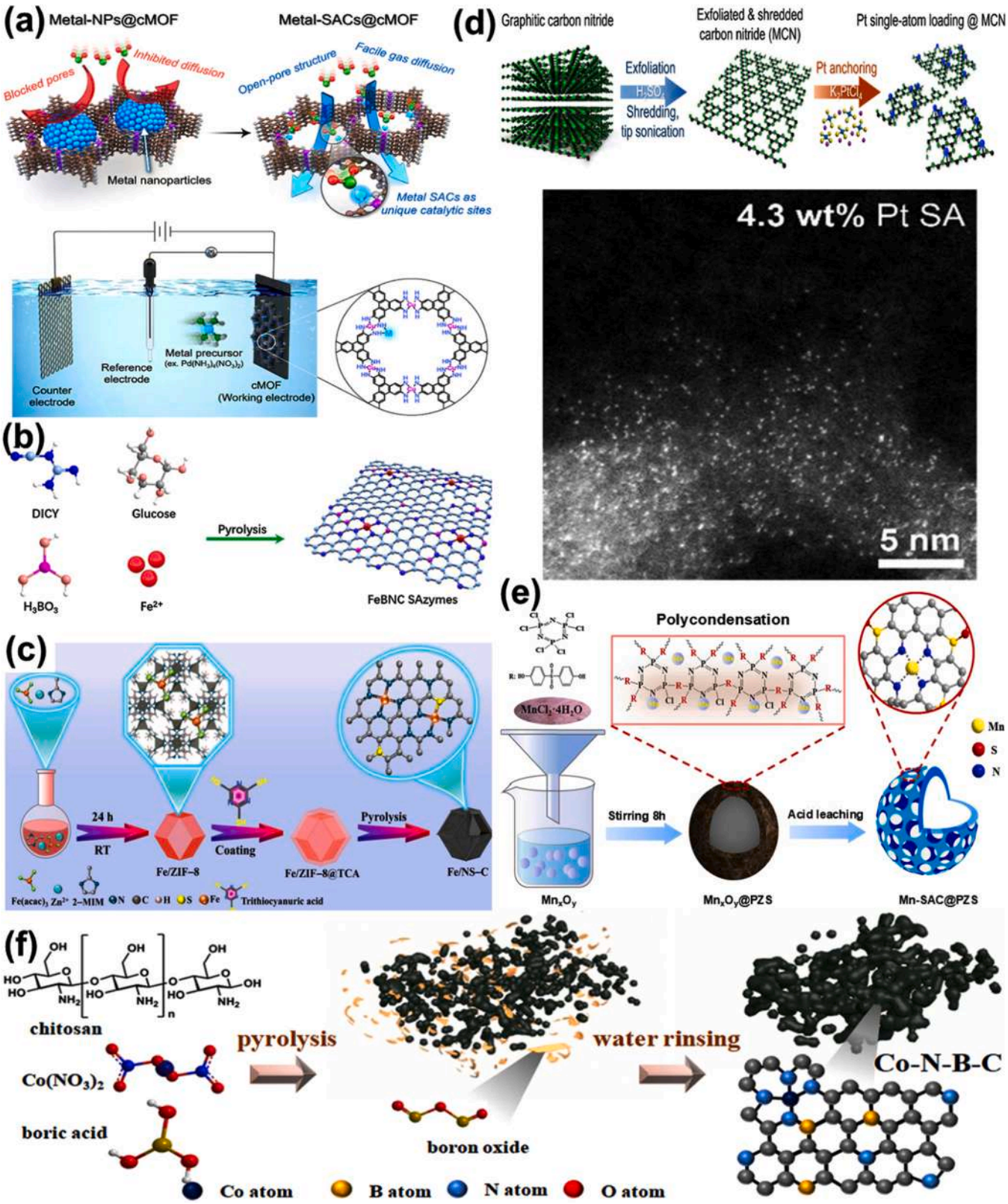

Fig. 2. Heteroatom- coordinated single atoms (Cu, Fe, Pt, Mn, and Co) on various substrates. (a) N moiety conductive metal-organic frameworks. Reprinted with permission from Ref. [95]. (b) B, N moiety carbon frame. Reprinted with permission from Ref. [96]. (c) N, S moiety carbon frame. Reprinted with permission from Ref. [97]. (d) N moiety graphitic carbon structure and STEM image of Pt SAs. Reprinted with permission from Ref. [72]. (e) N, S moiety porous carbon frame. Reprinted with permission from Ref. [98]. (f) B, N moiety has porous carbon frame Reprinted with permission from Ref. [99].

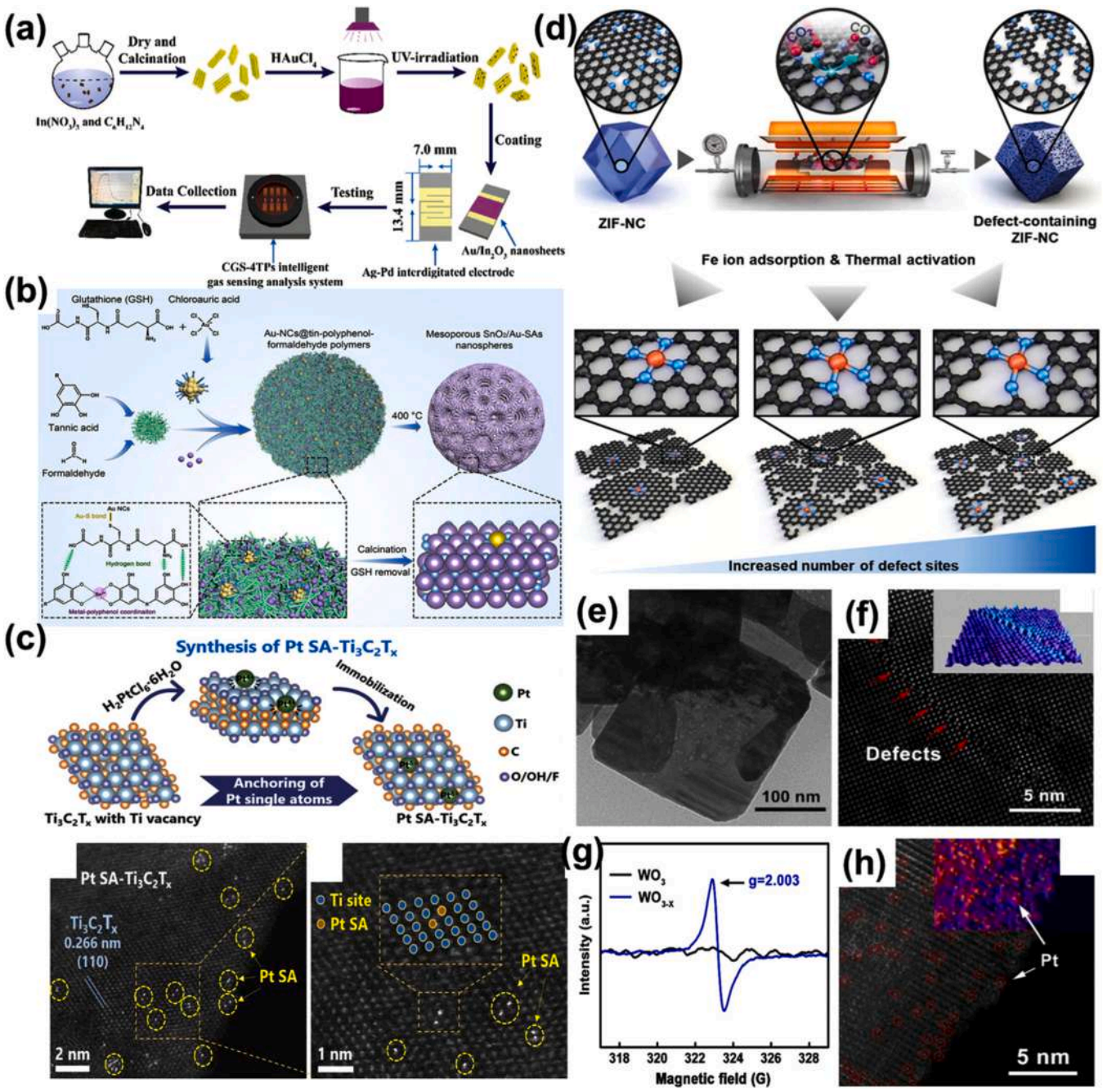

Fig. 3. Defect engineering anchored various SAs. (a, b) defect sites metal oxide nanoparticles anchored SAs Reprinted with permission from Ref. [105, 106]. (c) Pt SAs onto Ti vacancy positions of $Ti_3C_2T_x$ (MXene) substrate and HAADF-STEM images. Reprinted with permission from Ref. [70]. (d) Defect site carbon substrate anchored Fe SAs. Reprinted with permission from Ref. [107]. (e-h) TEM and HAADF STEM images and EPR spectra of WO_3 nanoplate with oxygen vacancy defects can effectively accommodate Pt SAs. Reprinted with permission from Ref. [108].

abundant active sites with high atom efficiency, enabling ultra-low-level detection of target analytes. For instance, a novel UV light reduction method has been employed to dope In_2O_3 with a trace amount of Au SAs, significantly enhancing its sensing performance (Fig. 3a) [105]. In the Au SAs@In_2O_3 MOS sensor, Au SAs extract electrons from In_2O_3, triggering an electron transfer phenomenon that enhances the performance of the MOS gas sensor. Similarly, introducing Au SAs into the interstitial sites of porous SnO_2 with lattice deffects prevents their agglomeration while forming Au-O-Sn bonds, which provide additional active sites [106].

The Au-embedded porous SnO_2 improves sensing performance through both chemical and electric sensitization effects (Fig. 3b). These defect engineering strategies effectively facilitate the fabrication of SAs metal oxide semiconductor gas sensors, enabling highly sensitive detection at lower working temperatures. B. Zong et al. successfully anchored Pt SAs onto Ti vacancy positions of $Ti_3C_2T_x$ (MXene) substrate using a self-reduction immobilization method, which has been confirmed in HAADF-STEM images (Fig. 3c) [70]. The PtSAs@$Ti_3C_2T_x$ structure enhances chemical sensitization and gas adsorption, allowing for rapid detection of target gas molecules with high sensitivity. Another intriguing defect engineering approach involves tuning defect sites in a carbon substrate using a CO_2 activation strategy (Fig. 3d) [107]. This method modulates the oxidation and spin states of Fe single atom centers, altering the electronic configuration of Fe-NC SAs and enhancing

their intrinsic catalytic activity. The role of defect engineering in single-atom growth is clearly emphasized by T. Yuan et al. In their study, they used WO_3 nanoplates as a substrate with and without oxygen vacancy defects. Fig. 3e and f display the TEM and AC-HAADF STEM images of WO_3 nanoplates with high oxygen vacancy defects, while the inset 3D image provides a clear visualization of the defect-engineered WO_3 nanoplate. Furthermore, the presence of oxygen vacancy defects in WO_3 nanoplate was confirmed by EPR spectra ($g = 2.003$) (Fig. 3g). Their findings revealed that while pure WO_3 tends to form nanoparticles, WO_3 nanoplates with oxygen vacancy defects can effectively accommodate Pt SAs, which are resistant against agglomeration (Fig. 3h). The presence of Pt SAs enhances the adsorption and lowers the reaction activation energy. The PtSAs@WO_3 sensor demonstrated exceptional selectivity ($S_{best}/S_{second} = 2.8$) and a detection limit as low as 0.1 ppm for VOC detection [108].

Precise defect management plays a crucial role in controlling a material's electronic structure, thereby enhancing the sensitivity of sensors to specific analytes. Materials with a high density of defects exhibit increased surface reactivity and faster charge transfer kinetics [109]. The advantages of defect-engineered SAs in sensing applications include high sensitivity and selectivity, lower detection limits, improved stability in challenging environments, and enhanced flexibility for detecting a wide range of analytes.

2.3. Other physical parameters

The physical characteristics of SAs in sensors play a crucial role in enhancing measurement sensitivity and precision. Recent advancements in quantum sensing and electrochemical applications have highlighted the unique properties of SAs, including their high activity at low mass content, strong interactions, and exceptional ability to detect minute forces and fields. Key aspects of SAES include force sensitivity, electric and magnetic field sensing, and material properties. The force sensitivity of SA sensors, particularly those using trapped ions, can reach sub-attonewton levels. These measurements involve super-resolution imaging, which enables precise three-dimensional displacement detection [110]. Quantum sensors composed of SAs can monitor electric and magnetic fields at the atomic scale, facilitating the study of spin textures and interactions in quantum materials [111]. Additionally, single-atom materials have demonstrated enhanced electrochemical sensing capabilities, including improved sensitivity, selectivity, and stability. The careful design of these materials is crucial for optimizing their sensing performance, making them suitable for a wide range of applications.

3. Design of single atom-based sensors for the detection of VOCs

Accurate detection of VOCs is essential for ecological safety, healthcare, and disaster management, such as locating victims through VOCs emitted during human decomposition. Traditional detection methods, though highly accurate, rely on large and bulky laboratory instruments, making them unsuitable for on-site or real time applications. To address these limitations, portable alternatives, such as electronic noses (e-noses), have been developed. These devices attempt to mimic the mammalian olfactory systems using multi-sensor arrays that integrate optical, acoustic, semiconductive polymer, and electrochemical sensing technologies. However, despite their portability, e-noses often suffer from limited specificity, which hinders their particle deployment in complex environments. Several commonly used sensor technologies, MOS sensors, conducting polymer (CP) sensors, surface acoustic wave (SAW) sensors, and quartz crystal microbalance (QCM) sensors, operate through distinct mechanisms and offer unique advantages and limitations. MOS sensors, which function via a chemiresistive mechanism, are cost-effective and sensitive but typically exhibit poor selectivity and diminished performance in the presence of complex gas mixtures. CP sensors are capable of room-temperature operation and demonstrate high sensitivity, yet they are susceptible to environmental instability, particularly under varying humidity levels. SAW sensors, while offering high sensitivity and compact design, face issues with temperature fluctuations and material degradation. QCM sensors detect changes in mass with high precision but require advancements in material stability to achieve commercial viability. In addition, photoionization detectors (PIDs) and electrochemical sensors are also key technologies for VOC detection. PIDs offer broad-spectrum detection capabilities but suffer from poor selectivity. EC sensors, which rely on redox reactions facilitated by catalytic materials such as various inorganic nanoparticles, are relatively selective but can face challenges such as baseline drift and cross-sensitivity to other gases.

To address the limitations of conventional sensors, SACs have emerged as a promising advancement (Table 2) [112–143]. SACs significantly enhance sensor performance due to their unique catalytic properties, which improve both sensitivity and selectivity. When anchored onto MOS surfaces, SAs facilitate efficient electron transfer, thereby optimizing sensor responsiveness and accuracy. This innovation highlights the potential of SACs to address the inherent challenges associated with traditional sensing materials.

This review explores the fundamental principles of SAC-based VOC sensors, including their sensing mechanisms, integration with various substrates, and applications in advanced sensing platforms such as chemiresistive, electrochemical, FETs, and MEMS. The integration of SACs into these platforms offers the way for the development of highly sensitive, selective, and portable VOC detection systems suitable for real-world applications.

3.1. Working principle and significance of SAE VOCs sensor

Chemiresistive sensors represent a versatile and widely adopted class of devices for VOC detection, primarily leveraging electron transfer mechanisms during gas sensor interactions. Their popularity stems from advantages such as low power consumption, high sensitivity, and compatibility with advanced nanomaterials. The progression of chemiresistive sensor technology has been significantly driven by advances in material science and nanotechnology, resulting in improved selectivity, sensitivity, and operational stability.

Traditional chemiresistive sensors typically operate through the catalytic activity of sensing materials, wherein adsorbed gas molecules undergo oxidation or reduction reactions, leading to measurable changes in electrical signals. For example, metal oxide-based (MOX) chemiresistive sensors detect resistance changes upon gas adsorption and are classified as n-type or p-type, depending on the dominant charge carriers. Similarly, CP-based sensors, such as those using polyaniline or polypyrrole, exploit reversible electronic or structural changes in response to VOC exposure. Despite their effectiveness, these conventional systems often suffer from limitations, including high operating temperatures, cross-sensitivity to other gases, and long-term performance degradation. To address these challenges, hybrid sensor architectures have emerged as promising alternatives. These designs integrate MOX materials with porous frameworks such as carbon allotropes, boron nitride nanotubes, and MOFs, and 2D materials like transition metal carbides (MXenes) and chalcogenides. By combining the complementary properties of these components, such hybrid systems enhance gas adsorption capacity, promote efficient electron transfer, and improve operational robustness under varying humidity and temperature conditions.

Among these advancements, SAs embedded in MOX, porous carbon frameworks, or MOFs have significantly improved sensor selectivity and stability. These systems enable rapid and precise detection of specific VOCs. The enhancement arises from the unique characteristics of single-atom active sites, which provide exceptionally high surface-to-volume ratios, tunable electronic structures, and superior catalytic activity. The evolution of VOC sensors, propelled by advances in material science and nanotechnology, has enabled the development of efficient, selective, and reliable VOC detection mechanisms. The integration of SACs

Table 2
Summary table of various SAC-based catalytic sensors for detecting multiple analytes.

S.No.	Category	Analyte	Catalyst	Detection Limit	Linear range	Ref
1.	Electrochemical sensor	NO	Ni SACs/N-C	1.8×10^3μM	~1.3 μM	[112]
2.	Electrochemical sensor	OPs	SA-Ir/NC	0.17 ng ML^{-1}	0.5–500 ng ML^{-1}	[113]
3.	Electrochemical sensor	H_2O_2	Fe-SASC/NW	46.35×10^{-9} m	5.0×10^{-10} m to 0.5 m	[114]
4.	Electrochemical sensor	H_2O_2	FeSAs-N/C	0.34 μM	764–9664 μM	[115]
5.	Electrochemical sensor	H_2O_2	Fe_3C@C/Fe-N-C	0.26 μM	1–6000 μM	[116]
6.	Electrochemical sensor	H_2O_2	Co-N-C−800	0.13 μM	0.3–1 × 10^4 μM	[117]
7.	Electrochemical sensor	H_2O_2	Co-N/CNT	0.0324 μM	0.05–5 × 10^4 μM	[118]
8.	Electrochemical sensor	As(III)	Co SAC	0.02 ppb	0.1–3 ppb	[119]
9.	Electrochemical sensor	As(III)	Pt_1/MoS_2	0.05 ppb	0.5–8 ppb	[120]
10.	Electrochemical sensor	As(III)	FeN_3P	0.01 ppb	0.5–8 ppb	[121]
11.	Electrochemical sensor	Pb(II)	Mn/g-C_3N_4	0.01 μM	0.1–0.8 μM	[122]
12.	Electrochemical sensor	HQ	Mo SAs/NPO-C	0.005 μM	0.02–200 μM	[123]
13.	Electrochemical sensor	Nitrobenzene	Nb-BNC	0.70 μM	2–100 μM 100–600 μM	[124]
14.	Electrochemical biosensor	Glucose	Pt_1/Ni_6Co_1LDHs/NG	10 μM	10–2180 μM	[125]
15.	Electrochemical biosensor	Glucose	NCA-Co	0.1 μM	0.5–1000 μM	[126]
16.	Electrochemical biosensor	Glucose	NCA-Fe	0.5 μM	2–2000 μM	[127]
17.	Electrochemical biosensor	Glucose	Pt_1/Cu_2O@CF	1 μM	2–560 μM	[128]
18.	Electrochemical biosensor	L-dopa	PtHPCN−222	0.003 μM	0.1–1 μM	[129]
19.	Electrochemical biosensor	Uric Acid	A-Co-NG	0.0333 μM	0.4–1055 μM	[130]
20.	Electrochemical biosensor	Uric Acid	Ru_3/NC	0.01 μM	0.05–1000 μM	[131]
21.	Electrochemical biosensor	Uric acid	Fe-N_5	27 μM	0.01–480 μM	[132]
22.	Electrochemical biosensor	Uric acid	Co-N-C/rGA	3.59 μM	4–300 μM	[133]
23	Electrochemical biosensor	Uric Acid	Ru-Ala-C_3N_4	170 μM	0.5–2135 μM	[134]
24.	Electrochemical biosensor	Uric Acid	SA Pt-Ti_3C_2	0.0125 μM	3.5–5.8 μM	[135]
25.	Electrochemical biosensor	Dopamine	Ni-MoS_2	1×10^{-6} μM	1 × 10–6–1000 μM	[136]
26.	Electrochemical biosensor	Dopamine	SA Pt-Ti_3C_2	0.0022 μM	4.3–5.7 μM	[135]
27.	Electrochemical biosensor	Dopamine	Fe-N_5	7×10^{-6} μM	0.005–500 μM	[132]
28.	Electrochemical biosensor	Dopamine	In_1-N-C	0.279 μM	0–500 μM	[137]
29.	Electrochemical biosensor	Dopamine	Co-N-C/rGA	0.32 μM	2–80 μM	[133]
30.	Electrochemical biosensor	Dopamine	Fe-SACs/$Ti_3C_2T_x$	0.001 μM	0.01–200 μM	[138]
31.	Electrochemical biosensor	Dopamine	Mn-MoS_2/PGS	5×10^{-5} μM	5 × 10–5–50 μM	[139]
32.	Electrochemical biosensor	Dopamine	Co-N-C SANs	0.04 μM	0.06–1200 μM	[117]
33.	Electrochemical biosensor	Dopamine	Ru-Ala-C_3N_4	20 nM	0.06–490 μM	[134]
34.	Electrochemical biosensor	Homo-vanillic acid	Fe-SACs/$Ti_3C_2T_x$	0.01 μM	0.02–200 μM	[138]
35.	Electrochemical biosensor	Vanillylmandelic acid	FeSACs/$Ti_3C_2T_x$	0.005 μM	0.01–200 μM	[138]
36.	Electrochemical biosensor	Ascorbic acid	Rh SAzymes	0.26 μM	10.0–53, 100 μM	[140]
37.	Electrochemical biosensor	Furazolidone	Pd_1/NC	0.0333 μM	0.01–50, 50–300 μM	[141]
38.	Photoelectrochemical sensor	Chlorpyrifos	Pd SA/TiO_2	0.01 ng/ML	0.03 ng/ML to 10 μg/ML	[142]
39.	Photoelectrochemical sensor	Prostate-specific antigen	SA Pt anchored $Zn_{0.5}Cd_{0.5}S$	0.22 pg/ML	1.0–10000 pg/ML	[143]

Abbreviations: OPs: Organophosphorus pesticides, HQ: hydroquinone

within MOX, porous materials, and 2D metal carbides as well as chalcogenides exemplifies the potential of hybrid approaches in revolutionizing sensor design. These strategies effectively address key challenges such as cross-sensitivity, high operating temperatures, and long-term stability [71–73]. As a result, VOC sensors are emerging as indispensable tools for environmental monitoring, healthcare diagnostics, and the development of next-generation portable technologies (Scheme 3c, d).

3.2. Metal oxide semiconductor-based SAE sensors

3.2.1. 1D material-supported SAE sensors

One-dimensional (1D) materials, such as nanotubes and nanowires, offer exceptional platforms for supporting SAs due to their high surface area, excellent conductivity, and mechanical flexibility. Anchoring SAs onto 1D materials enables the creation of hybrid sensors with enhanced charge transport properties and increased active sites for VOC interactions. This synergy makes 1D-supported SA sensors ideal for applications requiring high sensitivity and flexibility, such as wearable electronics. By optimizing SA placement on 1D structures, these sensors achieve rapid response times and robust performance.

Initial studies primarily focused on SACs supported by MOXs. MOX materials offer a broad set of features that make them ideal for SAES. Their high surface area, intrinsic oxygen vacancies, and ability to stabilize SAs via strong metal-support interactions provide a stable platform for supporting SAs. Moreover, MOXs can exhibit excellent electronic conductivity, thermal stability, and environmental durability, which are critical for long-term sensor performance. These materials also modulate the electronic structure of the anchored SAs, thereby fine-tuning their reactivity and selectivity toward specific analytes. The synergy between MOXs and SAs in sensor applications arises from their complementary roles. While SACs provide atomically dispersed active sites with high catalytic efficiency, MOXs serve as a dynamic interface for analyte adsorption, charge transfer, and reaction activation. For instance, the presence of surface oxygen vacancies in MOXs enhances their adsorption capability for gas molecules, facilitating electron transfer processes that are crucial for sensor response. Furthermore, the combination of SAs with MOXs enables the design of sensors with low detection limits, fast response times, and excellent resistance to interference, even under complex environmental conditions [68]. Various synthetic approaches have been employed to prepare 1D MOX supports, including the use of composites where MOXs are decorated or co-impregnated with SAs on nanotubes, polymer-derived nitrogen-doped carbon, and methods to fabricate metal oxide nanowires.

For instance, incorporating WO_3 into Pt/BN catalysts significantly enhances propane oxidation performance by introducing new active sites at the Pt-WO_3 interface [144]. These interfacial sites create a synergistic environment where propane (C_3H_8) adsorption and C-H bond activation are facilitated. The reaction mechanism is governed by the interaction between C_3H_8 adsorbed on Pt and surface hydroxyl groups on WO_x, which accelerates the rate-determining step and C-H bond cleavage. The Pt-WO_3 interface modifies the electronic structure of the

Pt species and introduces novel active sites. This interaction alters the reducibility and surface acidity of the catalyst, which directly impacts C_3H_8 adsorption and activation. Specifically, the WO_3 sites adjacent to Pt provide hydroxyl groups that participate in the oxidation reaction, enhancing the cleavage of C-H bonds and facilitating the subsequent oxidation steps. The promotional effect of WO_3 is evident from the significantly higher intrinsic activity of Pt-7 W/BN (7 wt% of W) compared to Pt/BN. The apparent activation energy (E_a) for the WO_3 -containing catalyst is reduced, suggesting an alternate reaction pathway. The reaction orders of C_3H_8 (~1) and oxygen (negative) underscore the importance of oxygen coverage on the Pt surface, which is modulated by the WO_3. Reduced oxygen inhibition on the Pt-7 W/BN catalyst indicates that the Pt-WO_3 interface mitigates excessive oxygen adsorption, thereby enhancing C_3H_8 activation. XPS analysis reveals that metallic Pt species alone are insufficient to account for the observed activity, highlighting the dominant role of $Pt^{\delta+}$ species at the Pt-WO_3 interface [144]. The interplay between enhanced C_3H_8 activation, increased reducibility, surface acidity, and stable active sites contributes to the overall promotional effects. These results underscore the potential of MOX-promoted catalysts for efficient light alkane oxidation.

A notable example reported by Shin et al. involved polymer-derived nitrogen-doped carbon, where Pt SAs were impregnated onto SnO_2 nanowires using a melamine-based sacrificial carbon nitride (MCN) template [72]. Electrospinning was employed to form nanofibers, which were subsequently converted into a tubular structure. The post-calcination ensured uniform Pt dispersion within the SnO_2 lattice. XPS analysis confirmed the presence of Pt^{4+}, validating the successful incorporation of Pt SAs.

The sensing performance of the designed SA-based sensor for formaldehyde (HCHO) was systematically evaluated and compared against

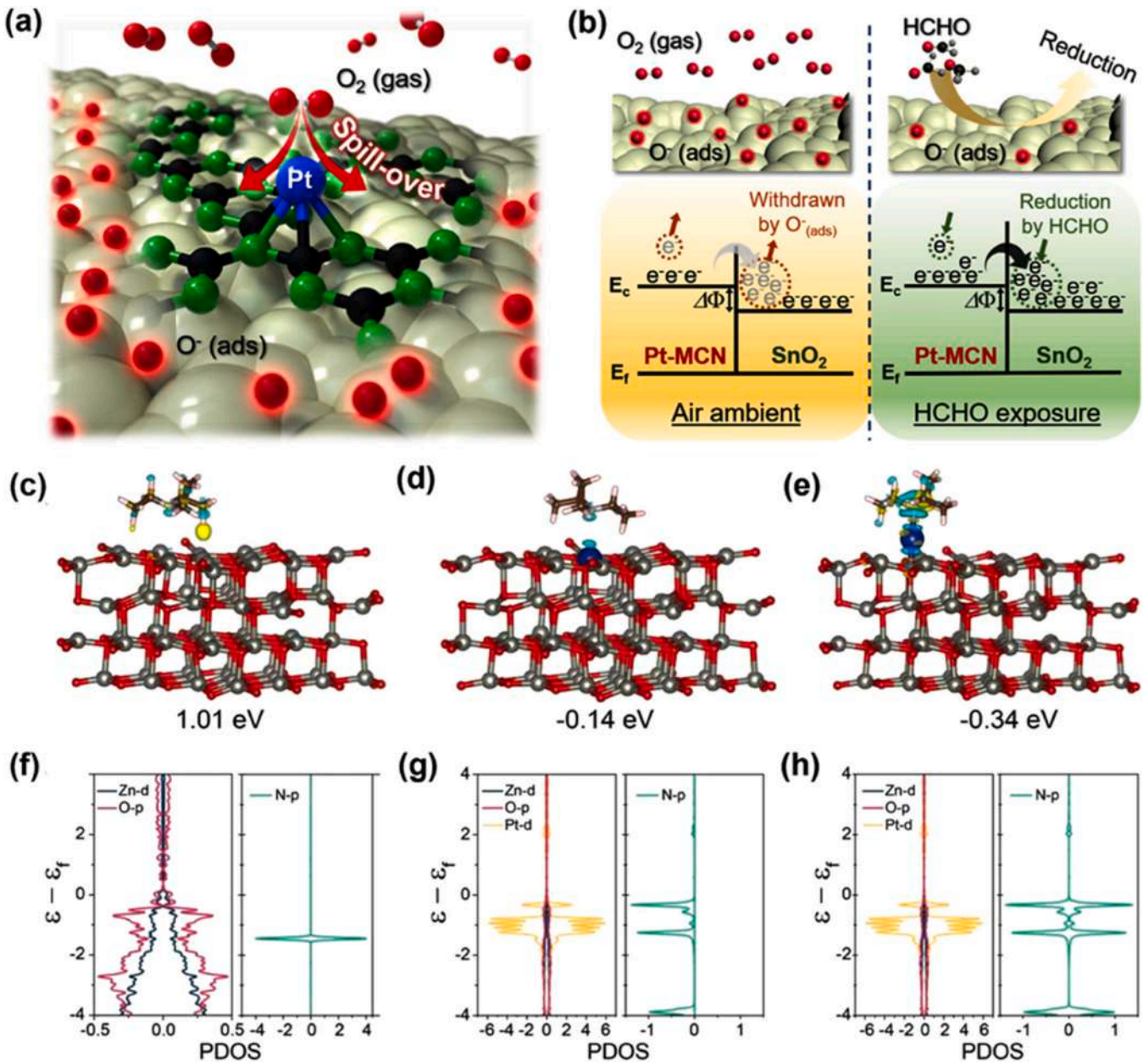

Fig. 4. (a) Schematic of O_2 dissociation on Pt SAs@Pt-MCN-SnO_2 with chemisorbed O^-(ads). (b) HCHO-sensing mechanism and MCN/SnO_2 heterojunction band diagram Reprinted with permission from Ref. [72]. Optimized geometries of TEA adsorption on (c) Pt@ZnO with an oxygen vacancy. (d) Pt@ZnO with Zn substitution by Pt, and (e) Pt SAs on ZnO near an oxygen vacancy. (f–h) Corresponding DFT-calculated band structures and DOS Reprinted with permission from Ref. [145].

Pt-doped SnO_2 nanofibers (Pt-SnO_2), MCN-SnO_2 without Pt, and pristine SnO_2. The SA-based sensor exhibited 2.2-fold and 1.4-fold higher responses than pristine SnO_2 and MNC-SnO_2, respectively, owing to enhanced catalytic activity and heterojunction formation. Among these, Pt-MCN-SnO_2 demonstrated the best performance, with a response (R_{air}/R_{gas}) of 33.9 at 5 ppm HCHO. This enhancement was attributed to synergistic effects, including the maximized atomic efficiency of Pt, heterojunctions between MCN and SnO_2, and morphological optimization. Mechanistically, the Pt-N/C active site enhances O_2 adsorption

and dissociation (Fig. 4a), evidenced by an adsorption energy of −1.93 eV and an elongated O−O bond compared to bulk Pt. This increases the concentration of chemisorbed oxygen species, facilitating HCHO adsorption and reaction. Electron transfer from Pt-MCN to SnO_2 reduces the work function (from 4.48 eV to 4.38 eV) and forms electron accumulation layers, amplifying resistance variations upon HCHO exposure (Fig. 4b). The increased baseline resistance of the sensor was supported by XPS data showing a higher O^-/O^{2-} ratio (71.4 %) in Pt-MCN-SnO_2 compared to pristine SnO_2 (46.7 %).

Experimental validation of the PtNP-MCN-SnO_2 material confirmed the superior performance of atomically dispersed Pt, attributed to enhanced active site exposure and suppressed agglomeration. Furthermore, Pt-MCN-SnO_2 exhibited exceptional stability, maintaining atomically dispersed Pt after 170 h of operation at 275°C. The material showed only a 7.1 % decrease in HCHO response after two months of storage, compared to 30.0 % for Pt-SnO_2 and 54.1 % for pristine SnO_2. This stability was ascribed to dual stabilization provided by MCN and SnO_2 nanograins, which prevented Pt migration and aggregation. These findings highlight the potential of N-doped carbon and MOX-supported SACs for high-performance, durable gas sensors, offering scalable synthesis and tunable selectivity for diverse VOCs applications.

Next, Pt SAs supported on ZnO nanorods were synthesized via a hydrothermal method for triethylamine (TEA) detection [145]. Notably, the Pt@ZnO sensor achieved an ultra-high response value of 4170 at 200 °C, with rapid response and recovery times of 34 and 76 s, respectively, and a low detection limit of 7.5 ppb. The enhanced sensitivity and specificity of SACs stem from their atomic dispersion, which maximizes active sites for gas interaction. In Pt@ZnO sensors, surface oxygen vacancies play a critical role in activating adsorbed oxygen species such as O^- and O_2. These species facilitate oxidative reaction with TEA, as TEA molecules are adsorbed and chemically activated through interactions with Pt SAs, particularly via bonding with nitrogen atoms. This activation lowers the energy barrier for TEA oxidation, resulting in products like CO_2, H_2O, and NO_2, which desorb efficiently, ensuring sensor repeatability and long-term stability. Moreover, Pt incorporation alters

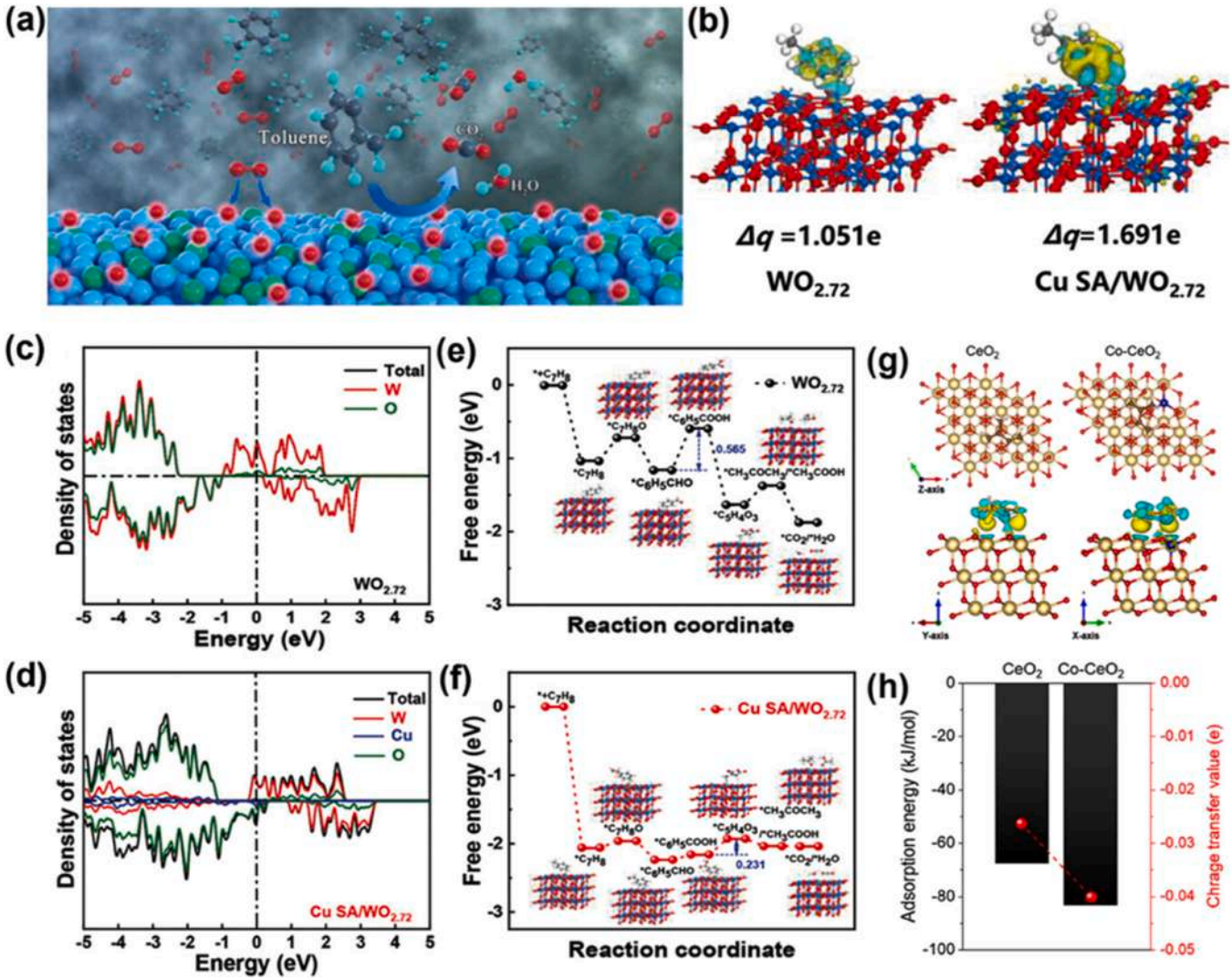

Fig. 5. (a) Schematic of the toluene sensing mechanism on the Cu SA/WO2.72 sensor. (b, c) DOS of pristine WO2.72 and Cu SA/WO2.72₂. (d) Differential charge density and Bader charge (Δq) of toluene adsorption on both samples. (e, f) Energy pathways for toluene oxidation to CO2 and H₂O on pristine WO2.72 and Cu SA/WO2.72. Reprinted with permission from Ref. [146]. (g) Optimized binding configurations and charge density differences of C5H8 adsorption on CeO2 and Co-CeO2. (h) Adsorption energy and charge transfer comparison of C5H8 on CeO2 and Co-CeO2. Reprinted with permission from Ref. [147].

the ZnO electronic structure, enhancing sensing performance. Defect level formations and a higher conduction band position (Fig. 4b-h) promote electron transfer to surface-adsorbed oxygen, increasing the concentration of reactive oxygen species. This mechanism is optimized by fine-tuning the Pt loading to preserve atomic dispersion and avoid nanoparticle aggregation that diminishes active site availability. These insights into the molecular adsorption, activation, and oxidation clarify the pathways for improved gas detection.

Transition metal SACs have also attracted attention for gas sensing, owing to their unique electronic structures, tunable d-band centers, and variable oxidation states, enabling modulation of catalytic activity for enhanced sensitivity and selectivity. Their abundance and coordination flexibility make them promising alternatives for VOC detection technologies. Further incorporating MOX to support transition metal SA is beneficial; for example, Cu sites anchored on ultrathin $WO_{2.72}$ nanowires (CuSA/$WO_{2.72}$) demonstrated exceptional sensing performance for toluene, with a detection limit of 10 ppb, ultrafast response and recovery times, and excellent reversibility [146] (Fig. 5a). The superior performance was attributed to synergistic effects between Cu SAs and $WO_{2.72}$ nanowires. Cu sites serve as active centers for toluene adsorption, facilitating charge transfer and modulating the MOX electronic structure. Toluene adsorption induces measurable resistance changes due to enhanced catalytic decomposition, validated by in situ IR spectroscopy, which confirms selective adsorption and dynamic surface interactions. Computational studies, including DFT and MD simulations, provide atomic-level insights into enhanced adsorption energy, binding sites, and toluene stability. Upon Cu SA incorporation, electron concentration in $WO_{2.72}$ increased from 1.051e to 1.691e (Fig. 5b). DOS analysis (Fig. 5c, d) showed Cu SA/$WO_{2.72}$ with continuous occupied states at the Fermi level and a conduction band closer to it, indicating improved charge transfer. Gibbs free energy profiles for toluene oxidation (Fig. 5e, f) indicate a six-step pathway ($*C_7H_8$- → $*C_7H_7-OH$ → $*C_6H_5-CHO$ → $*C_6H_5-COOH$ → $*C_5H_4O_3$ → $*CH_3COCH_3 + *CH_3COOH$ → $*CO_2 + *H_2O$), with Cu SAs significantly lowering the reaction energy barriers. These results validate the experimental findings and emphasize the potential of Cu SA/ $WO_{2.72}$ nanowires for sensitive and selective gas detection. Recent research suggests that combining MOX with other MOX phases can further enhance selectivity and sensitivity due to improved ionic and electronic charge transfer. For instance, Co-doped CeO_2 (Co–CeO_2) catalysts functionalized on SnO_2 nanofibers significantly improved sensitivity and selectivity for isoprene (C_5H_8) [147]. The catalytic activity of Co–CeO_2 stems from its ability to increase the density of reactive oxygen species, such as adsorbed oxygen (O_2^-, O^-) and lattice oxygen (O^{2-}), which are crucial for gas adsorption and activation. XPS analyses reveal that the ratio of adsorbed to lattice oxygen species is substantially higher for Co-CeO_2-modified SnO_2 compared to pristine SnO_2, facilitating stronger and more selective interactions with target gases. This enhancement is attributed to several factors: Co-CeO_2 promotes the spillover of reactive oxygen species across the sensing surface, increasing available active sites. Additionally, DFT calculations indicate greater charge transfer during gas adsorption. Charge density difference and Bader charge analyses (Fig. 5g, h) reveal increased charge transfer from 0.0263e for CeO_2 to 0.0401e for Co− CeO_2, demonstrating the role of Co doping in enhancing adsorption and activation. Co incorporation also strengthens C_5H_8 adsorption, as evidenced by the higher adsorption energy on Co− CeO_2 (-83.5 kJ/mol) compared to CeO_2 (−67.6 kJ/mol) (Fig. 5h). These findings confirm stronger gas-surface interactions in Co-doped CeO_2, reinforcing its potential for improved catalytic performance. Beyond catalytic performance, transition metal-doped MOX catalysts, such as Co-CeO_2, offer a cost-effective alternative to noble metals like Pt and Pd, whose high cost and scarcity limit large-scale deployment. In contrast, transition metal SAs-doped MOXs deliver comparable benefits at lower cost, supporting their practical use in advanced chemiresistive sensors. The integration of 1D nanomaterials with SACs is further facilitated by techniques like electrospinning, which enables the fabrication of porous nanostructures with uniform atomic dispersion. While challenges such as particle aggregation and limited nanoscale dispersion persist, using SAs-doped MOXs mitigates these issues by stabilizing reactive oxygen species and minimizing grain growth during synthesis.

Importantly, optimizing the oxygen spillover effect and tailoring interfacial f, such as electron transfer and adsorption energy modulation, significantly enhance the sensing capabilities of SAES.

3.2.2. 2D material supported SAE sensors

Two-dimensional (2D) nanomaterials exhibit unique properties such as large surface area, tunable band gaps, and high stability, making them highly suitable for sensing applications. As discussed in the previous section, MOS materials play a critical role in sensing mechanisms through the interplay of lattice oxygen vacancies and adsorbed oxygen species, optimizing the oxygen spillover effect depending on the type of VOC. The transformation of semiconducting MOS into 2D structures has rendered them particularly attractive for chemiresistive sensors due to their enhanced active surface area, low power consumption, excellent charge carrier mobility, high modifiability, and scalability.

Recent advancements in 2D MOS-supported SAES have revolutionized gas detection technologies. For example, WO_3, an n-type semiconductor with a narrow bandgap and superior charge transport properties, is widely employed in gas sensors. Functionalization of defective WO_3 nanoplates with single Pt atoms (SA-Pt@WO_{3-x}) has significantly enhanced sensing capabilities, particularly toward acetone detection [108]. The mechanism leverages defect sites on WO_{3-x} to anchor Pt SAs, forming highly active catalytic sites that facilitate oxygen adsorption and redox reactions. Adsorbed oxygen species extract electrons from the conduction band to form oxygen ions, resulting in the formation of an electron depletion layer (Fig. 6a). Upon exposure to acetone, redox reactions release electrons back into the conduction band, causing a measurable decrease in resistance. This process is accompanied by the formation of CO_2 and H_2O, as depicted in Fig. 6b. The isolated Pt SAs lower activation energy barriers, enhance electron transfer, and maintain uniform coordination, delivering exceptional

sensitivity (R_{air}/R_{gas} = 43.54 for 5 ppm acetone), selectivity, and ultralow detection limits (down to 0.1 ppm). The SA-Pt@WO_{3-x} platform exhibits rapid response and recovery times (7 s and 24 s, respectively), along with excellent reproducibility and long-term operational stability for up to 49 days.

In another study, SAs of Au on In_2O_3 nanosheets were employed to develop a highly sensitive method and selective for HCHO detection [105]. This design demonstrated that a minimal Au loading of 0.25 % significantly improved sensing performance, achieving an exceptional response (85.67) to 50 ppm HCHO at a low operating temperature (100 °C) with a detection limit of 1.42 ppb. The synthesis involved hydrothermal preparation of In_2O_3 nanosheets, followed by calcination at 300 °C. Au single atoms were uniformly loaded via UV irradiation of an $HAuCl_4$ solution. Mechanistically, Au SAs acts as electron sinks, promoting the adsorption of oxygen molecules and catalyzing redox reactions with HCHO to form CO_2 and H_2O (Fig. 6c). This interaction reduces the activation energy (Ea = 4.7 kJ/mol for 0.25 % Au/In_2O_3), enhances charge transfer efficiency, and provides uniformly distributed active sites for selective HCHO adsorption. The sensor also demonstrates high selectivity, long-term stability over 30 days, and excellent resistance to humidity in the 20–40 % RH range. This study highlights the critical role of Au SAs in tuning the surface chemistry of In_2O_3, improving sensitivity, and reducing the operating temperature, making it a promising candidate for practical applications in HCHO detection. 2D material-supported SA sensors represent a significant leap forward in VOC sensing, offering a combination of high sensitivity and robust operational stability. While SACs on 2D materials enable precise atomic-level modulation of adsorption and electron transfer, MOSs contribute high stability, cost-effectiveness, and efficient surface reactivity, together enabling highly efficient VOC detection.

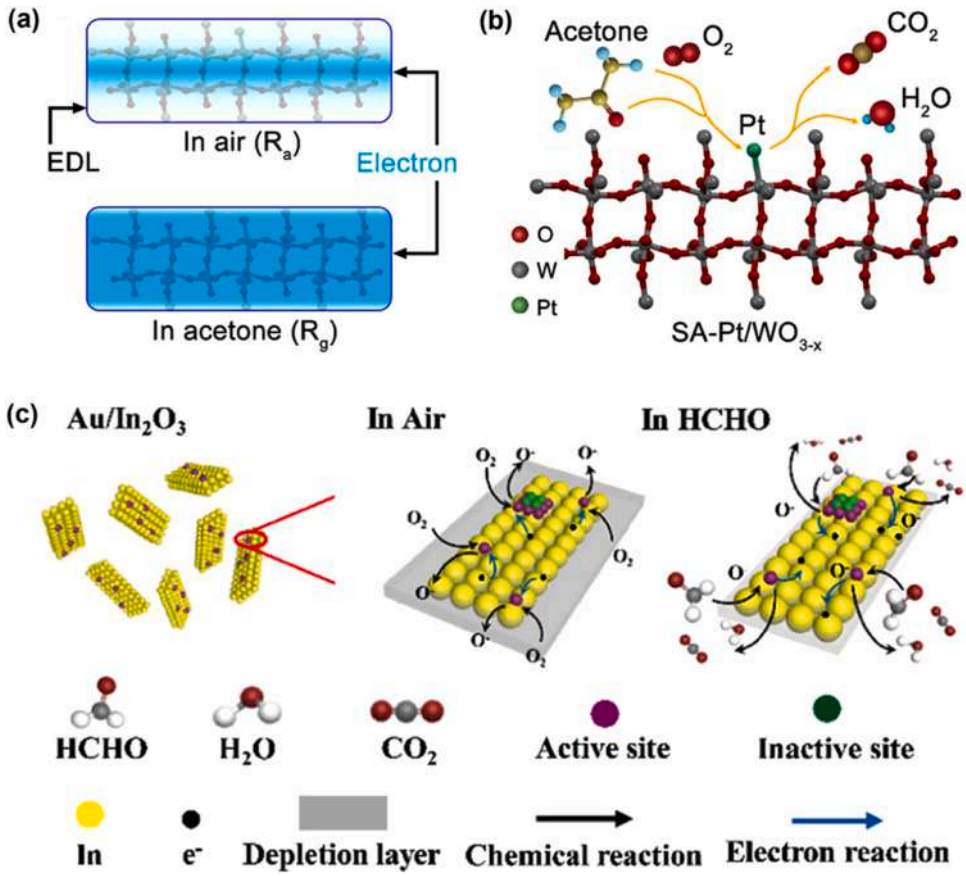

Fig. 6. (a) Variation in electron density of SA-Pt@WO_{3-x} under air and acetone exposure. (b) Acetone vapor interaction and sensing mechanism on the SA-Pt@WO_{3-x} surface. Reprinted with permission from Ref. [108]; (c) Schematic representation of the HCHO detection process on Au@In_2O_3. Reprinted with permission from Ref. [105].

3.2.3. 3D material-based SAE sensors

Beyond mesoporous oxides, three-dimensional (3D) MOS, metal-organic frameworks (MOFs), and conductive CMOFs have emerged as promising hosts for SAs. These porous architectures provide high surface areas, tunable pore structures, and abundant active sites, which significantly enhance oxygen adsorption. This increased oxygen uptake, in turn, facilitates greater electron depletion layer formation, leading to a stronger sensor response in VOC detection.

A novel chemiresistive gas sensor was developed by incorporating Pt-SAs into an Ag-$LaFeO_3$@ZnO core-shell structured material using a molecular imprinting-assisted sol-gel method [148]. The Pt-SAs were dispersed within a ZnO framework derived from the MOF precursor ZIF-8, ensuring strong Pt-O-Zn interactions that enhanced catalytic activity. The resulting Ag-$LaFeO_3$@ZnO-Pt sensor exhibited an exceptionally high specific surface area of 192.08 m^2/g, significantly improving the working temperature and detection limit for methanol. The sensor exhibited ultrahigh sensitivity of 453.02–5 ppm CH_3OH at 86 °C and retained a strong response even at 62 ppb (21.25). Compared to the Ag-$LaFeO_3$@ZnO sensor, the Pt-modified version exhibited a 6.69-fold increase in sensitivity, with a minimum detection limit of 3.27 ppb. DFT calculations revealed that the unoccupied 5d states of Pt SAs significantly enhanced oxygen and methanol adsorption, leading to stronger electron depletion effects and improved redox reaction kinetics. The methanol oxidation process on Ag-$LaFeO_3$@ZnO−Pt facilitated the formation of *CH_3O, *CH_2O, and *CO_2, with lower activation energy barriers compared to its non-Pt-counterpart, as shown in Fig. 7a. These findings confirmed that Pt SAs play a crucial role in boosting methanol sensing performance by promoting charge transfer and surface reaction efficiency.

Building on these findings, another study used a MOF-derived N-doped graphene (NG) framework to anchor atomically dispersed Pt SAs on In_2O_3 via a sacrificial templating route [73]. This synthesis approach integrates an MOF precursor with an NG template, effectively tuning the physicochemical properties of In_2O_3 and stabilizing single-atom Pt on its surface. The inclusion of Pt SACs increases the specific surface area, oxygen vacancies, and adsorbed oxygen species,

providing more active sites for gas adsorption. As a result, the Pt-In_2O_3-NG sensor exhibits a high response (750.4–100 ppm), rapid response time (2 s to 100 ppm), excellent selectivity, and a low theoretical detection limit (8.4 ppb). As shown in Fig. 7b, the sensing mechanism is based on electron transfer between HCHO molecules and chemisorbed oxygen species. Oxygen molecules adsorb onto the In_2O_3 surface, forming O_2^-, O^-, and O_2^{2-} species, which create an electron depletion layer, increasing resistance.

Upon HCHO exposure, oxidation reactions release electrons, reducing resistance and enabling detection. The Pt-In_2O_3-NG exhibits the highest concentration of active oxygen species participating in the sensing process. The introduction of Pt SAs also modifies the electronic structure of In_2O_3, reducing its band gap and facilitating stronger interactions between Pt and HCHO molecules, thus improving sensor performance. By leveraging the tunable porosity and electronic properties of MOF-derived structures, this work demonstrates the effectiveness of single-atom catalysts in enhancing the sensitivity, selectivity, and operational efficiency of chemiresistive gas sensors.

Further, synthesis strategies and the choice of cocatalysts play a pivotal role in determining the gas-sensing performance of metal oxide-based sensors. The structural and electronic modifications induced by different fabrication techniques can significantly influence the density of active sites, oxygen vacancy concentration, and charge transport properties, ultimately affecting sensitivity and selectivity. To illustrate this,

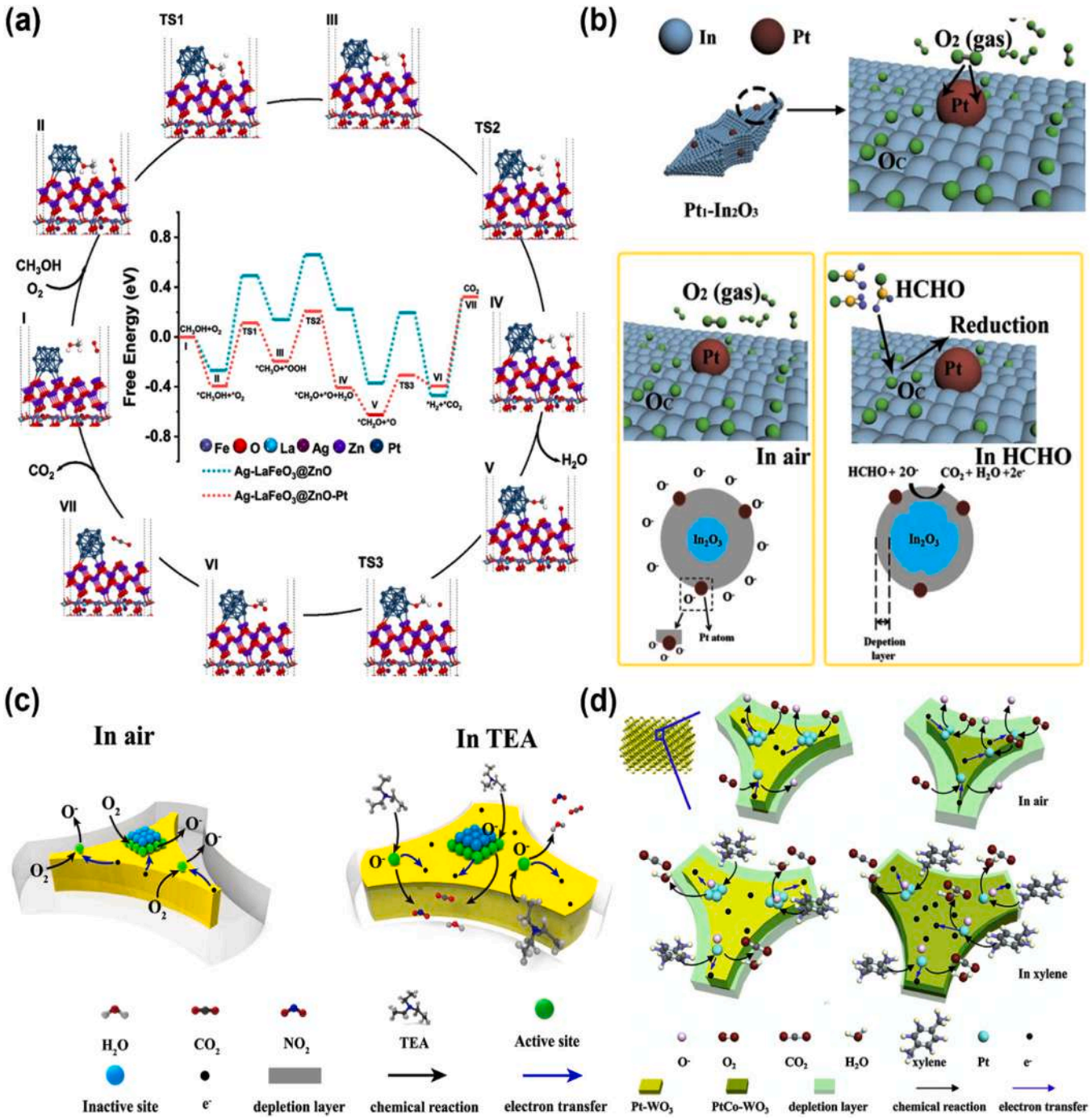

Fig. 7. (a) Schematic representation of the CH_3OH oxidation pathway on Ag−$LaFeO_3$@ZnO with Pt SAs. The inset illustrates the activation energy variations of ions and molecules in Ag−$LaFeO_3$@ZnO and Ag−$LaFeO_3$@ZnO−Pt at different reaction stages. The reaction cycle highlights the key intermediates and transition states (TSs). Reprinted with permission from Ref. [148]. (b) Conceptual depiction of the gas sensing mechanism in Pt-In_2O_3 [73]. (c) Mechanistic illustration of TEA detection and conversion on Pt@WO_3 Reprinted with permission from Ref. [149]. (d) Diagrammatic representation of the xylene sensing process in Pt@WIn_2O_3 and PtCo-WIn_2O_3 systems. Reprinted with permission from Ref. [150].

case studies on WO_3 coordinated with SAs through different cocatalyst choices and synthesis approaches have been explored. Gu et al. conducted a series of studies on 3D Pt SAs and Pt combined with transition metal SAs on WO_3 for detecting trimethylamine (TMA) and xylene, employing the colloidal crystal template method with a PMMA sacrificial template [149,150]. Their findings revealed that, compared to Pt-WO_3 nanoparticles, Pt SAs@WO_3 exhibited significantly enhanced sensitivity of 28.37 ppm and an ultralow LOD of 0.18 ppb for TMA. This improvement was attributed to reduced activation energy, which facilitates higher oxygen adsorption and improved gas-sensing performance. Additionally, the authors investigated the influence of Ni and Co transition metal SAs as cocatalysts in the 3D Pt SA-WO_3 structure. Among the studied materials, PtCo-SA@WO_3 demonstrated a superior sensitivity of 3.91 ppm and an LOD of 1.08 ppb for xylene detection. The incorporation of transition metals further increased oxygen vacancy concentration, leading to enhanced Pt SAs dispersion, a reduced band gap, and improved electron mobility within WO_3. The uniform distribution of Pt SAs played a crucial role in increasing the density of active

sites and the adsorption capacity for oxygen molecules. As shown in Fig. 7c and 7d, the heightened oxygen adsorption expanded the electron depletion layer, resulting in significant resistance variations in the sensing material and consequently improving gas-sensing performance.

Expanding upon this, Dai et al. employed a wet impregnation method to anchor Pt SAs onto WO_3, leveraging surface oxygen vacancies for stabilization [71]. To enhance WO_3-based chemiresistors, they combined chemical sensitization via Pt SAs with physical sensitization through pulsed temperature modulation (PTM). The incorporation of Pt SAs significantly improved sensor response to TMA and xylene, with 0.1 at% Pt SAs anchoring increasing response values from 2.7 to 7.8 for TMA and from 2.1 to 5.4 for xylene. PTM further amplified these responses to 6541.5 and 1001.1, respectively, achieving ultra-high sensitivity with theoretical detection limits as low as 0.78 ppt for TMA and 0.18 ppt for xylene. This study delves into the gas-sensing mechanism of Pt SAs on WO_3, emphasizing the role of surface chemistry and dynamic oxygen species in enhancing chemiresistive performance. Pt SAs modulate the electronic structure of WO_3, thereby improving VOC adsorption and catalytic activation. The enhancement is attributed to dynamic oxygen species modulation and improved analyte diffusion, facilitated by PTM. Mechanistically, Pt SAs promote the formation and replenishment of active oxygen species (O_2^-, O^-), which are crucial for VOC oxidation. Under PTM, periodic high-temperature pulses regenerate these oxygen species, preventing sensor saturation and

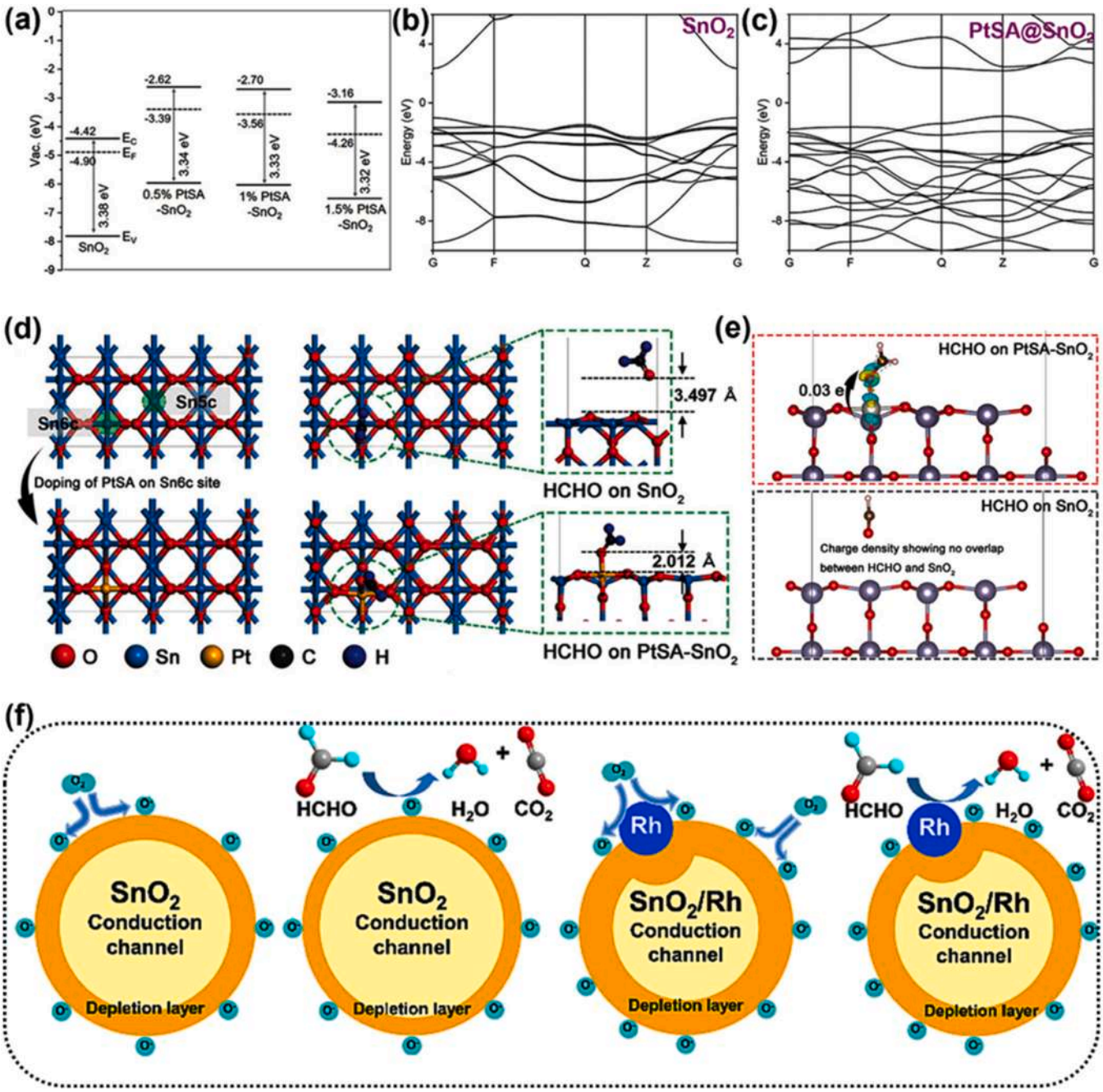

Fig. 8. (a) Electronic band structure of PtSA@SnO_2. (b-c) DOS comparison between pristine SnO_2 and PtSA@SnO_2. (d) Schematic representation of PtSA@SnO_2 surface formation, along with the most stable configurations of HCHO adsorption on SnO_2 and PtSA@SnO_2 surfaces. (e) Charge density difference analysis for HCHO adsorption on SnO_2 and PtSA@SnO_2. Reprinted with permission from Ref. [151]. (f) Illustration of the gas sensing mechanism of SnO_2 and RhSA-SnO_2 under ambient conditions and formaldehyde exposure. Reprinted with permission from Ref. [74].

accelerating response/recovery kinetics. This dynamic modulation significantly enhances sensing performance, enabling ultra-low detection limits. Furthermore, Pt SAs serve as catalytic sites, lowering the activation energy for VOC oxidation while ensuring long-term sensor stability. PTM further optimizes gas diffusion and surface reactions by periodically desorbing surface-bound intermediates, maintaining high sensitivity over multiple sensing cycles. These findings offer a comprehensive perspective on how the choice of synthesis methods and co-catalysts impacts the sensitivity of the materials.

As discussed in the 1D SAs sensors section, in the detection of HCHO, SnO_2 is well reported due to its selectivity towards HCHO. A 3D Pt SA-decorated SnO_2 material was synthesized using a carbonization–oxidation strategy combined with ultrasonic spray pyrolysis to obtain Pt SA substitutionally doped SnO_2 (PtSA@SnO_2) [151]. The structural analysis confirms that Pt SAs are embedded within the SnO_2 lattice, modifying its electrical properties and band structure, resulting in a low-resistivity state (Fig. 8a-c). The PtSA@SnO_2 sensor enables humidity-independent detection of trace-level HCHO (10 ppb) with high response, fast response speed, and excellent selectivity, even under 70 % RH conditions. Unlike conventional sensors, increasing Pt SA doping decreases resistance, which benefits circuit integration. DFT calculations revealed that Pt SA doping narrows the band gap (from 3.34 eV in SnO_2 to 3.08 eV in PtSA@SnO_2), while the Pt 5d orbital introduces new electronic states, enhancing electron transfer and conductivity (Fig. 8a). HCHO adsorption energy on PtSA@SnO_2 is significantly higher (−1.123 eV vs. −0.327 eV for pure SnO_2), indicating stronger gas interactions (Fig. 8d). As depicted in Fig. 8e, the presence of Pt SA significantly boosts charge transfer, improving both sensor selectivity and sensitivity. The PtSA@SnO_2 sensor demonstrates ultra-low detection limits (10 ppb), a rapid response time (24 s), excellent selectivity, and long-term stability.

Rh SAs have been employed to enhance the gas-sensing performance of SnO_2 sensors through atomic layer deposition (ALD) [74]. Gas-sensing investigations reveal that RhSA-SnO_2 exhibits a remarkable response of 36.3–20 ppm formaldehyde, representing a nearly 23-fold improvement over pure SnO_2. This sensor also demonstrates high sensitivity and rapid response-recovery times (4–29 s). Optimizing the Rh SA loading, RhSA-SnO_2 with 25 ALD cycles of Rh achieves the highest response to HCHO at 250 °C, further confirming the 23-fold enhancement compared to pristine SnO_2. Additionally, RhSA-SnO_2 maintains outstanding selectivity and stability, with an ultralow detection limit of 55 ppb. The superior sensing performance of Rh-doped SnO_2 is attributed to enhanced HCHO adsorption and charge transfer, as illustrated in Fig. 8f. The interaction energy between HCHO and RhSA-SnO_2 (-1.99 eV) is significantly higher than that of pure SnO_2 (-1.69 eV), leading to stronger analyte binding. Furthermore, charge transfer is greatly increased (2.27 e vs. 0.125 e), substantially improving sensor sensitivity. Selectivity for HCHO over other gases is also enhanced due to the stronger interaction energy. Density of states analysis confirms that Rh acts as the primary active site, with Rh–O interactions playing a pivotal role in adsorption. Moreover, Rh doping facilitates oxygen adsorption and desorption, increasing the surface oxygen content, which contributes to superior sensing performance. Hybridization between O-p and Rh-d orbitals is identified as the key factor driving the improved HCHO response in RhSA-SnO_2.

These findings collectively underscore the significance of 3D SA@MOS-based VOC sensors in achieving enhanced sensitivity, selectivity, and stability. The advancements in 3D SA-based materials integrated into MOS have significantly enhanced the performance of VOC sensors. These architectures provide higher surface areas, tunable pore structures, and abundant active sites, facilitating superior oxygen adsorption and improving electron depletion layer formation. The incorporation of single-atom catalysts, such as Pt and Rh, has demonstrated remarkable improvements in sensor sensitivity, selectivity, and operational stability by modulating electronic structures and catalytic activity. Notably, studies on Pt-SA-modified ZnO, In_2O_3, and WO_3 have revealed enhanced gas adsorption, charge transfer efficiency, and reduced activation energy barriers, leading to ultralow detection limits and rapid response times. The interplay between SACs and transition metal cocatalysts, such as Ni and Co, has further optimized oxygen vacancy concentration and electronic properties, improving the overall sensing mechanism. Additionally, the application of PTM in WO_3-based sensors has been pivotal in regenerating active oxygen species, sustaining sensor performance over multiple cycles. The introduction of Pt and Rh SAs in SnO_2-based sensors has demonstrated a profound impact on HCHO detection, with significant band gap reduction, enhanced charge density, and improved humidity tolerance. The synergistic effect of SAs and host materials underlines the importance of rational material design in developing next-generation chemiresistive VOC sensors. These findings collectively highlight the transformative role of 3D SA@MOS-based sensors in advancing gas-sensing technologies, emphasizing the critical influence of synthesis strategies, cocatalyst selection, and electronic structure engineering in achieving superior sensor performance.

3.3. Electrochemical SAE sensors

Electrochemical sensors based on SAs have emerged as powerful tools for detecting environmental pollutants with high sensitivity and selectivity. The unique electronic structure and well-defined active sites of SACs facilitate efficient electron transfer and catalytic activity, making them ideal candidates for electrochemical sensing applications. Incorporating SAs into conductive support materials enhances sensor performance by improving charge transport, increasing active surface area, and tailoring adsorption properties. Transition metal SAs have received considerable attention for their potential in gas sensing applications. Their unique electronic configuration and variable oxidation states offer opportunities to fine-tune catalytic sites, improving both sensitivity and selectivity. Their abundance and versatile coordination chemistry further establish them as promising candidates for advancing VOC detection technologies.

A notable example is the Nb@BNT sensor for nitrobenzene (NB) detection, reported by Li et al. synthesized via a co-precipitation method followed by high-temperature pyrolysis [124]. The SA Nb-BCN-modified glassy carbon electrode (GCE) exhibited a superior electrochemical response, underscoring the critical role of SACs in pollutant sensing. Mechanistic studies revealed that the incorporation of isolated Nb atoms into the boron-carbon-nitrogen (BCN) framework generated highly active sites that enhanced catalytic activity and enabled selective adsorption of Nb molecules. The synergistic interaction between Nb SAs and the surrounding matrix significantly lowered the energy barrier for Nb reduction, evidenced by a positive shift in reduction peak potential (0.6 V) and a remarkable 42-fold increase in peak current compared to the bare GCE. Further investigations into the catalytic mechanism confirmed that Nb SAs played a crucial role in stabilizing reaction intermediates and facilitating a multi-electron transfer process for Nb reduction. The electrochemical behavior of the sensor was systematically optimized by tuning parameters such as enrichment time, applied potential, and pH, leading to an ultralow detection limit of 0.70 mM. Additionally, the sensor exhibited dual linear response ranges for different NB concentrations, enhancing its adaptability to diverse environmental conditions. Real-world validation was performed through NB detection in tap and lake water samples, where high recovery rates confirmed the practical applicability of SAES in environmental monitoring. These advancements demonstrate the remarkable potential of SA-based electrochemical sensors in VOC detection, particularly through improvements in selectivity, sensitivity, and stability under complex and fluctuating environmental conditions. Notably, the ability of these sensors to maintain robust performance across a wide pH range is particularly crucial for real-world applications, given the variable acidity and alkalinity of environmental and industrial samples. Despite their promising attributes, SA-based electrochemical sensors remain relatively underexplored, and further investigations could unlock their

full potential in gas sensing technologies. Additionally, DFT studies could provide deeper mechanistic insights into the electronic structure, adsorption behavior, and reaction pathways of SA sites, thereby enabling the rational design of electrochemical sensors with improved sensitivity, selectivity, and stability. Such innovative approaches will drive the development of next-generation electrochemical sensors with superior durability, selectivity, and real-world applicability in environmental monitoring and beyond.

3.4. SAE Field effect transistor sensors

FET sensors, including metal-oxide-semiconductor FET (MOSFET), thin-film transistor (TFT), and chemical field-effect transistor (ChemFET), function by modulating the conductivity of a semiconducting channel upon exposure to analyte gases. This modulation arises from charge transfer or dipole interactions between the gas molecules and the channel material, imparting high sensitivity, rapid response/recovery times, and room temperature operability. These features render FETs well-suited for detecting a wide range of gases, including VOCs (Table 3). However, conventional FET sensors are often limited by poor selectivity, limited long-term stability, and performance degradation under humid conditions (Table 4) [152–157]. To overcome these limitations, MXenes have emerged as promising channel materials due to their metallic conductivity, tunable surface terminations, and large specific surface area, which provide abundant active sites for gas adsorption. Additionally, MXenes offer excellent platforms for stabilizing SACs, owing to their ability to anchor metal adatoms effectively. Incorporating SAs onto MXenes substrates introduces highly reactive catalytic sites that significantly enhance gas adsorption and charge transfer processes.

Table 3
Comparison of FET architectures and their suitability for VOC sensing.

S. No	Parameter	MOSFET (Metal-oxide-semiconductor FET)	TFT (Thin-film transistor)	ChemFET (Chemical field-effect transistor)
1	Structure	Bulk or planar silicon-based architecture	Uses thin-film semiconductors on substrates	Modified FET with chemically sensitive gate
2	Material Flexibility	Low (mainly Si-based)	High (can use organic/ inorganic materials)	High (gate surface can be functionalized with receptors)
3	Sensitivity to VOCs	Limited (requires surface functionalization)	Moderate to high (depending on material)	High (direct chemical interaction with gate)
4	Selectivity	Low (without modification)	Moderate (enhanced by nanomaterials)	High (with specific receptors or SAMs)
5	Response Time	Fast	Moderate to fast	Fast to moderate (depends on diffusion)
6	Operating Voltage	Moderate to high	Low to moderate	Low
7	Fabrication Cost	High (CMOS processes)	Low (solution-processable materials possible)	Moderate
8	Integration with Flexible Substrates	Poor	Excellent	Good
9	Scalability	Excellent (mature CMOS technology)	Good	Moderate
10	Real-world Applicability	Limited in VOC sensing	Suitable for low-cost, flexible sensors	Highly suitable for selective VOC sensing

A recent study reported a FET sensor based on Pt SAs anchored onto ultrathin $Ti_3C_2T_x$ nanosheets for detecting TEA gas at room temperature [70]. Pristine $Ti_3C_2T_x$ nanosheets were obtained through liquid-phase exfoliation and lithium fluoride/hydrochloric acid etching, generating Ti vacancies that acted as anchoring sites for Pt SAs. The Pt SAs were immobilized via self-reduction of Pt^{4+} under argon agitation, with $Ti_3C_2T_x$ acting as the reductant. Introducing Pt SAs lowered the activation energy for gas adsorption and improved selectivity toward TEA. Mechanistically, Pt SAs catalyzed the dissociation of oxygen molecules through the spillover effect, generating active O^- species that oxidized TEA into NO_2, CO_2, and H_2O (Fig. 9c). This reaction released electrons into the $Ti_3C_2T_x$ matrix, reducing the hole density in the p-type semiconductor and thereby decreasing its conductivity. This sensor achieved an impressive detection limit of 14 ppb, rapid response times of 3 s at 1 ppm TEA, and excellent ambient stability. The study also investigated the adsorption energy of Pt SAs with various MXene terminations (-OH, -O-, and -F) for TEA, revealing that Pt SA-MXene with F-Pt sites exhibited the highest TEA binding affinity (Fig. 9d, e). Beyond MXenes, TMDs such as MoS_2, WS_2, and $MoSe_2$, stand out due to their semiconducting nature and direct band gaps, which enable effective FET-based sensing. Modifying 2D materials via doping or heterostructure formation further enhances their gas sensing capabilities by improving adsorption and catalytic activity. In this context, the incorporation of SAs into chalcogenide atom vacancies in TMDs strengthens their interaction with VOC molecules. One study demonstrated that functionalizing 2D materials (n-type MoS_2 and p-type WSe_2) with SAs (Pt, Co, Ru) significantly enhanced VOC detection performance. Notably, even a minimal Pt loading (0.1 %) on MoS_2 yielded a high sensitivity of 92.3 for detecting 50 ppm acetone at room temperature (25 °C), with improved selectivity over ethanol and water [159]. This sensor also demonstrated an impressive detection limit of 0.05 ppm, highlighting its capability for low-concentration detection.

The Pt@MoS_2 sensor was synthesized via a one-step UV light-assisted reduction process, wherein Pt SAs were deposited onto mechanically exfoliated MoS_2. Mechanistically, the n-type nature of MoS_2 facilitated electron transfer upon VOC adsorption, increasing surface electron density at the surface and lowering the activation energy (Ea = 23.5 kJ/mol for Pt/MoS_2), which enhanced both adsorption and desorption kinetics. Conversely, the p-type WSe_2 stabilized adsorbed VOC molecules through charge delocalization and selective binding (Fig. 10a), enabling efficient detection and recovery. These complementary properties of TMDs, combined with SAs decoration, optimize adsorption capacity, charge transfer, and selectivity. The sensor exhibited excellent selectivity toward acetone, operational stability for over 50 days, and robust performance under high humidity (30–60 % RH). These findings highlight the transformative role of SA catalysts in tuning the electronic properties of n-type and p-type TMD substrates, facilitating dynamic adsorption-desorption processes under variable environmental conditions. The synergy between n-type and p-type 2D materials enables high sensitivity, selectivity, and efficient low-temperature operation, making these systems promising candidates for environmental monitoring, industrial safety, low power consumption, and healthcare diagnostics.

In summary, the integration of SAs on MXenes and TMDs significantly enhances the sensing performance of FET-based sensors by optimizing gas adsorption kinetics and catalytic activity. This advancement underscores the versatility and potential of SA-decorated MXenes and TMDs for developing next-generation VOC sensors with ultrahigh sensitivity, selectivity, stability, and room temperature operation. Continued exploration of various SAs and support materials is expected to further expand their applicability across diverse sensing platforms.

3.5. Microelectromechanical system (MEMS)

SA-incorporated materials have emerged as a promising class of catalysts for enhancing the sensitivity, selectivity, and response time of

Table 4
Comparison of SA FETs and conventional nanomaterial-based FET sensors for VOC detection.

S.No	FET Type	Catalyst	Target VOC	Detection limit	Response time	Operating temperature (°C)	Ref
1	SA-FET	Pt SA-$Ti_3C_2T_x$	Triethylamine	14 ppb	5 s	Room Temp.	[70]
2	NP-FET	Pd nanoparticles on CNT	Benzene	~50 ppb	8 s	Room Temp.	[152]
3	NP-FET	SnO_2 mesoporous nanoparticles	Formaldehyde	~10 ppm	~15 s	~200 °C	[153]
4	s-CNTs-FET	s-CNTs	Formaldehyde	20 ppb	-	Room Temp.	[154]
5	NP-FET	RGO/ZnO	Formaldehyde	120 ppb	120 s	Room Temp.	[155]
6	NP-FET	1T-2H-MoS_2	Formaldehyde	1 ppm	150 s	Room Temp.	[156]
7	NP-FET	ZnO/WS_2	Benzene	500 ppb	90 s	Room Temp.	[157]

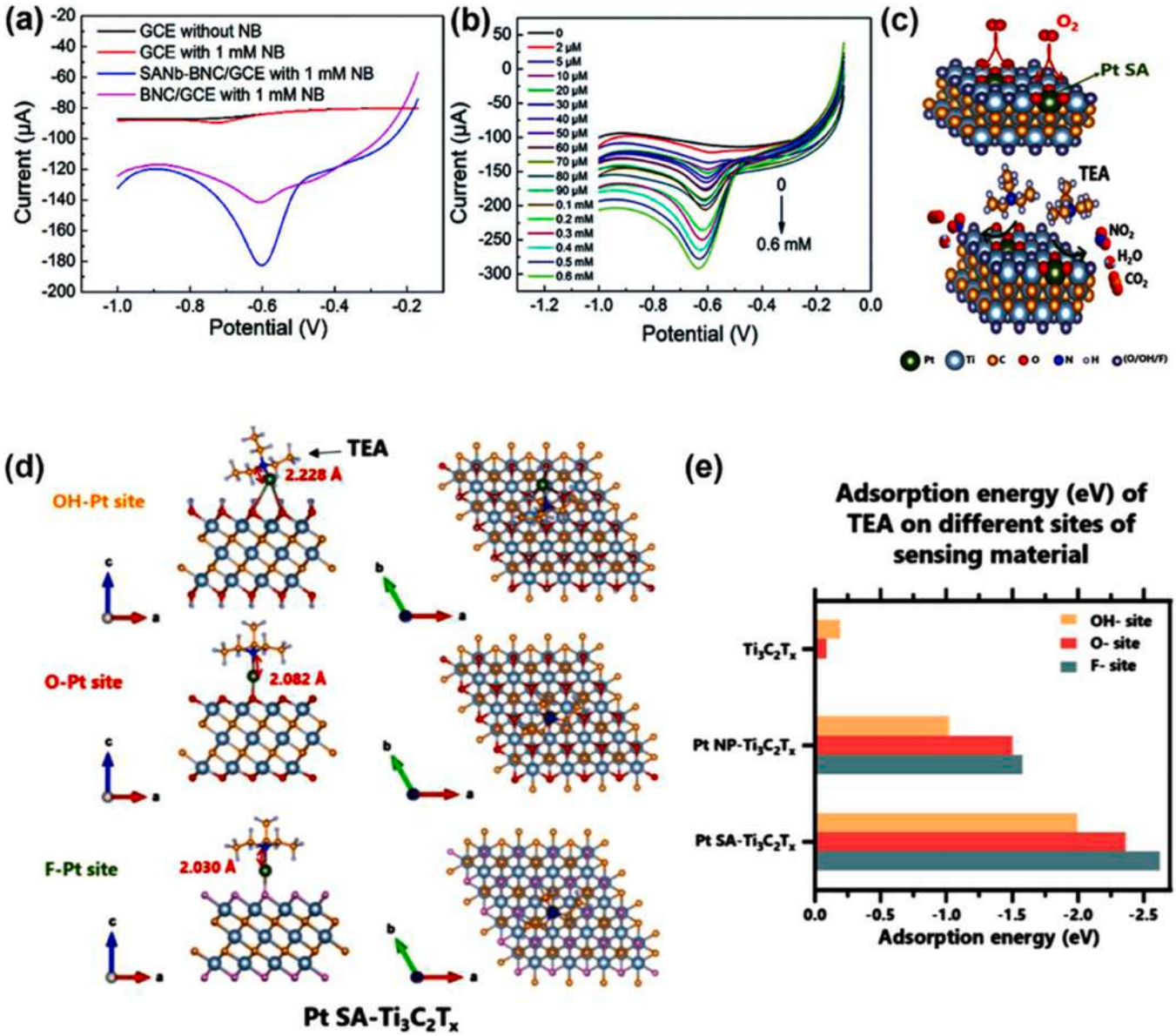

Fig. 9. (a) LSV curves of bare GCE, SANb-BNC/GCE, and BNC/GCE in 0.1 M PBS with 0.1 mM NB, including bare GCE without NB (scan rate: 50 mV s^{-1}). (b) LSV curves at varying NB concentrations (0-600 μM) under optimized conditions (pH 7.0, 0.1 M PBS). Reprinted with permission from Ref. [124]. (c) Schematic of Pt SA-facilitated TEA adsorption and surface reaction on Pt SA@$Ti_3C_2T_x$. (d, e) DFT models and adsorption energies of TEA with N-terminal atoms on OH^-, O^-, and F^- sites of Pt SA@$Ti_3C_2T_x$, Pt NP@$Ti_3C_2T_x$, and pristine $Ti_3C_2T_x$Reprinted with permission from Ref. [70].

MEMS sensors in VOC detection. The superior catalytic activity of these materials arises from atomically dispersed active metal sites, which provide abundant active centers, tunable surface interactions, and enhanced gas adsorption capabilities. These attributes facilitate efficient charge transfer and oxidation processes, enabling selective VOC detection even at low concentrations and reduced operating temperatures.

A representative case involves the detection of 3-hydroxy-2-butanone (3H-2B), a key biomarker VOC associated with *Listeria monocytogenes*, which can be selectively adsorbed and catalytically oxidized on SA sites, generating distinct and measurable signals. In this study Au-SAs were anchored on mesoporous SnO_2 nanospheres via a polyphenol-assisted assembly of glutathione-modified Au nanoclusters, followed by

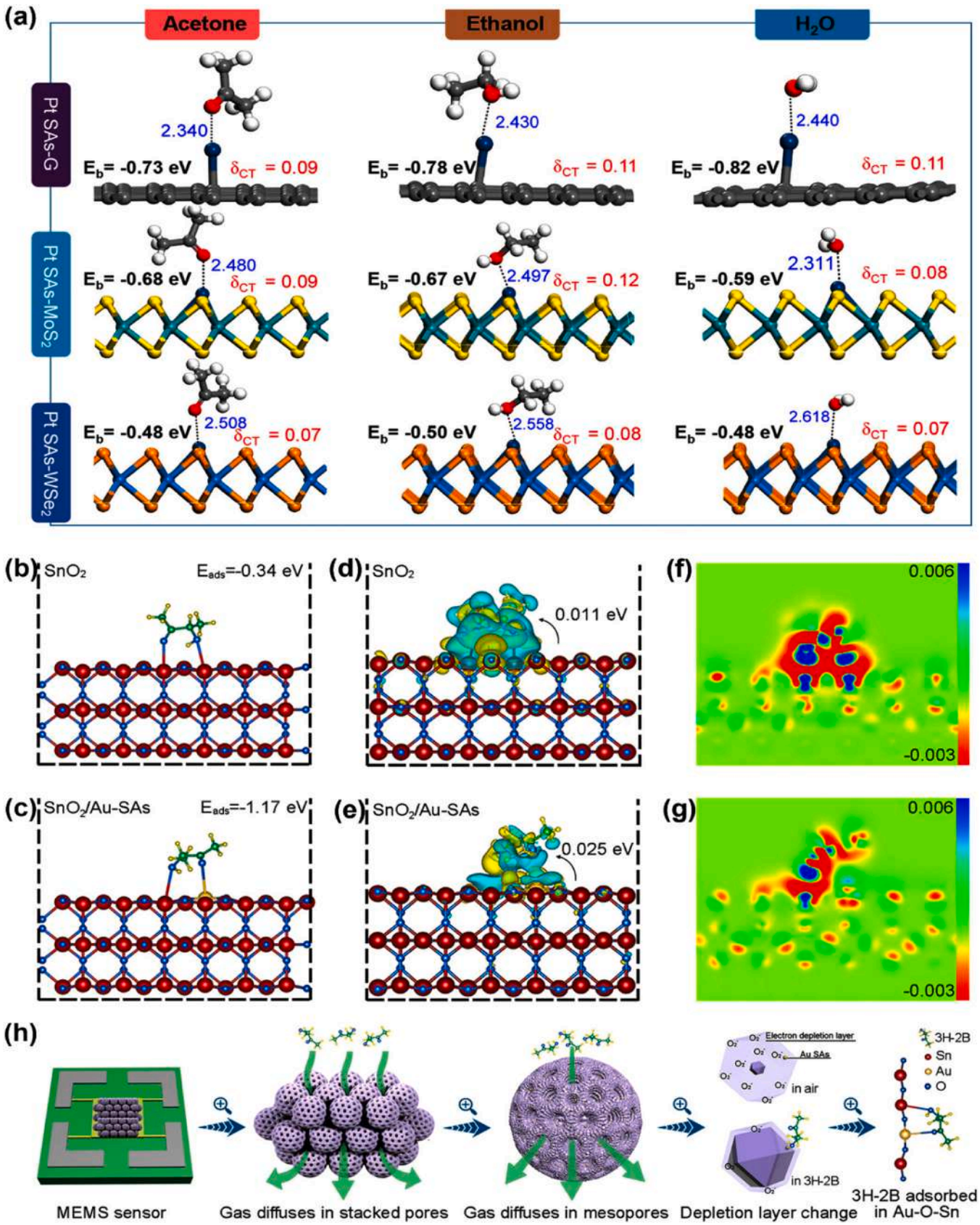

Fig. 10. (a) DFT-optimized structures of Pt SA-decorated graphene/MoS_2/WSe_2 with adsorbed VOCs (acetone, ethanol, and water), showing DM-O distances, binding energies (Eb, eV), and charge transfer (δ_{CT}, e). Reprinted with permission from Ref. [158]. Adsorption energies for 3H-2B on (b) SnO_2 and (c) SnO_2/Au-SAs. Charge distributions for (d) SnO_2 and (e) SnO_2/Au-SAs, and charge density differences in the 2D plane for (f) SnO_2 and (g) SnO_2/Au-SAs. (h) Schematic of SnO_2/Au-SAs enhanced performance for 3H-2B detection. Reprinted with permission from Ref. [159].

thermal calcination to generate atomically dispersed Au sites [158]. The resulting SA-functionalized sensor exhibited a remarkably high response (587.3) to 2 ppm of 3H-2B at just 50ºC, with a fast response time of 10 s and an ultra-low detection limit of 10 ppb. Compared to conventional SnO_2-based sensors, this SA-based material not only enhanced sensitivity by a factor of 183.5 but also significantly lowered the operational temperature from 100 °C to 50 ºC, making it highly energy-efficient. The superior sensing performance of SnO_2/Au-SA material was attributed to electronic and chemical sensitization mechanisms. These sensors were evaluated under air and nitrogen atmospheres using 2 ppm of 3H-2B as the target analyte. In a nitrogen atmosphere, the sensor exhibited a response of 300.3 with a resistance of 5.51 GΩ, while in air, the response significantly increased to 587.3. This notable enhancement suggests that Au SAs promote the adsorption and dissociation of O_2, increasing the concentration of ionized oxygen species, which amplifies the response. The high response observed even in nitrogen (300.3) indicates that both electronic and chemical sensitization mechanisms play critical roles in improving sensing efficiency. Mechanistically, Au has a higher work function than SnO_2, the functionalization of SnO_2 with Au SAs facilitating electron transfer from SnO_2 to Au until Fermi level equilibrium is achieved. This process increases the depletion layer thickness and electrical resistance, thereby intensifying the response upon exposure to 3H-2B vapor. Computational analysis further confirms this enhancement, with the adsorption energy increasing from −0.34 eV for pristine SnO_2 to −1.17 eV for AuSAs@SnO_2 (Fig. 10 b, c). Charge density difference analysis (Fig. 10 d-g) showed that the introduction of Au SA increased the local electron density from 0.011 to 0.022 eV, enhancing electron mobility. The synergistic effects of atomic-scale active sites, mesoporous architecture, and optimized charge transport and fast oxygen adsorption/dissociation kinetics significantly improved VOC detection (Fig. 10h).

Moreover, the significantly reduced energy demands of SA catalysts align perfectly with the low-power requirements of MEMS devices, making them highly suitable for portable and wearable applications. By integrating SA-functionalized materials into MEMS-based sensors, researchers can achieve high-performance VOC detection with minimal energy consumption, paving the way for next-generation smart sensing technologies (Table 5) [160].

4. Mechanistic insights from *in situ*, theoretical and machine learning studies

Understanding the synergistic interactions between SACs and target analytes is crucial for optimizing their performance in VOC sensing and catalytic applications. Advanced spectroscopic techniques, DFT calculations, and ML models offer significant mechanistic insights into these interactions.

4.1. *In Situ and operando spectroscopic investigations*

In situ and operando spectroscopic techniques play a pivotal role in the real-time monitoring of catalytic and sensing processes, providing crucial insights into reaction intermediates, pathways, active sites, and variations in electronic structures. These techniques facilitate a deeper understanding of catalytic mechanisms by enabling direct observation of dynamic transformations. Key spectroscopic techniques include diffuse reflectance infrared Fourier transform spectroscopy (DRIFTS), Raman spectroscopy, X-ray absorption near-edge structure (XANES), and extended X-ray absorption fine structure (EXAFS).

4.1.1. *Diffuse reflectance infrared Fourier transform Spectroscopy (DRIFTS)*

DRIFTS is a highly effective technique for investigating surface interactions in catalysts, particularly SACs. By analyzing the adsorption and transformation of probe molecules such as CO and VOCs, DRIFTS yields valuable insights into the electronic states, coordination environments, and reaction pathways of active sites.

4.1.1.1. Differentiating metal species via CO-DRIFTS. CO-DRIFTS is instrumental in distinguishing different metal species based on their electronic structures. Several studies have demonstrated the effectiveness of CO-DRIFTS in distinguishing different SA species based on their characteristic absorption peaks. For instance, specific CO absorption peaks at 2143 cm^{-1} (Pt^{+n}), 2112 cm^{-1} (Pt^0 isolated), and ~2094 cm^{-1} (Pt metallic clusters) represent oxidized, isolated, and metallic Pt species, respectively (Fig. 11a-c) [150]. The sharp and intense 2112 cm^{-1} peak observed in SA-Pt/WO_3 indicates a high density of isolated Pt atoms. Furthermore, changes in the full width at half maximum (FWHM) of these peaks provide information about the size distribution and dispersion of Pt species. Further investigations using DRIFTS have demonstrated how the introduction of transition metal co-catalysts influences the anchoring of SA sites. In a representative example, incorporation of Co and Ni into the Pt-WO_3 system alters CO adsorption behavior, indicating shifts in the Pt oxidation state. An increase in oxygen vacancies improves the anchoring and stability of SA-Pt sites, enhancing catalytic activity. In another case study on Au/In_2O_3 catalysts, CO peaks observed at 2112 cm^{-1} (Au-CO) and 2172 cm^{-1} (In_2O_3-CO) reveal details about the oxidation state and electronic interactions of Au atoms [105]. A shift in the Au-related peak with decreasing Au content indicates variations in oxidation cluster formation. The correlation of CO-DRIFTS data with XPS and HAADF-STEM further validates the atomic-level dispersion of Au atoms.

4.1.1.2. DRIFTS in understanding SA-based gas sensing mechanisms. DRIFTS is crucial in elucidating gas sensing mechanisms by providing

Table 5
Single atom-engineered VOC detection by various sensor techniques, detection limit, and working temperature.

S. No.	Type of sensor	VOC analyte	Support material	Detection limit (ppb)	Working temperature (ºC)	Ref
1.	Metal oxide semiconductor (MOS) gas sensor	Formaldehyde	Au/In_2O_3	1.42	100	[105]
2.	Metal oxide semiconductor (MOS) gas sensor	Methanol	Ag-$LaFeO_3$@ZnO-Pt	3.27	86	[148]
3.	Metal oxide semiconductor (MOS) gas sensor	Acetone	SA-Pt/WO_{3-x}	4.3	350	[108]
4.	Semiconductor-based gas sensor	Formaldehyde	Pt on MOF-derived In_2O_3	8.4	-	[73]
5.	Metal oxide semiconductor (MOS) gas sensor	Xylene	3DOM PtCo-WO_3	1.08	250	[150]
6.	Metal oxide semiconductor (MOS) gas sensor	Xylene	3DOM PtNi-WO_3	1.69	250	[150]
7.	Chemiresistive gas sensor	Toluene	Cu SA/$WO_{2.72}$	10	160	[146]
8.	Metal oxide semiconductor (MOS) gas sensor	Triethylamine	SA-Pt/WO_3	0.18	240	[149]
9.	Field-effect transistor (FET) gas sensor	Triethylamine	Pt SA-$Ti_3C_2T_x$	14	RT	[70]
10.	Chemiresistive gas sensor	Ethanol	Pt SAs-MoS_2	5 (ppm)	RT	[160]
11.	Metal oxide semiconductor (MOS) gas sensor	Formaldehyde	SA Rh-sensitized SnO_2	55	250	[74]
12.	Metal oxide semiconductor (MOS) gas sensor	Triethylamine	Pt Single atom loaded ZnO	17.8	200	[144]
13.	Chemiresistive gas sensor	Formaldehyde	PtSA-SnO_2	6	175	[151]
14	Microelectromechanical system (MEMS) sensor	3-hydroxy−2-butanone	SnO_2/Au-SA	10	50	[158]

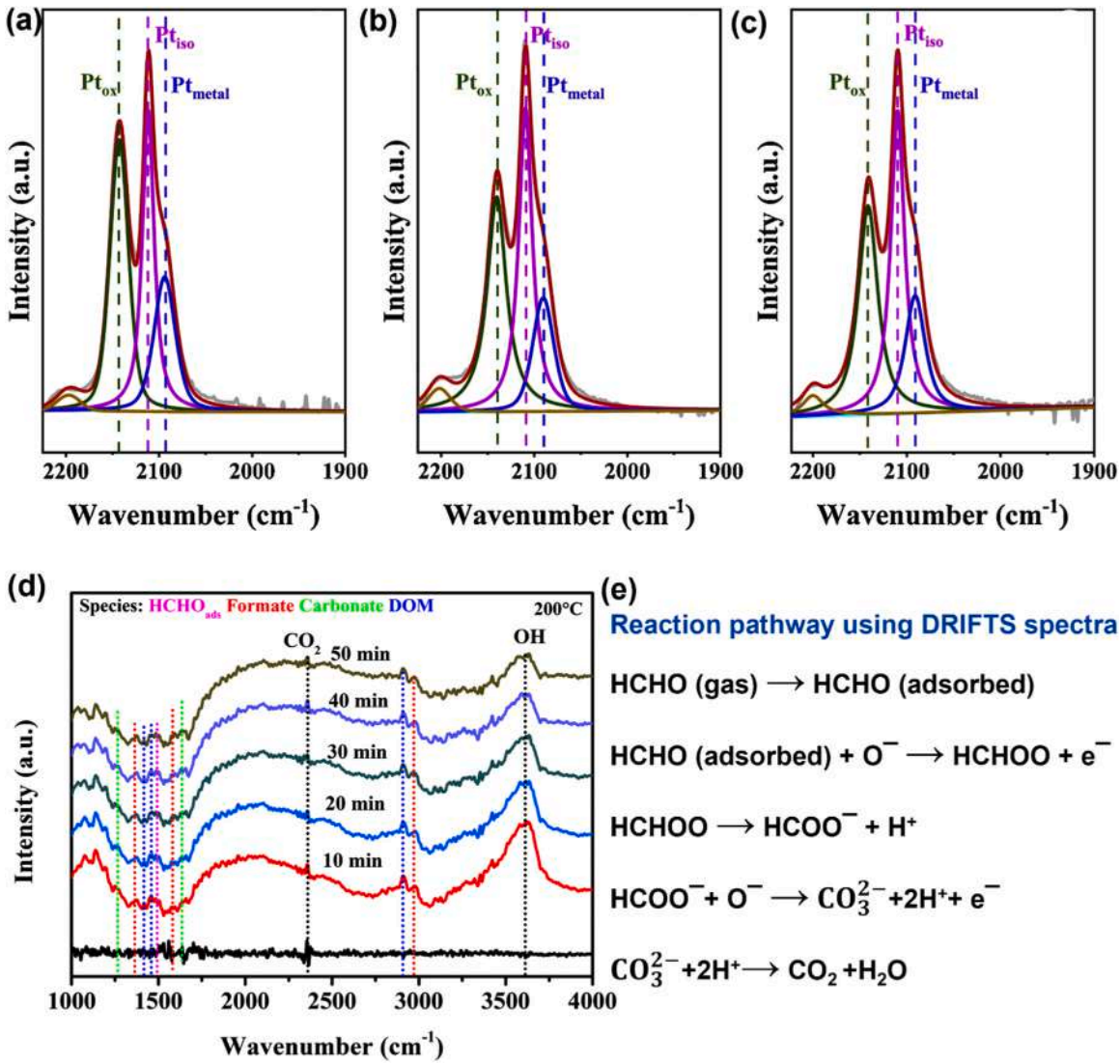

Fig. 11. CO-DRIFTS spectra of (a) Pt@WO_3, (b) PtCo@WO_3, and (c) PtNi@WO_3, highlighting surface interactions Reprinted with permission from Ref. [150]. (d) In situ, DRIFTS spectra of Pt@In_2O_3 exposed to 100 ppm HCHO at 200 °C, capturing the formation and evolution of key reaction intermediates. (e) Representative oxidation mechanism of HCHO proposed based on DRIFTS analysis. Reprinted with permission from Ref. [73].

real-time insights into surface interactions in SA catalysts. DRIFTS enhances the understanding of SA-based gas-sensing applications by identifying key surface intermediates, tracking reaction kinetics, and distinguishing atomic configurations. The real-time monitoring capabilities of DRIFTS have been effectively demonstrated in the study of Pt-In_2O_3 for HCHO detection [73]. As shown in Fig. 11d, exposure to 100 ppm HCHO at 200°C yields time-resolved in situ DRIFTS spectra with distinct vibrational peaks corresponding to key oxidation intermediates. Adsorbed HCHO (1495 cm^{-1}) undergoes transformation into formate (1356, 1584, and 2968 cm^{-1}), carbonate (1258 and 1645 cm^{-1}), and dioxymethylene species (1410, 1474, and 2872 cm^{-1}), alongside hydroxyl species (3620 cm^{-1}) and CO_2 (2359 cm^{-1}). These spectral changes confirm a sequential oxidation pathway ultimately leads to the formation of CO_2 and H_2O. The corresponding resistance variations observed in gas-sensing measurements align with these reaction steps, providing mechanistic insights into the role of surface-adsorbed oxygen in catalytic oxidation.

The reaction pathway, further supported by the proposed equations (Fig. 11e), deepens the fundamental understanding of the VOC oxidation mechanism in SA-based sensors. In situ DRIFTS conducted under oxygen-deficient and oxygen-rich conditions provides direct evidence of the distinct roles played by adsorbed oxygen species and lattice oxygen, offering a comprehensive understanding of their dynamic contributions to the catalytic process. For example, CO-DRIFTS studies during propane oxidation identify CO as a critical intermediate, underscoring the mechanistic involvement of oxygen species [144].

As shown in Fig. 12a, shifts in CO adsorption bands (2069–2012 cm) confirm the active participation of surface oxygen, while the emergence of hydroxyl-related bands (3688–3392 cm^{-1}) on WO_3 highlights their direct involvement in VOC oxidation. In oxygen-deficient conditions (Fig. 12a, b), CO forms initially on metallic Pt sites, indicating partial oxidation of propane. However, in Pt-WO_3/BN catalysts, the gradual depletion of hydroxyl bands (3688–3392 cm^{-1}) correlates with propane activation and subsequent oxidation to CO_2 (2326–2378 cm^{-1}), emphasizing the essential role of hydroxyl species in the reaction pathway. Temporal variations of CO and CO_2 band intensities reflect the dynamic consumption and regeneration of reactive oxygen species, illustrating the role of WO_3 in sustaining catalytic oxidation through oxygen renewal. Upon reintroduction of oxygen (Fig. 12c, d), the rapid structural recovery of WO_3 validates its contribution to catalytic stability and efficiency. These findings highlight that both oxygen and hydroxyl groups on WO_3 are critical to the oxidation mechanism,

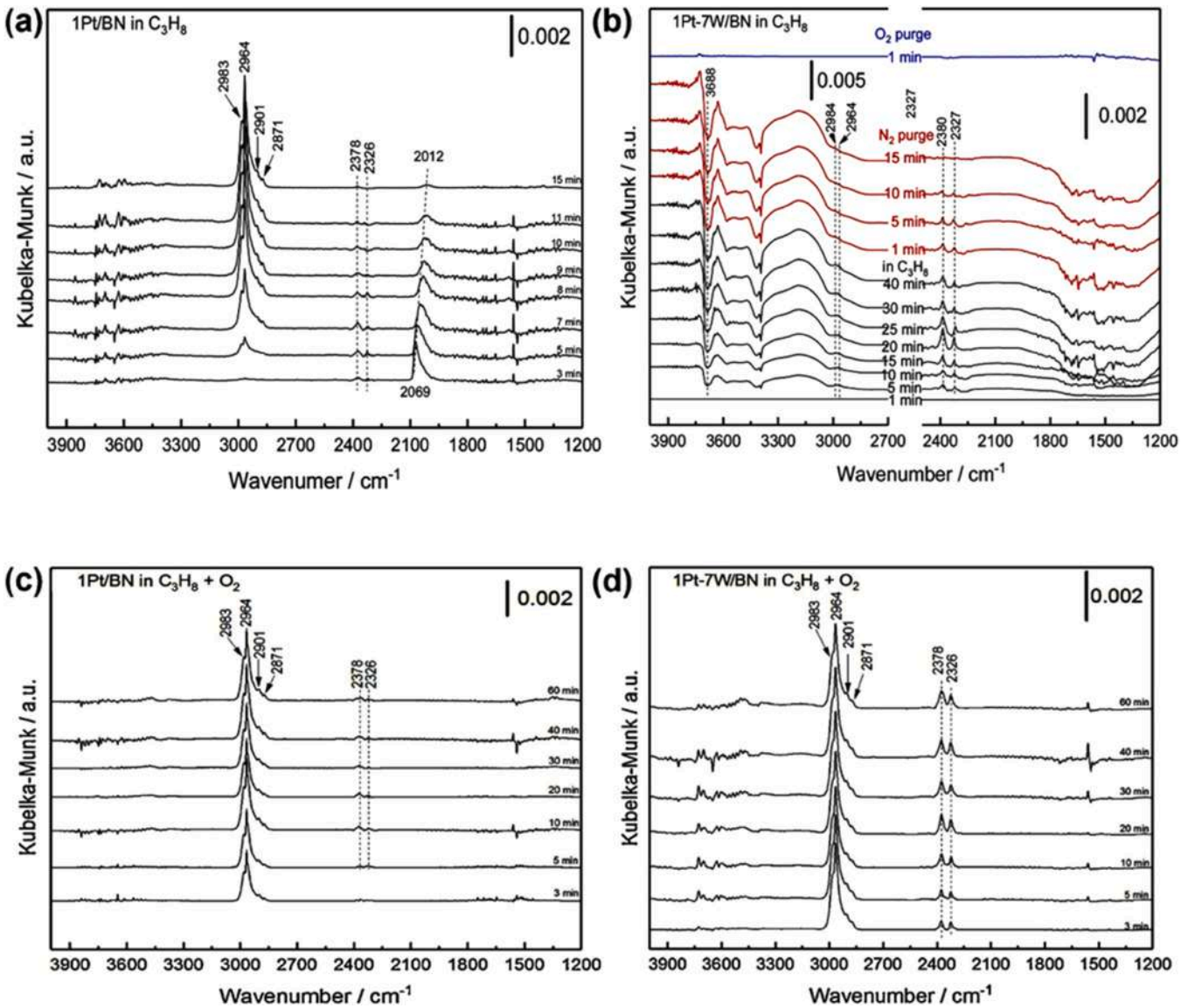

Fig. 12. In-situ DRIFT spectra for propane oxidation over (a, b) Pt/BN and Pt-WO_3/BN catalysts without oxygen, showing CO formation as an intermediate and hydroxyl group consumption on WO_3. (c, d) Spectra with oxygen present, highlighting increased CO_2 production and reversible structural restoration of Pt-WO_3/BN Reprinted with permission from Ref. [144].

particularly at the Pt-WO_3 interface, where they facilitate rate-determining steps and enhance overall catalytic activity. In situ DRIFTS thus serves as a vital tool for probing the electronic and structural characteristics of SACs. Correlating spectroscopic features with gas-sensing performance enables the rational design of high-performance VOC sensors. When combined with complementary techniques such as XPS and HAADF-STEM, DRIFTS enhances the robustness of experimental insight, offering a powerful framework for advancing SA-catalyst research.

4.1.2. Significance of in situ Raman Spectroscope in VOC Spectroscopy

Raman spectroscopy is a powerful technique for probing the structural and electronic properties of SACs. It offers valuable insights into defect states, chemical coordination, and the local environment of active sites. Specifically, Raman analysis can sensitively detect oxygen vacancies, strain effects, and electronic interactions with adsorbates, making it highly relevant for elucidating VOC sensing mechanisms. While *ex situ* Raman spectroscopy has been widely applied to characterize SACs in VOC-related studies, *in situ* and operando implementations remain relatively less explored. *In situ* Raman spectroscopy enables real-time monitoring of catalyst evolution under working conditions, offering a deeper understanding of reaction intermediates, structural transformations, and active site dynamics. This technique has been extensively utilized in electrochemical energy systems, including HER, ORR, OER, and batteries, where it has revealed crucial phenomena such as active site restructuring and degradation pathways. However, its potential in VOC sensing has yet to be fully realized.

For example, in HER and OER studies, *in situ* Raman spectroscopy has been employed to track the formation of hydroxide intermediates and their interactions with active sites. Similarly, in ORR investigations, the evolution of oxygen-containing species during the reaction process. Applying this methodology to VOC sensing could provide analogous insights by enabling the detection of VOC adsorption, intermediate species formation, and real-time transformation under sensing conditions.

Future work should aim to adapt *in situ* Raman techniques for VOC sensing applications to bridge this critical knowledge gap. Integration with complementary characterization tools such as XPS, XANES, and EXAFS can provide a more holistic mechanistic understanding, facilitating the rational design of high-performance SAC-based VOC sensors.

Furthermore, combining *operando* Raman spectroscopy with electrical resistance measurements could establish direct correlations between spectral changes and sensing behavior, thereby accelerating progress in SAC-enabled gas sensing technologies.

4.2. Computational approaches: DFT and Machine learning for SA VOC sensors

DFT plays a central role in understanding the electronic and geometric structures of SACs. It provides detailed information on adsorption energies, charge transfer mechanisms, and reaction pathways. In the context of VOC sensing, DFT enables the analysis of adsorption behavior, reaction mechanisms, and defect chemistry by calculating charge transfer dynamics, energy barriers, transition states, and formation energies. DFT has been extensively applied to 2D materials such as TMDs, including WS_2, MoS_2, SnS_2, and CrX_2, as well as dual-atom doped graphdiyne and 2D C_2N, owing to their tunable electronic structures, high surface areas, and strong metal-support interactions [161–165]. These properties make them highly suitable for electrocatalysis, energy storage, and gas sensing applications.

To evaluate the thermodynamic stability of SACs on supporting materials, the binding energy (E_b) is calculated as [166],

$$E_b = E(SA@Substrate) - E(Substrate) - E(SA) \quad (1)$$

where E(SA@Substrate) is the total energy of the SA-loaded system, E (Substrate) is th energy of pristine support, and E(SA) is the energy of the isolated SA.

A recent DFT study investigated the adsorption of eleven VOCs on pristine WS_2, sulfur-vacancy-induced WS_2 (V_S-WS_2), and metal-doped WS_2 (M@WS_2, where Co, Fe, Nb, and Ni). After geometry optimization, the VOC adsorption energy on WS_2 was evaluated using an equation.

$$E_{ads} = E(WS_2 with V_s - WS_2 \quad with M@WS_2@VOC) - E(WS_2 with V_s - WS_2 \quad with M@WS_2) - E(VOCs) \quad (2)$$

where E(WS_2 with V_S−WS_2 with M@WS_2@VOCs) is the total energy of the VOC-adsorbed system, E(WS_2 with V_S−WS_2 with M@WS_2) is the total energy of the substrate, and E(VOCs) is the energy of the isolated VOC molecule.

Adsorption energy trends revealed that octane exhibited the strongest interaction at −0.78 eV, followed by heptane at −0.72 eV, toluene and benzaldehyde (-0.61 eV each), while methylamine, 2-butanone, and dimethyl disulfide demonstrated weaker adsorption with values of −0.26 eV, −0.41 eV, and −0.45 eV, respectively (Fig. 13a). Partial density of states (PDOS) analysis revealed minor shifts due to contributions from O(p), N(p), C(p), and S(p) orbitals of the VOC molecules. The Fermi level shift towards the conduction band minimum indicated n-type semiconductor behavior (Fig. 13b). However, Bader charge analysis and electron localization function plots revealed negligible charge transfer and weak van der Waals interactions in pristine WS_2 (Fig. 13c).

To enhance VOC adsorption, a single sulfur vacancy (V_S-WS_2) was introduced, resulting in a formation energy of −6.19 eV. However, the corresponding adsorption energies (E_{ads}) showed marginal improvements, suggesting that defect engineering alone may not significantly enhance sensing performance. In contrast, transition metal doping led to substantial improvements; binding energies for Co, Fe, Ni, and Nb dopants were calculated as −4.72 eV, −4.06 eV, −4.88 eV, and −8.47 eV, respectively. Among these, Nb-doped WS_2 exhibited the highest affinity for VOCs, with 2-butanone, butanol, and hexanal demonstrating strong chemisorption, registering adsorption energies of −2.09 eV, −2.08 eV, and −1.89 eV, respectively. Bond lengths in the range of 1.96–2.35 Å further supported strong metal-VOC interactions. For optimal gas sensing, the adsorption energy should ideally lie between strong physisorption and weak chemisorption, with E_{ads} values in the range of −1.20 to −2.00 eV [167,168]. While pristine WS_2 and V_S-WS_2 fell outside this optimal range, metal doping, particularly with Nb-enabled favorable VOC adsorption, positioned Nb@WS_2 as a promising candidate for next-generation VOC sensors. Overall, DFT offers critical insights into the intrinsic properties of the SAC system, guiding experimental efforts and mechanistic understanding, as discussed in the previous section.

In parallel, ML has emerged as a prevailing tool to accelerate catalyst discovery and establish structure-activity relationships in SACs [169]. By leveraging extensive experimental and theoretical datasets, ML enhances predictive accuracy and computational efficiency, thereby accelerating the discovery of novel materials and improving the sensing performance of previously untested VOCs. ML-driven approaches facilitate the rapid screening of SAs materials by predicting key parameters such as adsorption energies, activation barriers, and charge transfer properties, enabling the identification of promising candidates with high catalytic activity. Moreover, ML models assist in recognizing key descriptors that govern SAC performance, such as coordination environments, electronic structures, and defect densities, thereby guiding the rational design of optimized catalysts [170]. Beyond accelerating the discovery process, ML-based models and neural networks effectively reduce the computational cost of DFT simulations while preserving accuracy, making large-scale screening of SAC materials feasible. In the context of VOC sensing, ML models have also played a crucial role in improving detection accuracy, selectivity, and response time [171]. Commonly employed models such as Principal Component Analysis (PCA), Support Vector Machines (SVM), Random Forest (RF), k-Nearest Neighbors (k-NN), Artificial Neural Networks (ANN), and Convolutional Neural Networks (CNN) are used to extract features, classify sensor responses, and identify VOC species with improved precision [172].

To illustrate the potential of ML in VOC sensing, advanced ML models like RF, CNNs, and SVMs have demonstrated exceptional performance in gas detection, offering insights applicable to SAC-based systems. RF, an ensemble-based model, aggregates decisions from multiple decision trees to achieve robust classification, even under sensor drift or low signal-to-noise conditions. In a study using SnO_2-based sensor arrays, RF achieved 99 % accuracy in distinguishing structurally similar VOCs, with feature importance metrics (e.g., adsorption energy) highlighting key descriptors relevant to SAC design [173,174].

$$Importance(f_i) = \sum_{t \in T(f_i)} \frac{N_t}{N} \quad \Delta i_t$$

where $T(f_i)$ is the set of nodes where f_i is used, N_t is the number of samples at node t, and Δi_t represents the impurity reduction. Similarly, CNNs excel at extracting spatiotemporal features from raw sensor signals, reducing reliance on manual feature engineering. For instance, a CNN framework integrating time-variant illumination in a μLED-based sensor achieved ~97 % accuracy in identifying methanol, ethanol, acetone, and NO_2 at sub-ppm levels, while another CNN model using grayscale-transformed resistance-time matrices classified acetone and formaldehyde with 100 % accuracy [175,176]. The CNN convolution operation is defined as [177]:

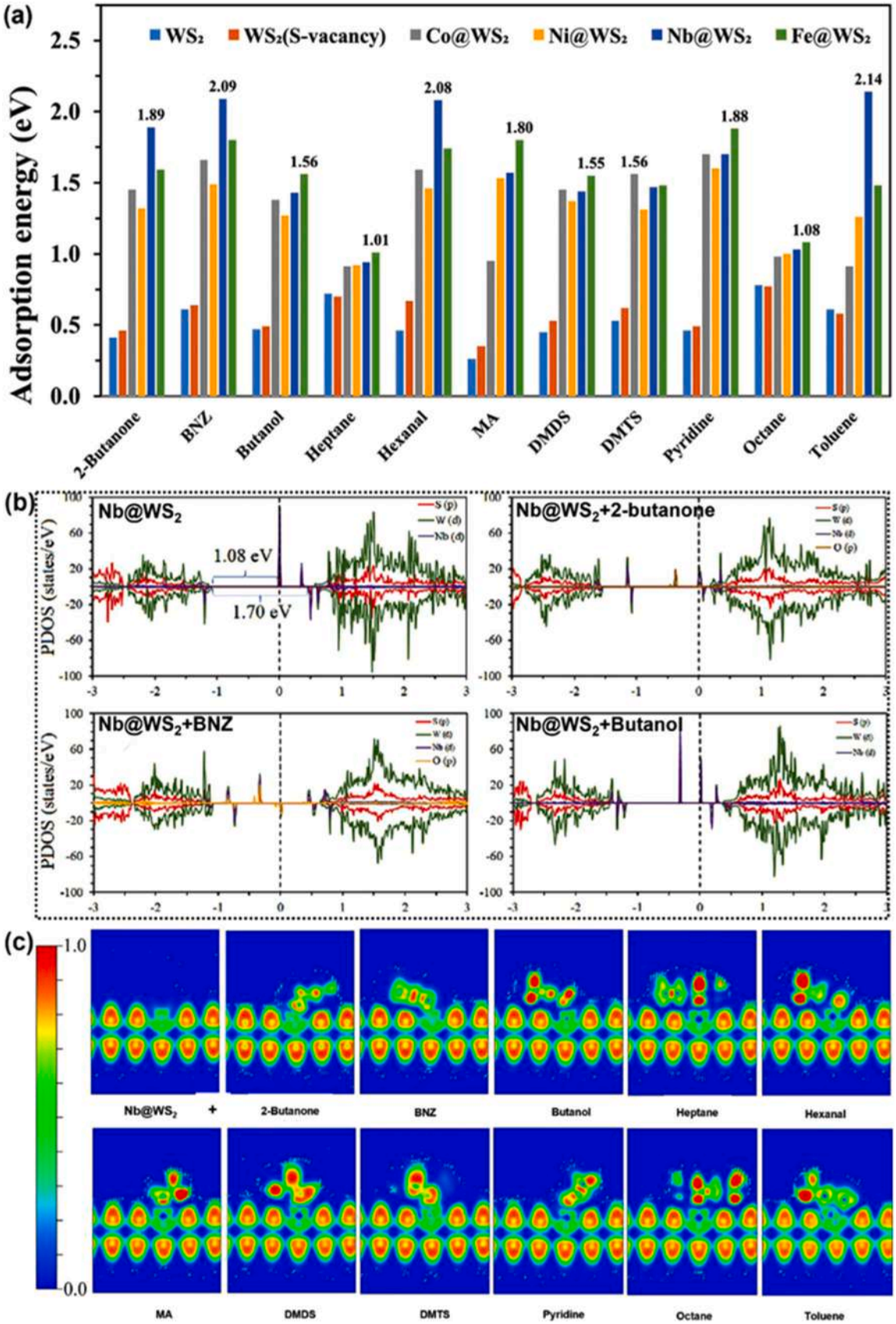

Fig. 13. (a) Adsorption energies (E_{ads}) of VOCs on WS_2, VS-WS_2, and M@WS_2 (M=Co, Fe, Nb, Ni). (b) DOS variations upon VOC adsorption. (c) ELF plots of Nb@WS_2 and its interactions with various VOCs, illustrating electron distribution (0: absent, ~0.5: uniform, 1: localized). Reprinted with permission from Ref. [161].

$$Output(i, \quad j) = \sum_{m=0}^{M-1} \sum_{n=0}^{N-1} Input(i+m, j+n) \quad .K(m,n)$$

SVMs, effective in low-data regimes, achieved up to 100 % accuracy in hybrid RF-SVM frameworks, using kernel-based decision functions [178,179].

$$f(x) \quad = sign(\sum_{i=1}^{n} \alpha_i y_i K(x_i, \quad x) + b)$$

These high accuracies (97–100 %) in non-SAC sensing materials suggest that RF, CNNs, and SVMs, when combined with DFT-derived SAC descriptors (e.g., adsorption energy, charge transfer), could significantly enhance the selectivity and sensitivity of SAC-based VOC sensors. Table 6 summarizes a range of ML models applied to conventional VOC sensors, highlighting their potential and outcomes, which serve as a foundation for advancing SAC-based sensing applications [173, 175, 176, 180–185]. Drawing on the ML approaches summarized in Table 6 [186], the integration of such models into SAC-based VOC sensor systems can follow a systematic workflow to ensure optimal performance, as shown in Fig. 14a. The process begins with data acquisition, where sensor response data is collected under controlled conditions to capture baseline signals and VOC-specific responses while monitoring environmental parameters like temperature and humidity to reduce noise. In the preprocessing stage, techniques such as data normalization, scaling, and outlier detection are applied to enhance data consistency and improve model reliability. Subsequently, feature extraction and selection methods, such as PCA or Recursive Feature Elimination (RFE), are utilized to identify critical features while eliminating redundant information. The refined dataset is then employed for model training and validation, where supervised algorithms are trained with labeled data and assessed using cross-validation methods to prevent overfitting and ensure model robustness. The trained model is then applied for prediction and classification, where it classifies unknown VOC samples based on sensor response patterns, improving real-time detection in practical applications. Following this, performance evaluation using metrics such as accuracy, precision, recall, and F1-score (combined precision and recall) ensures comprehensive model assessment, while confusion matrix analysis aids in refining model predictions. Lastly, the model is integrated into the sensor system for deployment and monitoring, enabling real-time VOC detection with periodic recalibration to maintain performance stability. Fig. 14b presents a representative scheme highlighting the role of ML in gas sensor detection and analysis of unknown gas inputs [187]. This integrated ML framework strengthens VOC sensor systems, ensuring precise detection, improved stability, and enhanced data interpretation, advancing their role in environmental monitoring, industrial safety, and healthcare applications.

In the discovery of new materials, the integration of DFT-calculated parameters with ML models has

shown significant potential in improving VOC sensor performance by enhancing predictive accuracy and identifying key material features. In a representative study, Hu and co-workers employed a data-enhanced network strategy to optimize gas-sensitive materials [188]. The workflow began with DFT calculations to extract critical parameters such as adsorption energy, bond distances (d), and structural distortions (Δd), which were used as input features for model training (Fig. 15a). Eight ML classifiers, including convolutional neural network (CNN), multilayer perceptron (MLP), random forest (RF), logistic regression (Logist), decision tree (Tree), support vector machine (SVM), bagging classifier (Bagging), and voting classifier (Voting), were evaluated to determine the most effective predictive model (Fig. 15b). Fig. 15c shows that the voting classifier achieved the highest accuracy (85.71 %), surpassing bagging (57.14 %) and other models (71.43 %). The receiver operating characteristic (ROC) curve analysis further validated the

robustness of the voting classifier, with its area under the curve (AUC) values closely approaching 1, signifying superior performance. Further, feature analysis identified adsorption energy, a key descriptor derived from DFT data, as one of the most influential features in predicting VOC response. Pearson correlation analysis and feature importance ranking reinforced that E_{ads}, along with selected structural parameters (d and Δd), played a pivotal role in enhancing model performance (Fig. 15 d, e). The confusion matrix shown in Fig. 15f further confirms the voting classifier's high prediction accuracy and robustness against misclassification. This approach highlights the synergistic combination of DFT data and ML algorithms, demonstrating how electronic structure insights can guide the rational design of VOC sensors with improved accuracy, selectivity, and stability. By leveraging data-driven strategies, VOC sensor development can be accelerated, offering innovative solutions for environmental monitoring and industrial safety.

While ML models have been extensively explored for VOC sensors [189], their application in SAC-based VOC sensors remains relatively limited. Leveraging DFT-derived SAC parameters, such as adsorption energies, charge transfer characteristics, and geometric descriptors, can significantly enhance the predictive capabilities of ML models in this

Table 6
Representative ML model in VOC sensing.

S. No	ML Model	Category	Potentials	Target VOCs	Case Sensor Systems	Ref
1	Random Forest	Supervised (Ensemble)	Robust to noise, ranks feature importance	Formaldehyde, methanol, 2-propanol, toluene, acetone, benzene, ethanol	SnO_2-based and noble-metal-decorated sensor arrays	[175,176]
2	Support Vector Machines	Supervised (Kernel-based)	Effective for small dataset, high precision	Benzene, toluene, acetone, ethanol	Pd-glass, zeolite–oxide systems, Metal oxides	[174,175, 180,181]
3	Convolution Neural Network	Deep Learning	Learns from raw signals, high dimensionality support	Ethanol, acetone, methanol, formaldehyde, benzene	μLED dynamic sensors, In_2O_3-based sensors	[182,183]
4	Artificial Neural Network	Supervised (Neural)	Capture non-linear relationships	Ethanol, Formaldehyde, benzene, toluene	Noble-metal In_2O_3 arrays, Cr and Pd doped In_2O_3	[183]
5	Multilayer Perception	Supervised, Feedforward	Flexible architecture for small to mid-size datasets	Methanol, toluene, formaldehyde, 2-propanol	SnO_2 and hybrid oxide sensors	[175]
6	Linear Regression	Supervised (Linear)	Interpretable, suitable for concentration estimation	Acetone, benzene, ethanol, toluene, formaldehyde, isobutanol	Metal oxide associated MEMS-based VOC sensor array	[184,185]
7	Principal Component Analysis	Unsupervised Feature Reduction	Reduces data dimensionality; enhances model performance	Acetone, ethanol, benzene, toluene formaldehyde, methanol	ZnO, In_2O_3-based sensor arrays	[180,183, 186]
8	K-Nearest Neighbor (k-NN)	Supervised, Distance-based	Easy to implement; no model training required	Ethanol, methanol, acetone	rGO/CuCoOx sensor system, metal oxides	[186] [190]
9	Deep Neural Network	Deep Learning	Learns complex patterns; scalable to multi-gas and mixture data	Ethanol, formaldehyde, benzene, toluene	Cr/Pd-doped In_2O_3 arrays	[183]

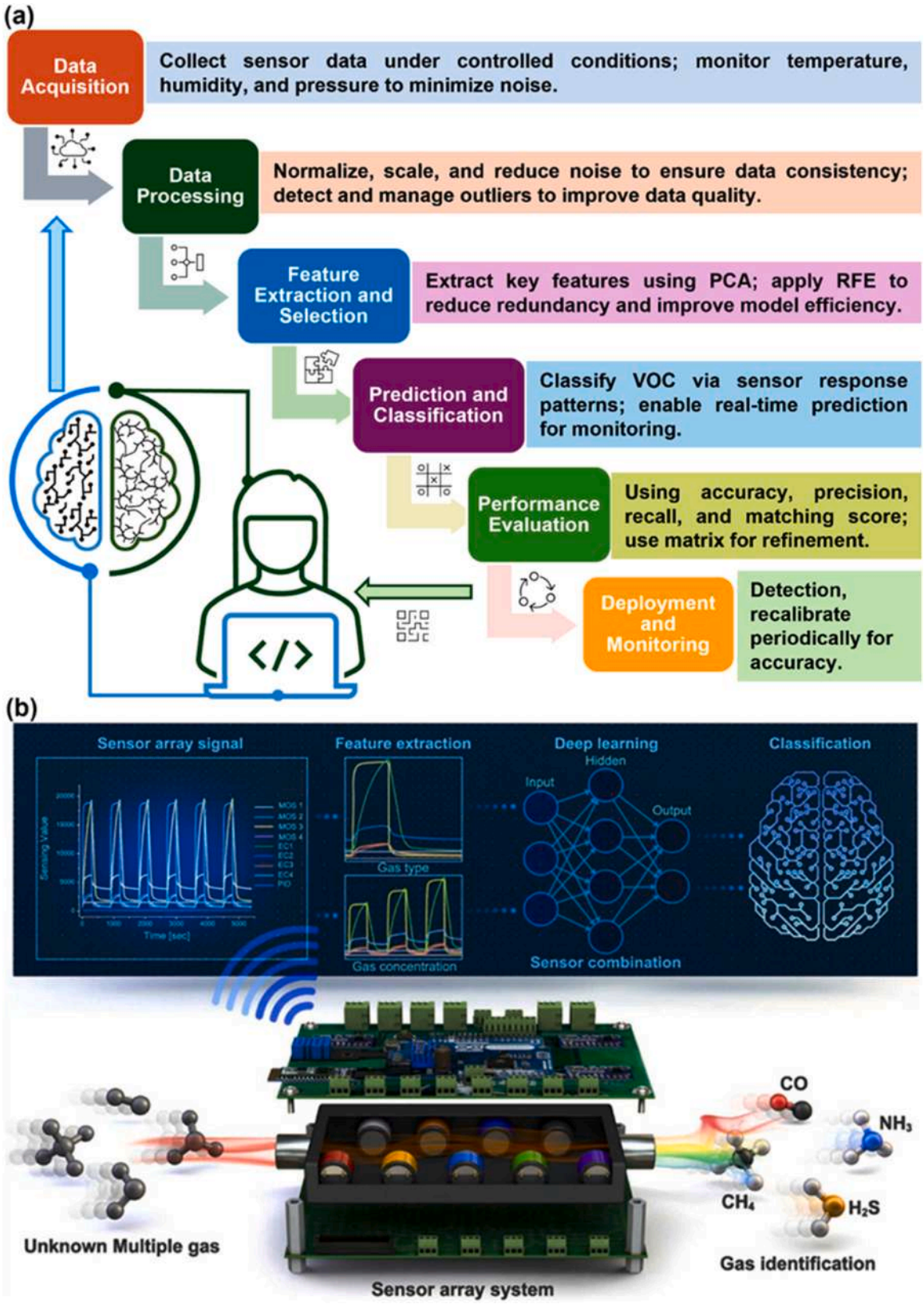

Fig. 14. (a) Machine learning framework for VOC detection and sensor material design. (b) Example of an integrated sensor system demonstrating the detection of unknown gases Reprinted with permission from Ref. [186].

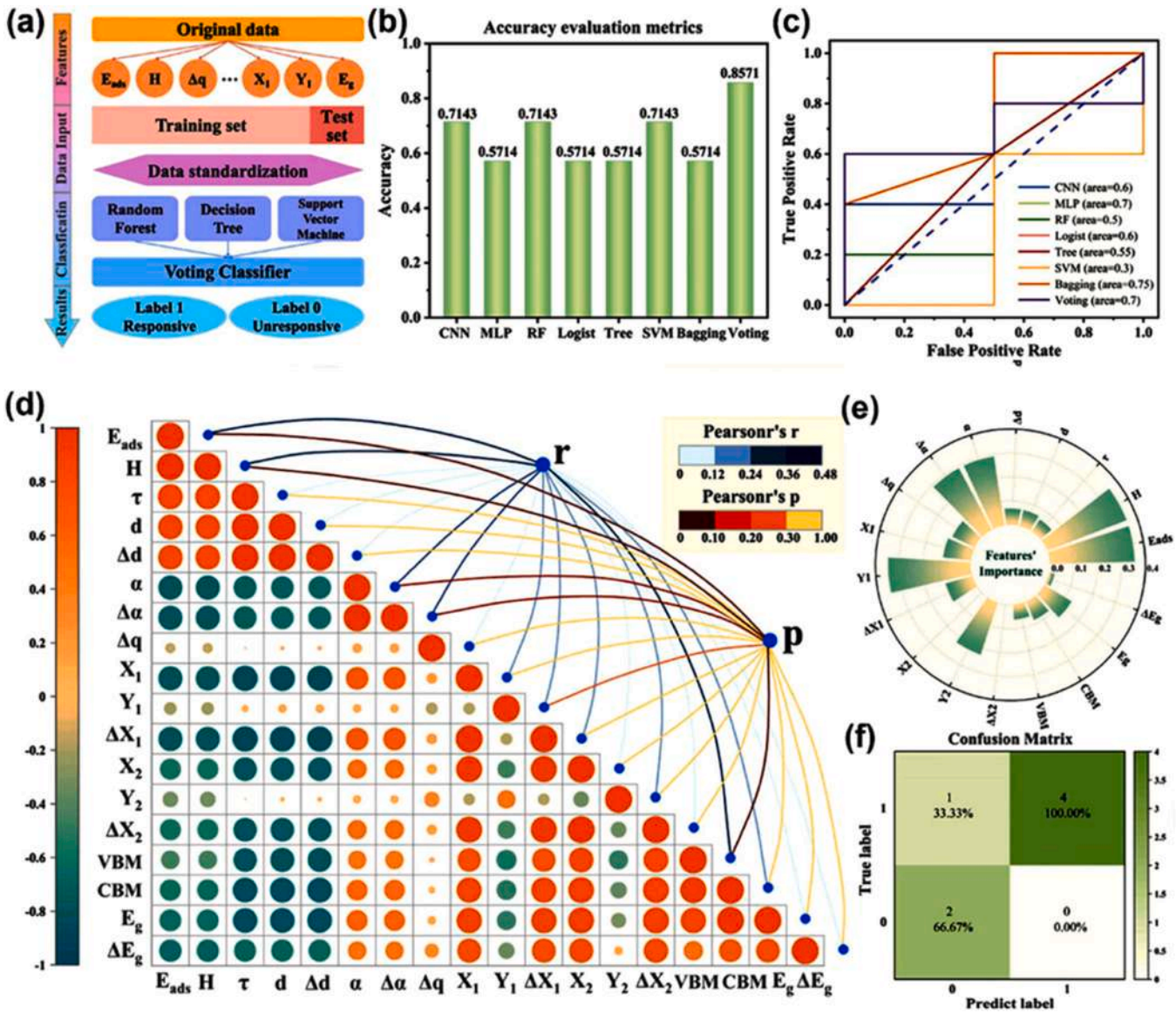

Fig. 15. Overview of the ML-based analysis framework for VOC sensing; (a) Workflow depicting data acquisition, preprocessing, model training, and evaluation. (b) Classification model accuracy comparison for VOC detection. (c) Receiver operating characteristic (ROC) curve highlighting model performance. (d) Pearson correlation analysis illustrating feature relevance to VOC classification. (e) Statistical significance of 18 selected features influencing sensor response. (f) Confusion matrix demonstrating model prediction outcomes for the test dataset Reprinted with permission from Ref. [188].

context. For instance, Liu et al. utilized ML to evaluate metal-2D SACs and predict their response intensity in SAC-based chemical sensors [158].

The gradient boosting regression (GBR) model exhibited superior predictive performance when incorporating four key descriptors; charge transfer (δ_{CT}), metal charge (q_M), metal-oxygen distance ($D_{M\text{-}O}$), and VOC type. Unlike conventional ML models that primarily predict binding energies (Fig. 16a), this approach introduced VOC classification (e.g., acetone, ethanol, and RH labeled as 1, 2, and 3, respectively) to refine response intensity predictions. As depicted in Fig. 16b, the integration of these four descriptors enabled accurate prediction of response intensity, achieving a Pearson correlation coefficient of approximately 0.79, thereby validating the model's robustness.

The integration of DFT with ML-driven methodologies offers a synergistic pathway for tailoring SACs with enhanced properties for VOC sensing. Future advancements in self-learning models,

capable of iteratively refining theoretical predictions based on experimental feedback, hold the potential to revolutionize the field, paving the way for more intelligent and efficient catalyst design strategies.

5. Current state of the art, limitations and future prospects

Although significant progress has been made in the development of SAES for VOC detection, further advancements are required to move beyond proof-of-concept studies and achieve reliable, real-world applications. This section outlines key research gaps, grounded in current successes and limitations, and proposes well justified research directions for future studies (Table 7).

1. Achievement: SAES exhibits ultra-high sensitivity and atom-efficient design.

   Problem: Many VOCs possess similar molecular weights, chemical structures, and binding affinities, making it extremely difficult to differentiate between analytes like methanol, ethanol, benzene, and toluene. In real-world environments, temperature and humidity

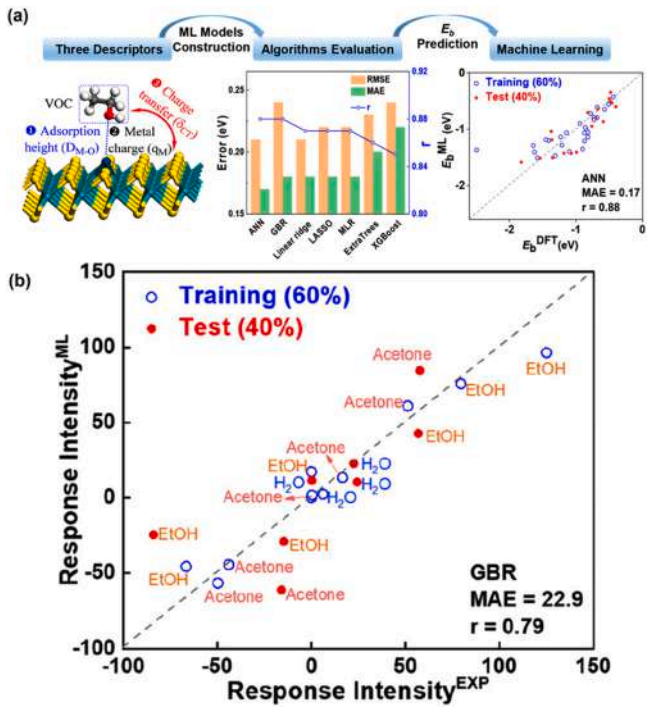

Fig. 16. (a) Schematic representation of ML-based prediction of E_{ads} using three key descriptors (δ_{CT}, q_M, and D_{M-O}), with performance assessed via RMSE, MAE, and r, highlighting ANN as the most effective model. (b) Comparison of ML-predicted and experimentally observed values using four descriptors (δ_{CT}, q_M, D_{M-O}, and VOC). Reprinted with permission from Ref. [158].

fluctuations further impair performance.

Future Research: Develop selectivity tuned SAES by engineering the coordination environment of the single atoms (e.g., via N, S, or P heteroatom anchoring) to introduce analyte specific recognition. Tune site specific functionalization (e.g., -OH, -COOH and -NH_2 groups) on the sensor surface to create chemical fingerprints for VOCs. Construct multichannel sensor arrays (e- nose systems) with different SA sites, coupled with machine learning algorithms for cross-analyte recognition under variable humidity and temperature.

2. Achievement: Atomic dispersion ensures maximum atom utilization and catalytic performance.

   Problem: The high surface energy of single atoms leads to agglomeration or migration, particularly under operational conditions or long-term storage, resulting in loss of sensitivity.

   Future Research: Apply defect-engineered supports (e.g., graphene vacancies, oxygen-rich MXenes, or doped carbon frameworks) to strongly anchor single atoms and prevent mobility. Investigate dual-atom or cluster-based strategies, where synergistic interactions between adjacent atoms prevent aggregation while enhancing sensing performance. Develop real-time operando STEM imaging and thermal stability studies to understand atom dynamics and sensor degradation over time.

3. Achievement: SAES shows rapid response and recovery times for real-time sensing.

   Problem: Signal fluctuations and poor reproducibility are observed in real-world scenarios due to interference from environmental factors and the dynamic interaction of VOCs with atomic sites.

   Future Research: Integrate dynamic compensation mechanisms, such as humidity tolerant layers or self-calibration feedback loops, in sensor devices. Embed nanoelectronic transducers (e.g., FET- based architectures) for enhanced signal-to-noise ratios and stable outputs. Use adaptive learning systems that train the sensor response over time for drift correction and stable performance in field settings.

Table 7
Summary of key challenges and potential solutions in SAES for VOC detection.

Challenges	Impact	Possible solutions
Agglomeration of single atoms	Loss of activity; cluster formation	Use of strong anchoring sites (N, O, S); defect engineering; MOF-derived and carbon supports
Low metal loading limits	Insufficient active sites; low signal strength	Optimized SA dispersion; dual-atom or cluster engineering
Uncontrolled coordination environment	Inconsistent sensor performance	Advanced synthesis methods like ALD, wet-chemistry control, and coordination-tuned precursors
Thermal and chemical instability	Degradation during sensing cycles	Design of thermally robust supports; hydrophobic coatings
Overlapping binding affinities among VOCs	Poor selectivity	Functional group engineering; heteroatom doping; sensor arrays with AI classifiers
Environmental interference (e.g., humidity, CO_2)	False signals or signal drift	Surface passivation; hydrophobic coatings; machine learning correction algorithms
Weak signal intensity	Low sensitivity	Signal amplification techniques (e.g., transducers, hybrid sensing platforms)
Irreversible VOC binding	Loss of reusability and sensitivity	Reversible binding designs; optimal binding energy tuning (via DFT)
Complex and inconsistent synthesis	Poor reproducibility	Green, scalable protocols like electrospinning, spray pyrolysis, ionic liquids
Limited real-time/ operando mechanistic data	Incomplete understanding of working principles	Adoption of operando XAS, XPS, DRIFTS, Raman, EPR
Lack of advanced characterization	Difficulty confirming SA dispersion or VOC interaction	STEM-EELS, HAADF-STEM, EXAFS, in-situ spectroscopy
Idealized DFT models	Theoretical predictions deviate from experiments	Combine DFT with solvent effects, machine learning, or experimental data
Trial-and-error material screening	Low efficiency in sensor design	ML-guided material selection; high-throughput DFT screening
Short operational lifespan	Limited real-world utility	Durability testing; encapsulation; environmental shielding
Incompatibility with flexible substrates	Hinders development of wearable/flexible sensors	Use of SA-hybrid materials on polymer or 2D conductive platforms
Poor signal reproducibility	Inaccurate detection; unreliable calibration	Device standardization and real-time calibration mechanisms
Difficult film uniformity during deposition	Batch-to-batch variation; noisy signals	Blade coating, inkjet printing, or self-assembled monolayer techniques
Low scalability of synthesis	Barrier to industrial translation	Scalable green routes: solvothermal, self-assembly, and spray deposition
High reliance on noble metals	Expensive and limited resource availability	Explore earth-abundant metals (Fe, Co, Ni, Mn, Cu, Al)
Poor technoeconomic viability	Cost outweighs performance gains	Optimize sensor performance per unit metal; replace noble metals with cost-effective alternatives
Limited validation under real sample conditions	Lab results may not translate to field conditions	Conduct testing in real air samples from industry, hospitals, and cities
Lack of standard benchmarking protocols	Hard to compare SAES across studies	Develop standard test protocols (gas exposure, humidity control, stability)
Unclear signal origin (SA vs support effect)	Misinterpretation of sensing mechanism	Combine operando spectroscopy with site-specific theoretical analysis

(*continued on next page*)

Table 7 (*continued*)

Challenges	Impact	Possible solutions
Insufficient integration into devices	Standalone materials, not usable devices	Integrate SAES into complete sensor platforms (chips, wireless modules, IoT systems)
Environmental and disposal issues	Toxicity and sustainability concerns	Use of eco-friendly synthesis, biodegradable supports, and recycling strategies

4. Achievement: Proof of concept SAES developed in laboratory settings.

   Problem: The scalability and process reproducibility of these sensors remain unproven for large- scale industrial production.

   Future Research: Develop green, low-temperature, and solution-processable synthesis routes such as UV-assisted photochemical reduction, ionic-liquid-mediated synthesis, electrospinning, or ultrasonic spray pyrolysis. Standardize scalable deposition techniques (e.g., inkjet printing, roll to roll coating) for sensor fabrication on flexible substrates. Design pilot-scale demonstration modules and field-testing prototypes to validate stability and reproducibility over months of operation.
5. Achievement: Initial mechanistic insights from DFT and basic spectroscopy.

   Problem: The fundamental sensing mechanism, including electron transfer, adsorption geometry, and reaction intermediates, remains poorly understood at the atomic scale.

   Future Research: Employ advanced in situ and operando spectroscopies (e.g., XPS, XAS, DRIFTS, EPR, Raman, and STEM) during VOC exposure to capture real-time changes in SA oxidation state and bonding configuration. Correlate experimental data with DFT calculated adsorption energies, charge distributions, and orbital overlaps for various VOCs on specific SA sites. Explore transient techniques (e.g., pulsed voltammetry-based sensing or TPD-MS coupling) to monitor fast electron transfer and desorption kinetics.
6. Achievement: DFT modeling has begun to assist material selection and screening.

Problem: The trial and error approach remains dominant; DFT alone cannot easily predict complex, real-world behavior involving competing analytes and interference.

Future Research: Combine machine learning (ML) with DFT databases to predict optimal metal support ligand configurations tailored for VOC sensing. Apply inverse design models to propose novel SAES systems with target performance metrics (e.g., selectivity for benzene in the presence of toluene). Create open-source knowledge platforms integrating theoretical predictions with experimental feedback to guide community wide sensor optimization.

5.1. Conclusions

Single-atom engineered sensors (SAES) represent a transformative advancement in the field of VOC detection due to their unparalleled atom efficiency, tunable electronic structures, and precise molecular recognition capabilities. Through the engineering of isolated atomic sites and their surrounding coordination environments, SAES provides superior sensitivity and selectivity, enabling the detection of trace level VOCs with rapid response and minimal cross interference. These attributes make them particularly suited for applications ranging from environmental monitoring to food safety and biomedical diagnostics. However, realizing the full potential of SAES demands overcoming persistent challenges related to their synthesis, long term stability, and large-scale fabrication. Preventing atom agglomeration, ensuring robust anchoring, and addressing environmental interferences remain critical hurdles. Furthermore, an incomplete mechanistic understanding of SAES VOC interactions continues to limit rational sensor design. In this regard, in situ and operando spectroscopies, along with density functional theory (DFT) calculations and machine learning algorithms, are essential tools for decoding the atomistic pathways that govern sensor behavior and performance. Looking forward, interdisciplinary efforts that integrate materials chemistry, surface science, and data driven modeling are crucial to optimize SAES for real world deployment. The use of earth abundant metals, advanced defect engineering, and dual or multi atom configurations will broaden the design space and functional applicability of these sensors. Furthermore, establishing industrially relevant testing protocols will be vital for scaling SAES technologies from laboratory prototypes to commercial sensor platforms. In essence, while SAES are still in their developmental stage, their promise is undeniable. With continued innovations in material design and mechanistic insight, SAES is poised to redefine how we monitor and respond to volatile organic pollutants in increasingly complex environments.

CRediT authorship contribution statement

Sowjanya Vallem: Writing review & editing, Writing original draft, Visualization, Conceptualization. **Malayil Gopalan Sibi:** Writing review & editing, Visualization. **K. Keerthi**: Writing review & editing. **Anam Giridhar Babu**: Writing review & editing. **Vishaka Goyal**: Writing review & editing. **Lohit EA**: Writing review & editing. **Jyothi N. V.V.**: Writing review & editing. **K. Praveena**: Writing review & editing. **Kasibhatta Sivakumar**: Writing review & editing. **T.G. Satheesh Babu**: Writing review & editing, Visualization. **P.V. Suneesh**: Writing review & editing. **Hari Bandi**: Writing review & editing, Visualization. **Daniel-Ioan Stroe**: Writing review & editing, Visualization. **Sada Venkateswarlu**: Conceptualization, Writing review & editing, Writing original draft, Visualization. **Aristides Bakandritsos**: Writing review & editing, Visualization, Supervision, Funding acquisition. **Rajenahally Jagadeesh**: Writing review & editing, Visualization, Validation, Supervision, Conceptualization. **Radek Zboril**: Writing review & editing, Validation, Supervision, Project administration, Funding acquisition, Conceptualization.

Data Statement

No data were generated for the production of this work.

Declaration of Competing Interest

The authors declared no conflict of interest

Acknowledgment

This article has been produced with the financial support of the European Union under the REFRESH – Research Excellence for REgion Sustainability and High-tech Industries project number CZ.10.03.01/00/22_003/0000048 via the Operational Programme Just Transition and also with the support of ERDF/ESF project TECHSCALE No. CZ.02.01.01/00/22_008/0004587. A.B. also acknowledges the support from the European Union and project 2D-BioPAD (project no. 101120706).

Data Availability

Data will be made available on request.

References

[1] M.C. Magnano, W. Ahmed, R. Wang, M.B. Marusic, S.J. Fowler, I.R. White, Exhaled volatile organic compounds and respiratory disease: recent progress and future outlook, Trends Anal. Chem. 176 (2024) 11773, https://doi.org/10.1016/j.trac.2024.117739.

[2] F.A. Pitten, J. Bremer, A. Kramer, Indoor air pollution caused by volatile organic compounds (VOCs) and health problems, Germ. Med. Wkly. 125 (2000) 545–550, https://doi.org/10.1055/s-2007-1024338.

[3] S.K. Brown, M.R. Sim, M.J. Abramson, C.N. Gray, Concentrations of volatile organic compounds in indoor air a review, Indoor Air 4 (1994) 123–134, https://doi.org/10.1111/j.1600-0668.1994.t01-2-00007.x.

[4] C. He, J. Cheng, X. Zhang, M. Douthwaite, S. Pattisson, Z. Hao, Recent advances in the catalytic oxidation of volatile organic compounds: a review based on pollutant sorts and sources, Chem. Rev. 119 (2019) 4471–4568, https://doi.org/10.1021/acs.chemrev.8b00408.

[5] Z. Cheng, B. Li, W. Yu, H. Wang, T. Zhang, J. Xiong, Z. Bu, Risk assessment of inhalation exposure to VOCs in dwellings in chongqing, china, Toxicol. Res. 7 (2017) 59–72, https://doi.org/10.1039/c7tx00191f.

[6] Q. Zhao, Q. Wang, Y. Li, P. Ning, S. Tian, Influence of volatile organic compounds (VOCs) on pulmonary surfactant monolayers at air-water interface: Implication for the pulmonary health, Colloids Surf. A Physicochem. Eng. Asp. 562 (2019) 402–408, https://doi.org/10.1016/j.colsurfa.2018.11.056.

[7] M. Hakim, Y.Y. Broza, O. Barash, N. Peled, M. Phillips, A. Amann, H. Haick, Volatile organic compounds of lung cancer and possible biochemical pathways, Chem. Rev. 112 (2012) 5949–5966, https://doi.org/10.1021/cr300174a.

[8] A.H. Jalal, F. Alam, S. Roychoudhury, Y. Umasankar, N. Pala, S. Bhansali, Prospects and challenges of volatile organic compound sensors in human healthcare, ACS Sens 3 (2018) 1246–1263, https://doi.org/10.1021/acssensors.8b00400.

[9] A. Panda, S.K. Arumugasamy, J. Lee, Y. Son, K. Yun, S. Venkateswarlu, M. Yoon, Chemical-free sustainable carbon nano-onion as a dual-mode sensor platform for noxious volatile organic compounds, Appl. Surf. Sci. 537 (2021) 147872, https://doi.org/10.1016/j.apsusc.2020.147872.

[10] P. Hajivand, J.C. Jansen, E. Pardo, D. Armentano, T.F. Mastropietro, A. Azadmehr, Application of metal-organic frameworks for sensing of VOCs and other volatile biomarkers, Coord. Chem. Rev. 501 (2024) 215558, https://doi.org/10.1016/j.ccr.2023.215558.

[11] M. Khatib, H. Haick, Sensors for volatile organic compounds, ACS Nano 16 (2022) 7080–7115, https://doi.org/10.1021/acsnano.1c10827.

[12] J. Dewulf, H. Van Langenhove, G. Wittmann, Analysis of volatile organic compounds using gas chromatography, Trends Anal. Chem. 21 (2002) 637–646, https://doi.org/10.1016/S0165-9936(02)00804-X.

[13.] A.J. Barbosa, A.R. Oliveira, A.C. Roque, Protein- and peptide-based biosensors in artificial olfaction, Trends Biotechnol. 36 (2018) 12441258, https://doi.org/10.1016/j.tibtech.2018.07.004.

[14] Y. Zhao, Y. Liu, B. Han, M. Wang, Q. Wang, Y. Zhang, Fiber optic volatile organic compound gas sensors: a review, Coord. Chem. Rev. 493 (2023) 215297, https://doi.org/10.1016/j.ccr.2023.215297.

[15] Z. Lin, J. Abbott, P. Karuso, D.K. Wong, Advances in electroanalytical sensing of volatile organic compounds towards field-deployable detection, Trends Anal. Chem. 183 (2025) 118101, https://doi.org/10.1016/j.trac.2024.118101.

[16] Sagnik Das, Subhajit Mojumder, Debdulal Saha, Mrinal Pal, Influence of major parameters on the sensing mechanism of semiconductor metal oxide based chemiresistive gas sensors: a review focused on personalized healthcare, Sens. Actuators B Chem. 352 (2022) 131066, https://doi.org/10.1016/j.snb.2021.131066.

[17] A. Mirzaei, S.G. Leonardi, G. Neri, Detection of hazardous volatile organic compounds (VOCs) by metal oxide nanostructures-based gas sensors: a review, Ceram. Int. 42 (2016) 15119–15141, https://doi.org/10.1016/j.ceramint.2016.06.145.

[18] Z. Li, W. Zeng, Q. Li, SnO_2 as a gas sensor in detection of volatile organic compounds: A review, Sens. Actuators A Phys. 346 (2022) 113845, https://doi.org/10.1016/j.sna.2022.113845.

[19] S. Deng, X. Liu, N. Chen, D. Deng, X. Xiao, Y. Wang, A highly sensitive VOC gas sensor using p-type mesoporous Co_3O_4 nanosheets prepared by a facile chemical coprecipitation method, Sens. Actuators B Chem. 233 (2016) 615–623, https://doi.org/10.1016/j.snb.2016.04.138.

[20] K. Swargiary, S. Thaneerat, N. Kongsawang, A.K. Pathak, C. Viphavakit, Highly sensitive and real-time detection of acetone biomarker for diabetes using a ZnO-coated optical fiber sensor, Biosens. Bioelectron. 271 (2025) 117061, https://doi.org/10.1016/j.bios.2024.117061.

[21] W. Geng, S. Ge, X. He, S. Zhang, J. Gu, X. Lai, H. Wang, Q. Zhang, Volatile organic compound gas-sensing properties of bimodal porous α-Fe_2O_3 with ultrahigh sensitivity and fast response, ACS Appl. Mater. Interfaces 10 (2018) 13702–13711, https://doi.org/10.1021/acsami.8b02435.

[22] L. Kong, Z. Yuan, H. Gao, F. Meng, Recent progress of gas sensors based on metal oxide composites derived from bimetallic metal-organic frameworks, Trends Anal. Chem. 166 (2023) 117199, https://doi.org/10.1016/j.trac.2023.117199.

[23] S.Y. Cho, H. Yoo, J.Y. Kim, W. Jung, M.L. Jin, J. Kim, H. Jeon, H. Jung, High-resolution p-type metal oxide semiconductor nanowire array as an ultrasensitive sensor for volatile organic compounds, Nano Lett. 16 (2016) 4508–4515, https://doi.org/10.1021/acs.nanolett.6b01713.

[24] J.M. Walker, S.A. Akbar, P.A. Morris, Synergistic effects in gas sensing semiconducting oxide nano-heterostructures: a review, Sens. Actuators B Chem. 286 (2019) 624–640, https://doi.org/10.1016/j.snb.2019.01.049.

[25] F. He, Y. Zhang, H. Chen, H. Wang, H. Li, Q. Qin, Y. Li, Highly sensitive and selective gas sensor based on SnO_2/Fe_2O_3@rGO nanocomposite for detection of formaldehyde, Mater. Chem. Phys. 312 (2014) 128646, https://doi.org/10.1016/j.matchemphys.2023.128646.

[26] F. Li, T. Zhang, X. Gao, R. Wang, B. Li, Coaxial electrospinning heterojunction SnO_2/Au-doped In_2O_3 core-shell nanofibers for acetone gas sensor, Sens. Actuators B Chem. 252 (2017) 822–830, https://doi.org/10.1016/j.snb.2017.06.077.

[27] L. Zhu, L. Ou, L. Mao, X. Wu, Y. Liu, H. Lu, Advances in noble metal-decorated metal oxide nanomaterials for chemiresistive gas sensors: overview, NanoMicro Lett. 15 (2023) 89, https://doi.org/10.1007/s40820-023-01047-z.

[28] R. Bhardwaj, V. Selamneni, U.N. Thakur, P. Sahatiya, A. Hazra, Detection and discrimination of volatile organic compounds by noble metal nanoparticle functionalized MoS_2 coated biodegradable paper sensors, N. J. Chem. 44 (2020) 16613–16625, https://doi.org/10.1039/D0NJ03491F.

[29] Md.R. Awual, Md.M. Hasan, H. Znad, Organic-inorganic based nano-conjugate adsorbent for selective palladium(II) detection, separation and recovery, Chem. Eng. J. 259 (2014) 611–619, https://doi.org/10.1016/j.cej.2014.08.028.

[30] Md.R. Awual, Md.M. Hasan, A.M. Asiri, M.M. Rahman, Novel optical composite material for efficient vanadium(III) capturing from wastewater, J. Mol. Liq. 283 (2019) 704–712, https://doi.org/10.1016/j.molliq.2019.03.119.

[31] Md.R. Awual, Md.M. Hasan, G.E. Eldesoky, Md.A. Khaleque, M.M. Rahman, Mu Naushad, Facile mercury detection and removal from aqueous media involving ligand impregnated conjugate nanomaterials, Chem. Eng. J. 290 (2016) 243–251, https://doi.org/10.1016/j.cej.2016.01.038.

[32] Md.R. Awual, A. Islam, M.M. Hasan, M.M. Rahman, A.M. Asiri, M.A. Khaleque, M.C. Sheikh, Introducing an alternate conjugated material for enhanced lead(II) capturing from wastewater, J. Clean. Prod. 224 (2019) 920–929, https://doi.org/10.1016/j.jclepro.2019.03.241.

[33] Md.R. Awual, N.H. Alharthi, Y. Okamoto, M.R. Karim, Md.E. Halim, Md. M. Hasan, M.M. Rahman, Md.M. Islam, Md.A. Khaleque, Md.C. Sheikh, Ligand field effect for dysprosium(III) and lutetium(III) adsorption and EXAFS coordination with novel composite nanomaterials, Chem. Eng. J. 320 (2017) 427–435, https://doi.org/10.1016/j.cej.2017.03.075.

[34] Md.R. Awual, New type mesoporous conjugate material for selective optical copper(II) ions monitoring & removal from polluted waters, Chem. Eng. J. 307 (2016) 85–94, https://doi.org/10.1016/j.cej.2016.07.110.

[35] Md.C. Sheikh, Md.M. Hasan, Md.N. Hasan, Md.S. Salman, K.T. Kubra, E. Awual, R.M. Waliullah, A.I. Rasee, A.I. Rehan, M.S. Hossain, H.M. Marwani, A. Islam, Md.A. Khaleque, Md.R. Awual, Toxic cadmium(II) monitoring and removal from aqueous solution using ligand-based facial composite adsorbent, J. Mol. Liq. 389 (2023) 122854, https://doi.org/10.1016/j.molliq.2023.122854.

[36] Md.R. Awual, A facile composite material for enhanced cadmium(II) ion capturing from wastewater, J. Environ. Chem. Eng. 7 (2019) 103378, https://doi.org/10.1016/j.jece.2019.103378.

[37] Md.S. Salman, Md.N. Hasan, K.T. Kubra, Md.M. Hasan, Optical detection and recovery of Yb(III) from waste sample using novel sensor ensemble nanomaterials, Microchem. J. 162 (2020) 105868, https://doi.org/10.1016/j.microc.2020.105868.

[38] Md.R. Awual, Md.M. Hasan, A. Shahat, Mu Naushad, H. Shiwaku, T. Yaita, Investigation of ligand immobilized nano-composite adsorbent for efficient cerium(III) detection and recovery, Chem. Eng. J. 265 (2014) 210–218, https://doi.org/10.1016/j.cej.2014.12.052.

[39] Md.R. Awual, A novel facial composite adsorbent for enhanced copper(II) detection and removal from wastewater, Chem. Eng. J. 266 (2015) 368–375, https://doi.org/10.1016/j.cej.2014.12.094.

[40] M.S. Hossain, M.A. Shenashen, E. Awual, A.I. Rehan, A.I. Rasee, R.M. Waliullah, K.T. Kubra, Md.S. Salman, Md.C. Sheikh, Md.N. Hasan, Md.M. Hasan, A. Islam, Md.A. Khaleque, H.M. Marwani, K.A. Alzahrani, A.M. Asiri, M.M. Rahman, Md. R. Awual, Benign separation, adsorption, and recovery of rare-earth Yb(III) ions with specific ligand-based composite adsorbent, Process Saf. Environ. Prot. 185 (2024) 367–374, https://doi.org/10.1016/j.psep.2024.03.026.

[41] E. Awual, Md.S. Salman, Md.M. Hasan, Md.N. Hasan, K.T. Kubra, Md.C. Sheikh, A.I. Rasee, A.I. Rehan, R.M. Waliullah, M.S. Hossain, H.M. Marwani, A.M. Asiri, M.M. Rahman, A. Islam, Md.A. Khaleque, Md.R. Awual, Ligand imprinted composite adsorbent for effective Ni(II) ion monitoring and removal from contaminated water, J. Ind. Eng. Chem. 131 (2023) 585–592, https://doi.org/10.1016/j.jiec.2023.10.062.

[42] A.I. Rasee, E. Awual, A.I. Rehan, M.S. Hossain, R.M. Waliullah, K.T. Kubra, Md. C. Sheikh, Md.S. Salman, Md.N. Hasan, Md.M. Hasan, H.M. Marwani, A. Islam, Md.A. Khaleque, Md.R. Awual, Efficient separation, adsorption, and recovery of samarium(III) ions using novel ligand-based composite adsorbent, Surf. Inter. 41 (2023) 103276, https://doi.org/10.1016/j.surfin.2023.103276.

[43] M. Li, Q. Shi, N. Song, Y. Xiao, L. Wang, Z. Chen, T.D. James, Current trends in the detection and removal of heavy metal ions using functional materials, Chem. Soc. Rev. 52 (2023) 5827–5860, https://doi.org/10.1039/d2cs00683a.

[44] Y. Song, D. Cho, S. Venkateswarlu, M. Yoon, Systematic study on preparation of copper nanoparticle embedded porous carbon by carbonization of metal organic framework for enzymatic glucose sensor, RSC Adv. 7 (2017) 10592–10600, https://doi.org/10.1039/C7RA00115K.

[45] M. Venu, S. Venkateswarlu, Y.V.M. Reddy, A.S. Reddy, V.K. Gupta, M. Yoon, G. Madhavi, Highly sensitive electrochemical sensor for anticancer drug by a zirconia nanoparticle-decorated reduced graphene oxide nanocomposite, ACS Omega 3 (2018) 14597–14605, https://doi.org/10.1021/acsomega.8b02129.

[46] M. Venu, V.K. Gupta, S. Agarwa, S. Venkateswarlu, G. Madhavi, Simultaneous determination of dopamine, uric acid and folic acid with electrochemical techniques based on Co_3O_4/rGO/CTAB modified carbon paste electrode, Int. J. Electrochem. Sci. 13 (2018) 11702–11719, https://doi.org/10.20964/2018.12.41.

[47] S. Venkateswarlu, B. Viswanath, A.S. Reddy, M. Yoon, Fungus-derived photoluminescent carbon nanodots for ultrasensitive detection of Hg^{2+} ions and

photoinduced bactericidal activity, Sens. Actuators B Chem. 258 (2017) 172–183, https://doi.org/10.1016/j.snb.2017.11.044.
[48] S. Venkateswarlu, A.S. Reddy, A. Panda, D. Sarkar, Y. Son, M. Yoon, Reversible fluorescence switching of Metal-Organic framework nanoparticles for use as security ink and detection of Pb^{2+} ions in aqueous media, ACS Appl. Nano Mater. 3 (2020) 3684–3692, https://doi.org/10.1021/acsanm.0c00392.
[49] A. Panda, Y. Yang, S. Venkateswarlu, Y. Son, T.-H. Bae, M. Yoon, Highly durable covalent organic framework for the simultaneous ultrasensitive detection and removal of noxious Hg^{2+}, Microporous Mesoporous Mater. 306 (2020) 110399 https://doi.org/10.1016/j.micromeso.2020.110399.
[50] A. Panda, S.K. Arumugasamy, J. Lee, Y. Son, K. Yun, S. Venkateswarlu, M. Yoon, Chemical-free sustainable carbon nano-onion as a dual-mode sensor platform for noxious volatile organic compounds, Appl. Surf. Sci. 537 (2020) 147872, https://doi.org/10.1016/j.apsusc.2020.147872.
[51] S. Kalytchuk, K. Poláková, Y. Wang, J.P. Froning, K. Cepe, A.L. Rogach, R. Zbořil, Carbon dot nanothermometry: intracellular photoluminescence lifetime thermal sensing, ACS Nano 11 (2017) 1432–1442, https://doi.org/10.1021/acsnano.6b06670.
[52] G. Chellasamy, S.K. Arumugasamy, M.J. Nam, S. Venkateswarlu, E. Varathan, K. Sekar, K. Manokaran, M.-J. Choi, S. Govindaraju, K. Yun, Experimental and simulation studies of bioinspired Au-enhanced copper single atom catalysts towards real-time expeditious dopamine sensing on human neuronal cell, Chem. Eng. J. 471 (2023) 144842, https://doi.org/10.1016/j.cej.2023.144842.
[53] A. Islam, A. Malek, Md.T. Islam, F.Y. Nipa, O. Raihan, H. Mahmud, Md.E. Uddin, M.L. Ibrahim, G. Abdulkareem-Alsultan, A.H. Mondal, Md.M. Hasan, Md. S. Salman, K.T. Kubra, Md.N. Hasan, Md.C. Sheikh, T. Uchida, A.I. Rasee, A. I. Rehan, E. Awual, M.S. Hossain, R.M. Waliullah, Md.R. Awual, Next frontier in photocatalytic hydrogen production through CdS heterojunctions, Int. J. Hydrog. Energy 101 (2024) 173–211, https://doi.org/10.1016/j.ijhydene.2024.12.300.
[54] A. Islam, S.H. Teo, Md.T. Islam, A.H. Mondal, H. Mahmud, S. Ahmed, M. Ibrahim, Y.H. Taufiq-Yap, A.-A. G, M.L. Hossain, Md.C. Sheikh, A.I. Rasee, A.I. Rehan, R. M. Waliullah, E. Awual, Md.M. Hasan, M.S. Hossain, K.T. Kubra, Md.S. Salman, Md.N. Hasan, Md.R. Awual, Harnessing visible light for sustainable biodiesel production with Ni/Si/MgO photocatalyst, Renew. Sustain. Energy Rev. 208 (2024) 115033, https://doi.org/10.1016/j.rser.2024.115033.
[55] S. Zhu, H. Fan, Y. Su, Y. Fan, W. Wang, Ultrahigh triethylamine sensitivity of WO_3-MoO_3 n-n heterojunction sensor operating at low-temperature, Chem. Eng. J. 507 (2025) 16060, https://doi.org/10.1016/j.cej.2025.160607.
[56] J. Jang, W. Koo, D. Kim, I. Kim, In situ coupling of multidimensional MOFs for heterogeneous metal-oxide architectures: toward sensitive chemiresistors, ACS Cent. Sci. 4 (2018) 929–937, https://doi.org/10.1021/acscentsci.8b00359.
[57] M. Zhang, G. Wang, J. Chen, X. Lu, Single atom catalysts for sensors, Trends Anal. Chem. 169 (2023) 11739, https://doi.org/10.1016/j.trac.2023.117399.
[58] M. Pumera, P. Thakkar, Single atom engineered materials for sensors, Trends Anal. Chem. 174 (2024) 117660, https://doi.org/10.1016/j.trac.2024.117660.
[59] G. Chellasamy, S.K. Arumugasamy, M.J. Nam, S. Venkateswarlu, E. Varathan, K. Sekar, K. Manokaran, M. Choi, S. Govindaraju, K. Yun, Experimental and simulation studies of bioinspired Au-enhanced copper single atom catalysts towards real-time expeditious dopamine sensing on human neuronal cell, Chem. Eng. J. 471 (2023) 144842, https://doi.org/10.1016/j.cej.2023.144842.
[60] B. Qiao, A. Wang, X. Yang, L.F. Allard, Z. Jiang, Y. Cui, J. Liu, J. Li, T. Zhang, Single-atom catalysis of CO oxidation using Pt1/FeOx, Nat. Chem. 3 (2011) 634–641, https://doi.org/10.1038/nchem.1095.
[61] B. Singh, M.B. Gawande, A.D. Kute, R.S. Varma, P. Fornasiero, P. McNeice, R. V. Jagadeesh, M. Beller, R. Zboril, Single-atom (iron-based) catalysts: synthesis and applications, Chem. Rev. 121 (2021) 13620–13697, https://doi.org/10.1021/acs.chemrev.1c00158.
[62] S. Kment, A. Bakandritsos, I. Tantis, H. Kmentová, Y. Zuo, O. Henrotte, A. Naldoni, M. Otyepka, R.S. Varma, R. Zboril, Single atom catalysts based on earth-abundant metals for energy-related applications, Chem. Rev. 124 (2024) 11767–11847, https://doi.org/10.1021/acs.chemrev.4c00155.
[63] Z. Ma, C. Kuloor, C. Kreyenschulte, S. Bartling, O. Malina, M. Haumann, P. W. Menezes, R. Zbořil, M. Beller, R.V. Jagadeesh, Development of iron-based single atom materials for general and efficient synthesis of amines, Angew. Chem. Inter. Ed. 63 (2024) e202407859, https://doi.org/10.1002/anie.202407859.
[64] S. Venkateswarlu, M. Umer, Y. Son, S. Govindaraju, G. Chellasamy, A. Panda, J. Park, S. Umer, J. Kim, S. Choi, K. Yun, M. Yoon, G. Lee, M.J. Kim, An amiable design of cobalt single atoms as the active sites for oxygen evolution reaction in desalinated seawater, Small 20 (2024) 2305289, https://doi.org/10.1002/smll.202305289.
[65] S. Vallem, S. Venkateswarlu, Y. Li, S. Song, M. Li, J. Bae, MXene-and MOF-based single-atom catalysts for next-generation batteries chemistry: A synergy of experimental and theoretical insights, Energy Storage Mater. 65 (2024) 103159, https://doi.org/10.1016/j.ensm.2023.103159.
[66] G. Chellasamy, E. Varathan, K. Sekar, S. Venkateswarlu, S. Govindaraju, K. Yun, Single-atom catalysts for biosensing: Progress in theoretical and mechanistic understanding, Coord. Chem. Rev. 502 (2024) 215606, https://doi.org/10.1016/j.ccr.2023.215606.
[67] Y. Qin, J. Wen, L. Zheng, H. Yan, L. Jiao, X. Wang, X. Cai, Y. Wu, G. Chen, L. Chen, L. Hu, W. Gu, C. Zhu, Single-atom-based heterojunction coupling with ion-exchange reaction for sensitive photoelectrochemical immunoassay, Nano Lett. 21 (2021) 1879–1887, https://doi.org/10.1021/acs.nanolett.1c00076.
[68] L. Liu, K. Yung, H. Yang, B. Liu, Emerging single-atom catalysts in the detection and purification of contaminated gases, Chem. Sci. 15 (2024) 6285–6313, https://doi.org/10.1039/d4sc01030b.
[69] X. Chen, P. Gao, L. Guo, Y. Wen, D. Fang, B. Gong, Y. Zhang, S. Zhang, High-efficient physical adsorption and detection of formaldehyde using Sc- and Ti-decorated graphdiyne, Phys. Lett. A 381 (2017) 879–885, https://doi.org/10.1016/j.physleta.2017.01.009.
[70] B. Zong, Q. Xu, S. Mao, Single-atom Pt-functionalized $Ti_3C_2T_x$ field-effect transistor for volatile organic compound gas detection, ACS Sens 7 (2022) 1874–1882, https://doi.org/10.1021/acssensors.2c00475.
[71] T. Dai, Z. Yan, M. Li, Y. Han, Z. Deng, S. Wang, R. Wang, X. Xu, L. Shi, W. Tong, J. Bao, Z. Qiao, L. Li, G. Meng, Boosting electrical response toward trace volatile organic compounds molecules via pulsed temperature modulation of Pt anchored WO_3 chemiresistor, Small Methods 6 (2022) 2200728, https://doi.org/10.1002/smtd.202200728.
[72] H. Shin, W. Jung, D. Kim, J. Jang, Y.H. Kim, W. Koo, J. Bae, C. Park, S. Cho, B. J. Kim, I. Kim, Single-atom Pt stabilized on one- dimensional nanostructure support via carbon nitride/SnO_2 heterojunction trapping, ACS Nano 14 (2020) 11394–11405, https://doi.org/10.1021/acsnano.0c03687.
[73] W. Bu, N. Liu, Y. Zhang, W. Han, X. Chuai, Z. Zhou, C. Hu, G. Lu, Atomically dispersed Pt on MOF-derived In_2O_3 for chemiresistive formaldehyde gas sensing, Sens. Actuators B Chem. 404 (2024) 135260, https://doi.org/10.1016/j.snb.2023.135260.
[74] L. Zhou, X. Chang, W. Zheng, X. Liu, J. Zhang, Single atom Rh-sensitized SnO_2 via atomic layer deposition for efficient formaldehyde detection, Chem. Eng. J. 475 (2023) 146300, https://doi.org/10.1016/j.cej.2023.146300.
[75] V.K. Sharma, X. Ma, R. Zboril, Single atom catalyst-mediated generation of reactive species in water treatment, Chem. Soc. Rev. 52 (2023) 7673, https://doi.org/10.1039/d3cs00627a.
[76] Y. Yu, Z. Zhu, H. Huang, Surface engineered single-atom systems for energy conversion, Adv. Mater. 36 (2024) 2311148, https://doi.org/10.1002/adma.202311148.
[77] W. Ma, H. Wan, L. Zhang, J.Y. Zheng, Z. Zhou, Single-atom catalysts for electrochemical energy storage and conversion, J. Energy Chem. 63 (2021) 170–194, https://doi.org/10.1016/j.jechem.2021.08.041.
[78] Y. Yu, Y. Tan, W. Niu, S. Zhao, J. Hao, Y. Shi, Y. Dong, H. Liu, C. Huan, C. Gao, P. Zhang, Y. Wu, L. Zeng, B. Du, Y. He, Advances in synthesis and applications of single-atom catalysts for metal oxide-based gas sensors, Materials 17 (2024) 1970, https://doi.org/10.3390/ma17091970.
[79] S. Lv, H. Wang, Y. Zhou, D. Tang, S. Bi, Recent advances in heterogeneous single-atom nanomaterials: From engineered metal-support interaction to applications in sensors, Coord. Chem. Rev. 478 (2023) 214976, https://doi.org/10.1016/j.ccr.2022.214976.
[80] Y. Chen, S. Ji, C. Chen, Q. Peng, D. Wang, Y. Li, Single-Atom catalysts: Synthetic strategies and electrochemical applications, Joule 2 (2018) 1242–1264, https://doi.org/10.1016/j.joule.2018.06.019.
[81] H. Ou, D. Wang, Y. Li, How to select effective electrocatalysts: Nano or single atom? Nano Sel. 2 (2020) 492–511, https://doi.org/10.1002/nano.202000239.
[82] X. Zhu, C. Xiong, H. Zhou, J. Wang, Y. Wu, Single-atom nanozymes for enhanced electrochemical biosensing: A review, Talanta 294 (2025) 128179, https://doi.org/10.1016/j.talanta.2025.128179.
[83] P.H. Li, M. Yang, Y.-X. Li, Z.-Y. Song, J.-H. Liu, C.-H. Lin, J. Zeng, X.-J. Huang, Ultra-Sensitive and selective detection of arsenic(III) via electroanalysis over cobalt single-atom catalysts, Anal. Chem. 92 (2020) 6128–6135, https://doi.org/10.1021/acs.analchem.0c00677.
[84] H. Wang, H. Zhang, J. Zhang, J. Han, H. Fang, M. Yu, Z. Chang, X. Bu, Innovative microstructure and morphology engineering of MOF-derived single-atom Sn-doped ZnO nanosheet showing highly sensitive acetone sensing, Adv. Funct. Mater. (2025), https://doi.org/10.1002/adfm.202422378.
[85] T. Chu, C. Rong, L. Zhou, X. Mao, B. Zhang, F. Xuan, Progress and perspectives of single-atom catalysts for gas sensing, Adv. Mater. 35 (2022), https://doi.org/10.1002/adma.202206783.
[86] G. Lei, H. Pan, H. Mei, X. Liu, G. Lu, C. Lou, Z. Li, J. Zhang, Emerging single atom catalysts in gas sensors, Chem. Soc. Rev. 51 (2022) 7260–7280, https://doi.org/10.1039/d2cs00257d.
[87] H. Zhang, G. Liu, L. Shi, J. Ye, Single-Atom catalysts: Emerging multifunctional materials in heterogeneous catalysis, Adv. Energy Mater. 8 (2017), https://doi.org/10.1002/aenm.201701343.
[88] H. Zhang, S. Zhang, Z. Zhang, Advancements and applications of single-atom nanozymes in sensing analysis, Chemosensors 12 (2024) 209, https://doi.org/10.3390/chemosensors12100209.
[89] J. Fu, Y. Liu, Single-Atom nanomaterials in electrochemical sensors applications, Chemosensors 11 (2023) 486, https://doi.org/10.3390/chemosensors11090486.
[90] X. Xu, D. Xu, S. Lu, X. Zhou, S. Yang, Z. Zhang, Atomically dispersed recognition unit for selective in vivo photoelectrochemical medicine detection, Nat. Commun. 15 (2024), https://doi.org/10.1038/s41467-024-53154-z.
[91] Z. Huang, X. Sun, P. Wang, H. Wan, Emerging single-atom catalysts in electrochemical biosensing, View 4 (2023), https://doi.org/10.1002/viw.20220058.
[92] S. Wang, S. Cao, L. Wang, X. Zhan, H. Yang, W. Yang, H. Hou, Enhanced photoelectrochemistry for energy conversion, environmental remediation, detection, and sensing through single-atom catalysts modified photoelectrodes: a comprehensive review, Mater. Today Energy 43 (2024) 101582, https://doi.org/10.1016/j.mtener.2024.101582.
[93] S. Zha, D. Wang, C. Liu, W. Wang, N. Mitsuzaki, Z. Chen, Heteroatom doped M–N–C single-atom catalysts for high-efficiency oxygen reduction reaction: regulation of coordination configurations, Sustain. Energ. Fuels 6 (2022) 3895–3906, https://doi.org/10.1039/d2se00896c.

[94] J. Liu, J. Zhu, H. Xu, D. Cheng, Rational design of Heteroatom-Doped Fe–N–C Single-Atom catalysts for oxygen reduction reaction via simple descriptor, ACS Catal. 14 (2024) 6952–6964, https://doi.org/10.1021/acscatal.4c01377.

[95] C. Park, H. Shin, M. Jeon, S. Cho, J. Kim, I. Kim, Single-atom catalysts in conductive Metal–Organic frameworks: enabling reversible gas sensing at room temperature, ACS Nano 18 (2024) 26066–26075, https://doi.org/10.1021/acsnano.4c05815.

[96] L. Jiao, W. Xu, Y. Zhang, Y. Wu, W. Gu, X. Ge, B. Chen, C. Zhu, S. Guo, Boron-doped Fe-N-C single-atom nanozymes specifically boost peroxidase-like activity, Nano Today 35 (2020) 100971, https://doi.org/10.1016/j.nantod.2020.100971.

[97] L. Cui, J. Hao, Y. Zhang, X. Kang, J. Zhang, X. Fu, J. Luo, N and S dual-coordinated Fe single-atoms in hierarchically porous hollow nanocarbon for efficient oxygen reduction, J. Colloid Interface Sci. 650 (2023) 603–612, https://doi.org/10.1016/j.jcis.2023.06.153.

[98] H. Zhou, H. Liu, Q. Lai, Z. Lei, S. Song, K. He, C. Liu, Y. Chen, Y. Hu, Electro-activating non-radical $^1O_2$/H* via single atom manganese modified cathode: The indispensable role of metal active site Mn*, J. Hazard. Mater. 426 (2021) 127794 https://doi.org/10.1016/j.jhazmat.2021.127794.

[99] C. Xu, J. Wu, L. Chen, Y. Gong, B. Mao, J. Zhang, J. Deng, M. Mao, Y. Shi, Z. Hou, M. Cao, H. Li, H. Zhou, Z. Huang, Y. Kuang, Boric acid-assisted pyrolysis for high-loading single-atom catalysts to boost oxygen reduction reaction in Zn-Air batteries, Energy Environ. Mater. 7 (2022) e12569, https://doi.org/10.1002/eem2.12569.

[100] T. Zheng, X. Han, J. Wang, Z. Xia, Role of heteroatom-doping in enhancing catalytic activities and the stability of single-atom catalysts for oxygen reduction and oxygen evolution reactions, Nanoscale 14 (2022) 16286–16294, https://doi.org/10.1039/d2nr04880a.

[101] Y. Qin, J. Wen, X. Wang, L. Jiao, X. Wei, H. Wang, J. Li, M. Liu, L. Zheng, L. Hu, W. Gu, C. Zhu, Iron single-atom catalysts boost photoelectrochemical detection by integrating interfacial oxygen reduction and enzyme-mimicking activity, ACS Nano 16 (2022) 2997–3007, https://doi.org/10.1021/acsnano.1c10303.

[102] M. Xi, H. Zhang, L. Yang, Y. Long, Y. Zhao, A. Chen, Q. Xiao, T. Liu, X. Xiao, G. Hu, Electronic structure engineering of Single-Atom tungsten on vacancy-enriched V_3S_4 nanosheets for efficient hydrogen evolution, Adv. Sci. 12 (2024) 2409855, https://doi.org/10.1002/advs.202409855.

[103] F. Opoku, O. Akoto, N.K. Asare-Donkor, A.A. Adimado, Defect-engineered two-dimensional layered gallium sulphide molecular gas sensors with ultrahigh selectivity and sensitivity, Appl. Surf. Sci. 562 (2021) 150188, https://doi.org/10.1016/j.apsusc.2021.150188.

[104] H. Khan, A. Naskar, S. Bera, Vacancy and Defect Structures in Metal Oxides, Elsevier eBooks, 2023, pp. 61–81, https://doi.org/10.1016/b978-0-323-85588-4.00007-6.

[105] R, M. Di, D. Han, S. Hong, Z. Wang, Atomically dispersed Au on In_2O_3 nanosheets for highly sensitive and selective detection of formaldehyde, ACS Sens 5 (2020) 2611–2619, https://doi.org/10.1021/acssensors.0c01074.

[106] B. Feng, Z. Wang, Y. Feng, P. Li, Y. Zhu, Y. Deng, L. Wu, Q. Yue, J. Wei, Single-atom Au-functionalized mesoporous SnO_2 nanospheres for ultrasensitive detection of listeria monocytogenes biomarker at low temperatures, ACS Nano 18 (2024) 22888–22900, https://doi.org/10.1021/acsnano.4c03566.

[107] S.Yeop Yi, E. Choi, H.Y. Jang, S. Lee, J. Park, D. Choi, Y. Jang, H. Kang, S. Back, S. Jang, J. Lee, Insight into Defect Engineering of Atomically Dispersed Iron Electrocatalysts for High-Performance Proton Exchange Membrane Fuel Cell, Adv. Mater. 35 (2023) 2302666, https://doi.org/10.1002/adma.202302666.

[108] T. Yuan, Z. Xue, Y. Chen, J. Xu, Single Pt atom-based gas sensor: break the detection limit and selectivity of acetone, Sens. Actuators B Chem. 397 (2023) 134139, https://doi.org/10.1016/j.snb.2023.134139.

[109] Y. Luo, Y. Wu, A. Braun, C. Huang, X. Li, C. Menon, P.K. Chu, Defect engineering to tailor metal vacancies in 2D conductive Metal–Organic frameworks: an example in Electrochemical Sensing, ACS Nano 16 (2022) 20820–20830, https://doi.org/10.1021/acsnano.2c08097.

[110] V. Blums, M. Piotrowski, M.I. Hussain, B.G. Norton, S.C. Connell, S. Gensemer, M. Lobino, E.W. Streed, A single-atom 3D sub-attonewton force sensor, Sci. Adv. 4 (2018) eaao4453, https://doi.org/10.1126/sciadv.aao4453.

[111] T. Esat, D. Borodin, J. Oh, A.J. Heinrich, F.S. Tautz, Y. Bae, R. Temirov, A quantum sensor for atomic-scale electric and magnetic fields, Nat. Nanotechnol. 19 (2024) 1466–1471, https://doi.org/10.1038/s41565-024-01724-z.

[112] M. Zhou, Y. Jiang, G. Wang, W. Wu, W. Chen, P. Yu, Y. Lin, J. Mao, L. Mao, Single-atom Ni-N_4 provides a robust cellular NO sensor, Nat. Commun. 11 (2020), https://doi.org/10.1038/s41467-020-17018-6.

[113] X. Luo, Z. Luo, X. Wei, L. Jiao, Q. Fang, H. Wang, J. Wang, W. Gu, L. Hu, C. Zhu, Iridium single-atomic site catalysts with superior oxygen reduction reaction activity for sensitive monitoring of organophosphorus pesticides, Anal. Chem. 94 (2021) 1390–1396, https://doi.org/10.1021/acs.analchem.1c04665.

[114] S. Ding, Z. Lyu, L. Fang, T. Li, W. Zhu, S. Li, X. Li, J. Li, D. Du, Y. Lin, Single-atomic site catalyst with heme enzymes-like active sites for electrochemical sensing of hydrogen peroxide, Small 17 (2021), https://doi.org/10.1002/smll.202100664.

[115] Y. Liang, P. Zhao, J. Zheng, Y. Chen, Y. Liu, J. Zheng, X. Luo, D. Huo, C. Hou, Fe Single-atom electrochemical sensors for H_2O_2 produced by living cells, ACS Appl. Nano Mater. 5 (2022) 11852–11863, https://doi.org/10.1021/acsanm.2c02853.

[116] X. Wei, S. Song, W. Song, W. Xu, L. Jiao, X. Luo, N. Wu, H. Yan, X. Wang, W. Gu, L. Zheng, C. Zhu, Fe_3C-Assisted single atomic Fe sites for sensitive electrochemical biosensing, Anal. Chem. 93 (2021) 5334–5342, https://doi.org/10.1021/acs.analchem.1c00635.

[117] Y. Shu, Z. Li, Y. Yang, J. Tan, Z. Liu, Y. Shi, C. Ye, Q. Gao, Isolated cobalt atoms on N-doped carbon as nanozymes for hydrogen peroxide and dopamine detection, ACS Appl. Nano Mater. 4 (2021) 7954–7962, https://doi.org/10.1021/acsanm.1c01278.

[118] Z. Li, R. Liu, C. Tang, Z. Wang, X. Chen, Y. Jiang, C. Wang, Y. Yuan, W. Wang, D. Wang, S. Chen, X. Zhang, Q. Zhang, J. Jiang, Cobalt nanoparticles and atomic sites in nitrogen-doped carbon frameworks for highly sensitive sensing of hydrogen peroxide, Small 16 (2019) 1902860, https://doi.org/10.1002/smll.201902860.

[119] P. Li, M. Yang, Y. Li, Z. Song, J. Liu, C. Lin, J. Zeng, X. Huang, Ultra-sensitive and selective detection of arsenic(III) via electroanalysis over cobalt single-atom catalysts, Anal. Chem. 92 (2020) 6128–6135, https://doi.org/10.1021/acs.analchem.0c00677.

[120] P. Li, M. Yang, Z. Song, S. Chen, X. Xiao, C. Lin, X. Huang, Highly sensitive and stable determination of As(III) under near-neutral conditions: benefit from the synergetic catalysis of Pt single atoms and active S Atoms over Pt_1/MoS_2, Anal. Chem. 93 (2021) 15115–15123, https://doi.org/10.1021/acs.analchem.1c03416.

[121] P. Li, Z. Song, X. Xiao, B. Liang, M. Yang, S. Chen, W. Liu, X. Huang, Coordination engineering strategy of iron single-atom catalysts boosts anti-Cu(II) interference detection of As(III) with a high sensitivity, J. Hazard. Mater. 442 (2022) 130122, https://doi.org/10.1016/j.jhazmat.2022.130122.

[122] Y. Li, Z. Song, X. Xiao, L. Zhang, H. Huang, W. Liu, X. Huang, In-situ electronic structure redistribution tuning of single-atom Mn/g-C_3N_4 catalyst to trap atomic-scale lead(II) for highly stable and accurate electroanalysis, J. Hazard. Mater. 435 (2022) 129009, https://doi.org/10.1016/j.jhazmat.2022.129009.

[123] W. Cong, P. Song, Y. Zhang, S. Yang, W. Liu, T. Zhang, J. Zhou, M. Wang, X. Liu, Supramolecular confinement pyrolysis to carbon-supported Mo nanostructures spanning four scales for hydroquinone determination, J. Hazard. Mater. 437 (2022) 129327, https://doi.org/10.1016/j.jhazmat.2022.129327.

[124] M. Li, X. Peng, X. Liu, H. Wang, S. Zhang, G. Hu, Single-atom niobium doped BCN nanotubes for highly sensitive electrochemical detection of nitrobenzene, RSC Adv. 11 (2021) 28988–28995, https://doi.org/10.1039/d1ra05517h.

[125] B. Long, Y. Zhao, P. Cao, W. Wei, Y. Mo, J. Liu, C. Sun, X. Guo, C. Shan, M. Zeng, Single-Atom Pt Boosting electrochemical nonenzymatic glucose sensing on Ni $(OH)_2$/N-doped graphene, Anal. Chem. 94 (2022) 1919–1924, https://doi.org/10.1021/acs.analchem.1c04912.

[126] Y. Song, T. He, Y. Zhang, C. Yin, Y. Chen, Q. Liu, Y. Zhang, S. Chen, Cobalt single atom sites in carbon aerogels for ultrasensitive enzyme-free electrochemical detection of glucose, J. Electroanal. Chem. 906 (2022) 116024, https://doi.org/10.1016/j.jelechem.2022.116024.

[127] X. Wu, Y. Sun, T. He, Y. Zhang, G. Zhang, Q. Liu, S. Chen, Iron, Nitrogen-doped carbon aerogels for fluorescent and electrochemical dual-mode detection of glucose, Langmuir 37 (2021) 11309–11315, https://doi.org/10.1021/acs.langmuir.1c01866.

[128] Z. Wang, J. Wu, W. Wei, M. Gao, Y. Zhang, Z.G. Yu, Y.C. Liang, C. Zhu, Pt single-atom electrocatalysts at Cu_2O nanowires for boosting electrochemical sensing toward glucose, Chem. Eng. J. 495 (2024) 153564, https://doi.org/10.1016/j.cej.2024.153564.

[129] L. Liu, F. Li, T. Liu, S. Chen, M. Zhang, Porphyrin zirconium-based MOF dispersed single Pt atom for electrocatalytic sensing levodopa, J. Electroanal. Chem. 921 (2022) 116701, https://doi.org/10.1016/j.jelechem.2022.116701.

[130] F.X. Hu, T. Hu, S. Chen, D. Wang, Q. Rao, Y. Liu, F. Dai, C. Guo, H.B. Yang, C. M. Li, Single-atom cobalt-based electrochemical biomimetic uric acid sensor with wide linear range and ultralow detection limit, Nanomicro Lett. 13 (2020), https://doi.org/10.1007/s40820-020-00536-9.

[131] N. Wu, H. Zhong, Y. Zhang, X. Wei, L. Jiao, Z. Wu, J. Huang, H. Wang, S. P. Beckman, W. Gu, C. Zhu, Atomically dispersed Ru3 site catalysts for electrochemical sensing of small molecules, Biosens. Bioelectron. 216 (2022) 114609, https://doi.org/10.1016/j.bios.2022.114609.

[132] F.A. Bushira, S.A. Kitte, H. Li, L. Zheng, P. Wang, Y. Jin, Enzyme-like Fe-N_5 single atom catalyst for simultaneous electrochemical detection of dopamine and uric acid, J. Electroanal. Chem. 904 (2021) 115956, https://doi.org/10.1016/j.jelechem.2021.115956.

[133] Y. Liu, P. Zhao, Y. Liang, Y. Chen, J. Pu, J. Wu, Y. Yang, Y. Ma, Z. Huang, H. Luo, D. Huo, C. Hou, Single-atom nanozymes Co–N–C as an electrochemical sensor for detection of bioactive molecules, Talanta 254 (2022) 124171, https://doi.org/10.1016/j.talanta.2022.124171.

[134] X. Xie, D.P. Wang, C. Guo, Y. Liu, Q. Rao, F. Lou, Q. Li, Y. Dong, Q. Li, H.B. Yang, F.X. Hu, Single-atom ruthenium biomimetic enzyme for simultaneous electrochemical detection of dopamine and uric acid, Anal. Chem. 93 (2021) 4916–4923, https://doi.org/10.1021/acs.analchem.0c05191.

[135] T. Chu, G. Wang, X. Zhang, Y. Jia, S. Dai, X. Liu, L. Zhang, X. Yang, B. Zhang, F. Xuan, High-density dual-structure single-atom Pt electrocatalyst for efficient hydrogen evolution and multimodal sensing, Nano Lett. 24 (2024) 9666–9674, https://doi.org/10.1021/acs.nanolett.4c02428.

[136] X. Sun, C. Chen, C. Xiong, C. Zhang, X. Zheng, J. Wang, X. Gao, Z. Yu, Y. Wu, Surface modification of MoS_2 nanosheets by single Ni atom for ultrasensitive dopamine detection, Nano Res 16 (2022) 917–924, https://doi.org/10.1007/s12274-022-4802-8.

[137] R. Li, W. Guo, Z. Zhu, Y. Zhai, G. Wang, Z. Liu, L. Jiao, C. Zhu, X. Lu, Single-atom indium boosts electrochemical dopamine sensing, Anal. Chem. 95 (2023) 7195–7201, https://doi.org/10.1021/acs.analchem.2c05679.

[138] S.S. Shetty, J.K. El-Demellawi, Y. Khan, M.N. Hedhili, P. Arul, V. Mani, H. N. Alshareef, K.N. Salama, Iron Single-Atom catalysts on MXenes for ultrasensitive monitoring of adrenal tumor markers and cellular dopamine, Adv. Mater. Technol. 8 (2023) 2202069, https://doi.org/10.1002/admt.202202069.

[139] Y. Lei, D. Butler, M.C. Lucking, F. Zhang, T. Xia, K. Fujisawa, T. Granzier-Nakajima, R. Cruz-Silva, M. Endo, H. Terrones, M. Terrones, A. Ebrahimi, Single-

atom doping of MoS_2 with manganese enables ultrasensitive detection of dopamine: Experimental and computational approach, Sci. Adv. 6 (2020), https://doi.org/10.1126/sciadv.abc4250.
[140] X. Shi, J. Li, Y. Xiong, Z. Liu, J. Zhan, B. Cai, Rh single-atom nanozymes for efficient ascorbic acid oxidation and detection, Nanoscale 15 (2023) 6629–6635, https://doi.org/10.1039/d3nr00488k.
[141] C. Han, W. Yi, Z. Li, C. Dong, H. Zhao, M. Liu, Single-atom palladium anchored N-doped carbon enhanced electrochemical detection of furazolidone, Electrochim. Acta 447 (2023) 142083, https://doi.org/10.1016/j.electacta.2023.142083.
[142] X. Ge, P. Zhou, Q. Zhang, Z. Xia, S. Chen, P. Gao, Z. Zhang, L. Gu, S. Guo, Palladium single atoms on TiO_2 as a photocatalytic sensing platform for analyzing the organophosphorus pesticide chlorpyrifos, Angew. Chem. Int. Ed. 59 (2019) 232–236, https://doi.org/10.1002/anie.201911516.
[143] B. Li, L. Guo, M. Chen, Y. Guo, L. Ge, H.F. Kwok, Single-atom Pt-anchored $Zn_{0.5}Cd_{0.5}S$ boosted photoelectrochemical immunoassay of prostate-specific antigen, Biosens. Bioelectron. 202 (2022) 114006, https://doi.org/10.1016/j.bios.2022.114006.
[144] W. Liao, X. Fang, B. Cen, J. Chen, Y. Liu, M. Luo, J. Lu, Deep oxidation of propane over WO_3 - promoted Pt/BN catalysts: the critical role of Pt - WO_3 interface, Appl. Catal. B Environ. Energy 272 (2020) 118858, https://doi.org/10.1016/j.apcatb.2020.118858.
[145] L. Liu, C. Mao, H. Fu, X. Qu, S. Zheng, ZnO Nanorod-immobilized Pt single-atoms as an ultrasensitive sensor for triethylamine detection, ACS Appl. Mater. Interfaces 15 (2023) 16654–16663, https://doi.org/10.1021/acsami.2c21410.
[146] P. Wang, S. Guo, Z. Hu, L. Zhou, T. Li, S. Pu, H. Mao, H. Cai, Z. Zhu, B. Chen, H. Li, H. Liu, Single-atom Cu stabilized on ultrathin $WO_{2.72}$ nanowire for highly selective and ultrasensitive ppb-level toluene detection, Adv. Sci. 10 (2023), https://doi.org/10.1002/advs.202302778.
[147] J.W. Baek, S. Han, S.E. Lee, J. Ahn, C. Park, J.S. Nam, Y.H. Kim, E. Shin, M. Kim, J. Jang, J. Kim, H.J. Park, I. Kim, Cobalt-doped ceria sensitizer effects on metal oxide nanofibers: Heightened surface reactivity for high-performing chemiresistive sensors, ACS Nano 18 (2024) 19568–19580, https://doi.org/10.1021/acsnano.4c03168.
[148] T. Y, B. Xiao, J. Zeng, R. Yu, B. Zi, G. Zhang, Z. Zhu, J. Zhang, J. Wu, Q. Liu, Pt Single atom-induced activation energy and adsorption enhancement for an ultrasensitive ppb-level methanol gas sensor, ACS Sens 7 (2022) 199–206, https://doi.org/10.1021/acssensors.1c01959.
[149] F. Gu, Y. Cui, D. Han, S. Hong, M. Flytzani-Stephanopoulos, Z. Wang, Atomically dispersed Pt (II) on WO_3 for highly selestive sensing and catalytic oxidation of triethylamine, Appl. Catal. B Environ. 256 (2019) 117809, https://doi.org/10.1016/j.apcatb.2019.117809.
[150] F. Gu, C. Luo, D. Han, S. Hong, Z. Wang, Atomically dispersed Pt on 3DOM WO_3 promoted with cobalt and nickel oxides for highly selective and highly sensitive detection of xylene, Sens. Actuators B Chem. 297 (2019) 126772, https://doi.org/10.1016/j.snb.2019.126772.
[151] N. Wang, Z. Liu, Y. Zhou, L. Zhao, X. Kou, T. Wang, Y. Wang, P. Sun, G. Lu, Imparting chemiresistor with humidity-independent sensivity toward trace-level formaldehyde via substitutional doping platinum single atom, Small 20 (2024) 2310465, https://doi.org/10.1002/smll.202310465.
[152] H.H. Choi, J. Lee, K.-Y. Dong, B.-K. Ju, W. Lee, Noxious gas detection using carbon nanotubes with Pd nanoparticles, Nanoscale Res. Lett. 6 (2011), https://doi.org/10.1186/1556-276x-6-605.
[153] P. Liu, J. Wang, H. Jin, M. Ge, F. Zhang, C. Wang, Y. Sun, N. Dai, SnO_2 mesoporous nanoparticle-based gas sensor for highly sensitive and low concentration formaldehyde detection, RSC Adv. 13 (2023) 2256–2264, https://doi.org/10.1039/d2ra06745e.
[154] C. Liu, J. Hu, G. Wu, J. Cao, Z. Zhang, Y. Zhang, Carbon nanotube-based field-effect transistor-type sensor with a sensing gate for ppb-level formaldehyde detection, ACS Appl. Mater. Interfaces 13 (2021) 56309–56319, https://doi.org/10.1021/acsami.1c17044.
[155] N.M. Triet, L.T. Duy, B.-U. Hwang, A. Hanif, S. Siddiqui, K.-H. Park, C.-Y. Cho, N.-E. Lee, High-Performance schottky diode gas sensor based on the heterojunction of three-dimensional nanohybrids of reduced graphene oxide-vertical ZnO nanorods on an AlGaN/GaN layer, ACS Appl. Mater. Interfaces 9 (2017) 30722–30732, https://doi.org/10.1021/acsami.7b06461.
[156] B. Zong, Q. Xu, Q. Li, X. Fang, X. Chen, C. Liu, J. Zang, Z. Bo, S. Mao, Novel insights into the unique intrinsic sensing behaviors of 2D nanomaterials for volatile organic compounds: from graphene to MoS_2 and black phosphorous, J. Mater. Chem. A 9 (2021) 14411–14421, https://doi.org/10.1039/d1ta02383g.
[157] R. Cao, Z. Lu, J. Hu, Y. Zhang, Carbon-Based FET-Type gas sensor for the detection of ppb-level benzene at room temperature, Chemosensors 12 (2024) 179, https://doi.org/10.3390/chemosensors12090179.
[158] Z. LZu, Q. Zhu, Y. Pan, F. Huang, L. Tang, C. Liu, Z. Cheng, P. Wang, J. Ma, M. Ding, Single-atom tailoring of two-dimensional atomic crystals enables highly efficient detection and pattern recognition of chemical vapors, ACS Sens 7 (2022) 1533–1543, https://doi.org/10.1021/acssensors.2c00356.
[159] B. Feng, Z. Wang, Y. Feng, P. Li, Y. Zhu, Y. Deng, L. Wu, Q. Yue, J. Wei, Single-atom Au-functionalized mesoporous SnO_2 nanospheres for ultrasensitive detection of listeria monocytogenes biomarker at low temperatures, ACS Nano 18 (2024) 22888–22900, https://doi.org/10.1021/acsnano.4c03566.
[160] B. Liu, Q. Zhu, Y. Pan, F. Huang, L. Tang, C. Liu, Z. Cheng, P. Wang, J. Ma, M. Ding, Single-Atom tailoring of Two-Dimensional atomic crystals enables highly efficient detection and pattern recognition of chemical vapors, ACS Sens 7 (2022) 1533–1543, https://doi.org/10.1021/acssensors.2c00356.
[161] M. Ueland, H. Bae, A. Udomkijmongkol, K. Kotmool, V. Gulati, T. Hussain, Single atom dispersed tungsten disulfide (WS_2) based nanosensors for VOCs detection related to decomposed humans in disaster events, FlatChem 45 (2024) 100666, https://doi.org/10.1016/j.flatc.2024.100666.
[162] T. Liu, Z. Cui, X. Li, H. Cui, Y. Liu, AI-doped $MoSe_2$ monolayer as a promising biosensor for exhaled breath analysis: a DFT study, ACS Omega 6 (2021) 988–995, https://doi.org/10.1021/acsomega.0c05654.
[163] Q. Wan, X. Chen, Y. Gui, First-principles insight into a Ru-doped SnS_2 monolayer as a promosing biosensor for exhale gas analysis, ACS Omega 5 (2020) 8919–8926, https://doi.org/10.1021/acsomega.0c00651.
[164] H. Vovusha, P. Panigrahi, Y. Pal, H. Bae, M. Park, S.K. Son, M.J.A. Shiddiky, T. Hussain, H. Lee, Efficient detection of specific volatile organic compounds associated with COVID-19 using CrX_2 (X=Se, Te) monolayers, FlatChem 43 (2024) 100604, https://doi.org/10.1016/j.flatc.2023.100604.
[165] Z. Zhu, H. Tao, R. Zhang, L. Gan, Y. Zhou, Synergistic effect of diatomic materials on efficient formaldehyde sensing and degradation, J. Mater. Chem. A 12 (2024) 419–427, https://doi.org/10.1039/D3TA06132A.
[166] S. Vallem, S. Song, Y. Oh, J. Bae, Small methods sustainable ZIF-67/Mo-MXene-derived nanoarchitecture synthesis: an enhanced durable performance of lithium-selenium batteries, Small Methods 8 (2024) 2400294, https://doi.org/10.1002/smtd.202400294.
[167] A. Singh, A. Singh, S. Lee, H. Bae, T. Hussain, H. Lee, Density functional theory study on sensing and dielectric properties of arsenic trisulfide nanosheets for detecting volatile organic compounds, ACS Appl. Nano Mater. 4 (2021) 5444–5453, https://doi.org/10.1021/acsanm.1c00771.
[168] H. Vovusha, H. Bae, S. Lee, J. Park, A. Raza, K. Kotmool, T. Hussain, H. Lee, Density functional theory studies of MXene-based nanosensors for detecting volatile organic compounds in meat spoilage assessment, ACS Appl. Nano Mater. 6 (2023) 18592–18601, https://doi.org/10.1021/acsanm.3c03846.
[169] J. Sun, R. Tu, Y. Xu, H. Yang, T. Yu, D. Zhai, X. Ci, W. Deng, Machine learning aided design of single-atom alloy catalysts for methane cracking, Nat. Comm. 15 (2024) 6036, https://doi.org/10.1038/s41467-024-50417-7.
[170] M. Tamtaji, H. Gao, M.D. Hossain, P.R. Galligan, H. Wong, Z. Liu, H. Liu, Y. Cai, W.A. Goddard, Z. Luo, J. Mater. Chem. A 10 (2022) 15309–15331, https://doi.org/10.1039/D2TA02039D.
[171] M. Huang, R. Shi, H. Liu, W. Ding, J. Fan, B. Zhou, B. Da, Z. Gao, H. Li, W. Yang, Computational single-atom catalyst database empowers the machine learning assisted design of high-performance catalysts, J. Phys. Chem. C. 129 (2025) 5043–5053, https://doi.org/10.1021/acs.jpcc.5c00491.
[172] Z. Yuan, X. Luo, F. Meng, Machine learning-assisted research and development of chemiresistive gas sensors, Adv. Eng. Mater. 26 (2024) 2400782, https://doi.org/10.1002/adem.202400782.
[173] B. Wang, J. Zhang, T. Wang, W. Li, Q. Lu, H. Sun, L. Huang, X. Liang, F. Liu, F. Liu, P. Sun, G. Lu, Machine Learning-Assisted Volatile Organic Compound Gas Classification Based on Polarized Mixed-Potential Gas Sensors, ACS Appl. Mater. Interfaces 15 (2023) 6047–6057, https://doi.org/10.1021/acsami.2c17348.
[174] L. Breiman, Random forests, Mach. Learn 45 (2001) 5–32, https://doi.org/10.1023/A:1010933404324.
[175] S. Acharyya, B. Jana, S. Nag, G. Saha, P.K. Guha, Single resistive sensor for selective detection of multiple VOCs employing SnO_2 hollow spheres and machine learning algorithm: A proof of concept, Sens. Actuators B Chem. 321 (2020) 128484, https://doi.org/10.1016/j.snb.2020.128484.
[176] M. Tonezzer, J.-H. Kim, J.-H. Lee, S. Iannotta, S.S. Kim, Predictive gas sensor based on thermal fingerprints from Pt-SnO_2 nanowires, Sens. Actuators B Chem. 281 (2019) 670–678, https://doi.org/10.1016/j.snb.2018.10.102.
[177] F.F. Li, E. Adeli, J. Johnson, Z. Durante. CS231n: Convolutional Neural Networks for Visual Recognition, Stanford University, (2024). https://cs231n.github.io/convolutional-networks/.
[178] M. Pardo, G. Sberveglieri, Classification of electronic nose data with support vector machines, Sens. Actuators B Chem. 107 (2005) 730–737, https://doi.org/10.1016/j.snb.2004.12.005.
[179] H. Ye, Z. Du, H. Lu, J. Tian, L. Chen, W. Lin, Using machine learning methods to predict VOC emissions in chemical production with hourly process parameters, J. Clean. Prod. 369 (2022) 133406, https://doi.org/10.1016/j.jclepro.2022.133406.
[180] J.-Y. Kim, S.S. Kim, M. Tonezzer, Selective gas detection and quantification using a resistive sensor based on Pd-decorated soda-lime glass, Sens. Actuators B Chem. 335 (2021) 129714, https://doi.org/10.1016/j.snb.2021.129714.
[181] D.C. Pugh, S.M.V. Hailes, I.P. Parkin, A gas-sensing array produced from screen-printed, zeolite-modified chromium titanate, Meas. Sci. Technol. 26 (2015) 085102, https://doi.org/10.1088/0957-0233/26/8/085102.
[182] I. Cho, K. Lee, Y.C. Sim, J.S. Jeong, M. Cho, H. Jung, M. Kang, Y.H. Cho, S.C. Ha, K.J. Yoon, I. Park, Deep-learning-based gas identification by time-variant illumination of a single micro-LED-embedded gas sensor, Light Sci. Appl. 12 (2023), https://doi.org/10.1038/s41377-023-01120-7.
[183] J. Oh, S.H. Kim, M.-J. Lee, H. Hwang, W. Ku, J. Lim, I.-S. Hwang, J.-H. Lee, J.-H. Hwang, Machine learning-based discrimination of indoor pollutants using an oxide gas sensor array: High endurance against ambient humidity and temperature, Sens. Actuators B Chem. 364 (2022) 131894, https://doi.org/10.1016/j.snb.2022.131894.
[184] C. Zha, L. Li, F. Zhu, Y. Zhao, The classification of VOCs based on sensor images using a lightweight neural network for lung cancer diagnosis, Sensors 24 (2024), https://doi.org/10.3390/s24092818.
[185] Z. Tang, Y. Liu, M. Xiang, D. Cui, Q. Li, Discrimination of VOCs with e-nose consisting of a single MEMS sensor using lightweight deep learning model based on SqueezeNet, Sens. Actuators B Chem. 422 (2025) 136640, https://doi.org/10.1016/j.snb.2024.136640.

[186] O. Ogbeide, G. Bae, W. Yu, E. Morrin, Y. Song, W. Song, Y. Li, B.-L. Su, K.-S. An, T. Hasan, Inkjet-Printed rGO/binary metal oxide sensor for predictive gas sensing in a mixed environment, Adv. Funct. Mater. 32 (2022) 2113348, https://doi.org/10.1002/adfm.202113348.
[187] W. Ku, G. Lee, J.Y. Lee, D.H. Kim, K.H. Park, J. Lim, D. Cho, S.C. Ha, B.G. Jung, H. Hwang, W. Lee, H. Shin, H.S. Jang, J.O. Lee, J.H. Hwang, Rational design of hybrid sensor arrays combined synergistically with machine learning for rapid response to a hazardous gas leak environment in chemical plants, J. Hazard. Mater. 466 (2024) 133649, https://doi.org/10.1016/j.jhazmat.2024.133649.
[188] D. Hu, Z. Yang, S. Huang, Machine learning prediction of perovskite sensors for monitoring the gas in lithium-ion battery, Sen. Actuators A Phys. 369 (2024) 115162, https://doi.org/10.1016/j.sna.2024.115162.
[189] S. Acharyya, P.K. Bhowmick, P.K. Guha, Selective identification and quantification of VOCs using metal nanoparticles decorated SnO_2 hollow-spheres based sensor array and machine learning, J. Alloy. Compd. 968 (2023) 171891, https://doi.org/10.1016/j.jallcom.2023.171891.
[190] J. Lozano, G. Paredes, J.I. Suárez, A. Vergara, D. Gil, J. Fonollosa, S. Marco, Multiclass classification of n-butanol concentrations with k-nearest neighbor algorithm and support vector machine in an electronic nose, Sens. Actuators B Chem. 166-167 (2012) 721–725, https://doi.org/10.1016/j.snb.2012.03.047.

Sowjanya Vallem earned her Ph.D. in Physics from the National Institute of Technology Karnataka, India, in 2019. She is currently a postdoctoral researcher at Amrita Vishwa Vidyapeetham, working on advanced electrochemical sensors for glucose and chlorine detection, aimed at healthcare and environmental monitoring. Her expertise spans nanomaterials, electrocatalysis, and energy storage, with previous research focused on Li-chalcogenide batteries and supercapacitors. Dr. Vallem's interdisciplinary work bridges materials science and applied technologies, contributing to next-generation diagnostic and sustainable energy solutions.

Sibi Malayil Gopalan earned his Ph.D. in Chemical Science from AcSIR-IIP Dehradun in 2016. He held postdoctoral positions at the University of the Western Cape, Université Laval, and Sungkyunkwan University under the BK21 + program. Currently, he is a Marie Skłodowska-Curie Actions (MSCA) fellow and senior researcher at VSB-Technical University of Ostrava, Nanotechnology Centre. Mentored by Prof. Radek Zbořil, his research focuses on the design of single-atom heterogeneous catalysts for sustainable catalytic processes, including the production of sustainable aviation fuel (SAF) from biomass and CO_2.

K. Keerthi obtained her M.Sc., degree from Sri Padmavati Mahila Visvavidyalam, Tirupati, India in 2019. She is currently pursuing Ph. D under the supervision of Prof. N.V.V. Jyothi at Sri Venkateswara University. Her research work focuses on the development of efficient and eco-friendly catalysts for Oxygen evolution reaction and Hydrogen evolution reactions.

Giridhar Babu Anam is an Associate Professor in the Department of Basic Sciences at SR University, Telangana, India. He received his Ph.D. from the Department of Biotechnology and Environmental Sciences, Thapar University, India in 2011 and has held research positions at leading South Korean institutions including Chonbuk National University, Kangwon National University, and the Pohang Institute of Science and Technology. Currently, his research focuses on cyanobacterial bloom hazards, cyanophage and chemical based elimination strategies, microbial metagenomics, and renewable energy. He aims to develop sustainable solutions for pollution control and environmental remediation, effectively bridging the gap between academia, industry, and policy-making.

Vishakha Goyal completed her Ph.D. degree in catalysis and organic transformations at Academy of Scientific and Innovative Research (AcSIR), India in 2022. Subsequently, she joined in VSB-Technical University of Ostrava, as postdoctoral scientist in the group of Prof. Radek Zboril. Further, she worked as postdoctoral fellow in Leibniz Institute for Catalysis (LIKAT), Germany in 2024. In the following year, she started working as Marie Skłodowska-Curie Actions (MSCA) Postdoctoral Fellow-CZ in VSB-Technical University of Ostrava. Her research interest focuses on designing on homogeneous and heterogeneous (single atom catalysts) catalysts for sustainable organic synthesis and energy technologies.

EA Lohith received his M.Sc degree from Sri Venkateswara University, Tirupati, India in 2019. He is currently pursuing Ph. D under the supervision of Prof. N.V.V. Jyothi at Sri Venkateswara University. His research work focuses on the development of sustainable catalysts for energy sector particularly in hydrogen production through water splitting.

N.V.V. Jyothi obtained her Ph.D. in Chemistry from Sri Venkateswara University, Tirupati, in 2003. She received a UGC Postdoctoral Fellowship (UGC-PDF) in 2007 and currently serves as the Coordinator for the M.Sc. Organic Chemistry (SSC) program. In 2019, she was elected as an Associate Fellow of the Andhra Pradesh Academy of Sciences (APAS). She organized a national conference in 2017 and has published 40 research papers and two book chapters in reputed journals. Her research interests include voltammetric method development for trace metal analysis, nanomaterial synthesis, and the thermodynamic properties of binary organic liquids.

K. Praveena received her M.Sc. degree in Organic Chemistry from Sri Venkateswara University, Tirupati, India, in 2012. She worked as a lecturer at Kasturba Gandhi Balika Vidyalayas (KGBVs), Nellore, India, during 2023–2024. Currently, she is a Ph.D. scholar under the guidance of Prof. K. Sivakumar in the Department of Chemistry, Sri Venkateswara Arts College (TTD), Tirupati 517502, India. Her research interests include designing nanocatalyst for energy and environmental applications.

Kasibhatta Sivakumar is currently working as a Professor of Chemistry at S.V. Arts College (Autonomous), managed by TTD, Tirupati, India. He was awarded an M.Phil. and Ph.D. in Physical Chemistry from the same university in 1990 and 1992, respectively. His research areas include thermophysical characterization of liquid mixtures, molecular interactions in binary and ternary systems, physicochemical properties of ionic liquids, analytical determination of drugs, and biosorption of heavy metals. He has published 90 research articles and 6 book chapters in reputed national and international journals. In 2022, he was elected as a Fellow of the Royal Society of Chemistry (UK).

T. G. Satheesh Babu, Professor at Amrita Vishwa Vidyapeetham, leads cutting-edge research in non-enzymatic biosensors, immunosensors, and POCT devices. With over 75 publications, US patents, and significant project funding, he advances sensor technologies through the Amrita Biomedical Engineering Centre, driving impactful innovations in biomedical diagnostics.

Suneesh P. V., Associate Professor at Amrita Vishwa Vidyapeetham, specializes in nanomaterials for biosensors and energy storage. Active in the Biosensor Research Lab since 2008, his work focuses on developing affordable diagnostic tools, microfluidic systems, and next-generation energy devices for real-world healthcare and sustainable energy applications.

Hari Bandi earned his Bachelor of Science (B. Sc, 2015) and Master of Science (M. Sc, 2017) degrees in condensed matter physics from Sri Venkateshwara University, India. At present, he is pursuing a Ph.D. degree at Kyung Hee University in the Republic of Korea, where he is under the supervision of Professor Jae Su Yu. His primary research interests include transition metal oxides for the development of high-performance lithium-ion batteries, zinc-ion batteries, and supercapacitors.

Daniel-I. Stroe, Associate Professor at Aalborg University, leads the Batteries Research Group, specializing in lithium-ion battery testing, predictive modeling, diagnostics, and lifetime estimation. With over 270 peer-reviewed publications, his work advances energy storage for grid and e-mobility applications. His research supports UN SDGs through sustainable, data-driven battery technologies and modeling.

Sada Venkateswarlu received his Ph.D. in Chemistry from Sri Venkateswara University, Tirupati, India, in 2014. He worked with Prof. Minyoung Yoon (Gachon University) as a Postdoctoral Researcher and Assistant Professor (2015–2021), and with Prof. Myung Jong Kim (2021–2023). He has authored over 35 peer-reviewed publications (h-index: 21, 2000 + citations). Currently, he is a Senior Researcher in Prof. Radek Zbořil's group at the VSB–Technical University of Ostrava, Czech Republic. His research focuses on single-atom engineering, MOFs, carbon materials, and BNNTs for developing electrochemical catalysts in sensing and energy conversion applications.

Aristeidis Bakandritsos (ORCID 0000–0003–4411–9348) is a group leader and senior researcher at CATRIN-RCPTM, Palacký University Olomouc and VSB-TUO, CEET, MELab in Ostrava, Czech Republic. He received his Ph.D. in Greece in 2006, and he was faculty member at the Dept. of Materials Science, University of Patras, before joining RCPTM. He has more than 120 peer-reviewed publications, h-index 39, and > 6000 citations (Scopus). His research is focused on the synthesis and functionalization of nanomaterials targeting advances in the fields of energy storage, catalysis, environmental remediation and biomedicine.

Jagadeesh Rajenahally is currently a Group Leader at Leibniz Institute for Catalysis (LIKAT), Germany and Nanotechnology Center, CEET, VSB-Technical University of Ostrava, Czech Republic. He obtained PhD (2006) in Chemistry from Bangalore University, India. After having performed Postdoctoral Research (2006–2008) at the University of Florida, USA and worked as Assistant Professor (2009–2010) at VIT University, India he joined the Leibniz Institute for Catalysis in the year 2010 initially as a Scientist in the Department of Prof. Matthias Beller and then became Group Leader. His research focuses on catalysis, sustainable organic synthesis, valorization of renewable feedstocks and recycling/upscaling of waste-materials.

Radek Zbořil is the Scientific Director of RCPTM division of Czech Advanced Technology and Research Institute (CATRIN) at Palacky University Olomouc and a head of the Materials-Envi Lab at VSB-Technical University Ostrava, Czech Republic. After receiving PhD in 2000 from Palacký University he stayed at several universities including the University of Delaware and the University of Tokyo. He was a Founding Director (2010–2020) of the RCPTM. He is an expert in nanotechnologies and author of > 700 papers with > 78,000 citations and 128H-index. He has appeared several times on the list of Highly Cited Researchers announced by Clarivate Analytics.